UNIVERSITY OF PADUA
SCHOOL OF ENGINEERING

—

DEPARTMENT OF INDUSTRIAL ENGINEERING

—

MASTERS THESIS IN BIOENGINEERING

IDENTIFICATION OF UPPER LIMB MOTOR MODULES BASED ON ELECTROMYOGRAPHIC DATA ANALYSIS

SUPERVISOR: PROF. ENG. GIULIO ROSATI

AUTHOR: ANNA LORENZIN

ACADEMIC YEAR 2012-2013

"When making a decision of minor importance, I have always found it advantageous to consider all the pros and cons. In vital matters, however, such as the choice of a mate or a profession, the decision should come from the unconscious, from somewhere within ourselves. In the important decisions of personal life, we should be governed, I think, by the deep inner needs of our nature. "

FREUD

Contents

Abstract

How the central nervous system (CNS) selects the appropriate muscle activation patterns to achieve a behavioral goal is still an open question. Recently it was hypothesized that the CNS might rely on a modular control. Previous studies have shown that the coordination of human voluntary movements may be accomplished using combinations of a small number of muscular coordination patterns, or motor modules.

This thesis investigates the possibility of finding coordination patterns that could explain motor control of the upper extremity in many different situations. Our hypothesis is that motor coordination of a wide variety of movements can be explained by a small set of motor modules that are shared throughout most movements, but that can show minor movement-specific tweaks. We also hypothesize that this modular organization presents significant similarities among subjects and among dominant and non-dominant sides. This study also aims at examining if changes in muscle coordination after stroke can be explained by changes in motor modules.

15 healthy subject and 15 hemiparetic patients participated in the study. We recorded their EMG activity and movement kinematics while they performed six different reaching tasks. Tasks were chosen so as to cover a significant subset of all possible movements in the subject's workspace. Motor modules relative to all pooled movement and to each individual movement were extracted with non-negative matrix factorization from the processed EMG signals.

Regarding healthy subjects, results show that, on average, all movements could be described by a linear combination of about 4 modules, both for the dominant and the non-dominant side.

We also found that, even though not all subjects share the exact same coordination patterns, all modules of all subjects can be grouped into eight clusters. In addition, we found that modules extracted from single movements match those extracted from all pooled movements, although certain muscle weights change on a movement-specific basis in order to adapt to different performance requirements.

Introduction

To date it is not yet fully clear how the central nervous system (CNS) copes with the complex problem of muscle coordination during the execution of voluntary movements. Previously, various simplifying strategies have been hypothesized such as reflexes, unit burst generator model and spinal force fields.

In the past decades a new and promising way to explain motor control has gained ground, claiming that the number of variables controlled by the CNS can be greatly reduced by a modular organization of muscles.

The first studies regarding motor modules were carried out on animals: they provided clear evidence of the existence of a muscle pattern underlying postural responses and motor behavior as walking and swimming. Similar muscle modules robustness was demonstrated also in human subjects. Modular organization has been proposed as a strategy for muscle coordination during gait, and it was shown that a limited number of modules are sufficient to account for muscle activation during human walking.

The theory of motor modules was also applied to the upper limb. This is a much more challenging area, as the upper limb has a wide variety of possible movements due to the degree of freedom of the shoulder, elbow and wrist joints. For this reason, most of the literature focuses on muscle coordination during well-defined tasks, which are usually a very limited subset of all possible movements achievable by the upper extremity. It is therefore not yet clear if muscle modules used during such tasks can also explain muscle coordination during other movements.

Besides describing muscle coordination in healthy people, modules have also been used to describe changes in motor control after a neurological injury, and especially after stroke. Evidence suggests that motor impairment after stroke can be explained by alterations in the modular organization of muscles. Although many studies have focused on the changes in motor modules after stroke, most of these changes where reported only with respect to very specific tasks. The lack of a more comprehensive model of the upper extremity for healthy people makes hard to find a reference to which one can compare post-stroke muscle coordination.

Based on the theory of motor modules, the goal of this thesis is to investigate how well modules explain coordination of the upper extremity in many different situations and not just for a very specific task, and to provide useful information about motor control. This study also aims to examine if muscle activity of different subjects can be explained with similar modules and if changes in muscle coordination after stroke can be explained by changes in motor modules. In order to get there, healthy and hemiparetic subjects were asked to perform a set of tasks designed so as to cover a wide variety of movements in the subject's workspace. During the execution of these tasks EMG activity and movement kinematics were recorded and were then used to extract muscle modules.

The first chapter gives an introduction to the problem of muscle coordination and the theories that followed one another to explain it.

The second chapter gives a short overview on the nature of electromyographic signals and describes part of the instrumentation that was used to record EMG data.

In the third chapter the laboratory where the tests were performed, its instrumentation and its software tools are presented. In addition, the experimental protocol and the setup used for the data acquisitions are described in detail.

Chapter four shows how the data was processed and analyzed in order to extract modules from the EMG signals.

In the fifth chapter the results are illustrated. We first analyzed modules extracted from all combined tasks, comparing them between dominant and non-dominant side and among subjects.

We then identified those modules that are shared by most subjects and that could therefore represent fundamental structures used for motor control. These modules were then examined on a task-by-task basis in order to capture movement-specific adaptations, and were associated with a biomechanical function.

Chapter 1

Motor control

This chapter aims at giving a general overview on motor control, explaining fundamental concepts of how the CNS might achieve such a complex task. In the second part of this chapter we introduce the concept of motor modules as a strategy to simplify motor control and we show how the underlying theory developed throughout the years. The end of the chapter is dedicated to stroke, on its effects on motor control and on how recent studies try to explain the resulting motor impairments by alterations in motor modules.

1.1 Motor control: a quick overview

Motor control is a multidisciplinary field, which combines aspects of biomechanics, neuroscience, cognitive science and other scientific areas, to study how movements of the human body can be generated [1]. From a mechanical point of view, movement is initiated by the presence of a force, generated by the activity of one or more skeletal muscles. By contracting these muscles, forces and torques are generated in the joints of the skeletal system and, when properly coordinated, they allow humans to perform a wide variety of motor tasks. Each muscle consists of many muscle fibers, their number depending on the type of muscle, which act in parallel. Muscle fibers are the main force generators, each of them adding a fraction of the total muscle force. Normally not all fibers are active at the same time but follow a cyclic recruitment pattern that alternates active periods with

resting periods in order to reduce fatigue. The higher the force generated by the muscle, the more fibers will be active at the same time, and the shorter the force can be maintained before fatigue occurs [2].

The activity of muscle fibers is controlled by motoneurons. A single motoneuron may innervate multiple muscle fibers, the union of the motoneuron and all its muscle fibers is called motor unit. All muscle fibers within a motor unit activate together and almost at the same time. The axon of the motoneuron connects to the muscle fibers through specialized synapses, called neuromuscular junctions, which transmit the activation signal (action potential) to the fiber. The motoneuron is in turn connected to the descending neural pathways in the spinal cord, thereby forming a bridge between the central nervous system (CNS) and the muscles (see figure 1.1).

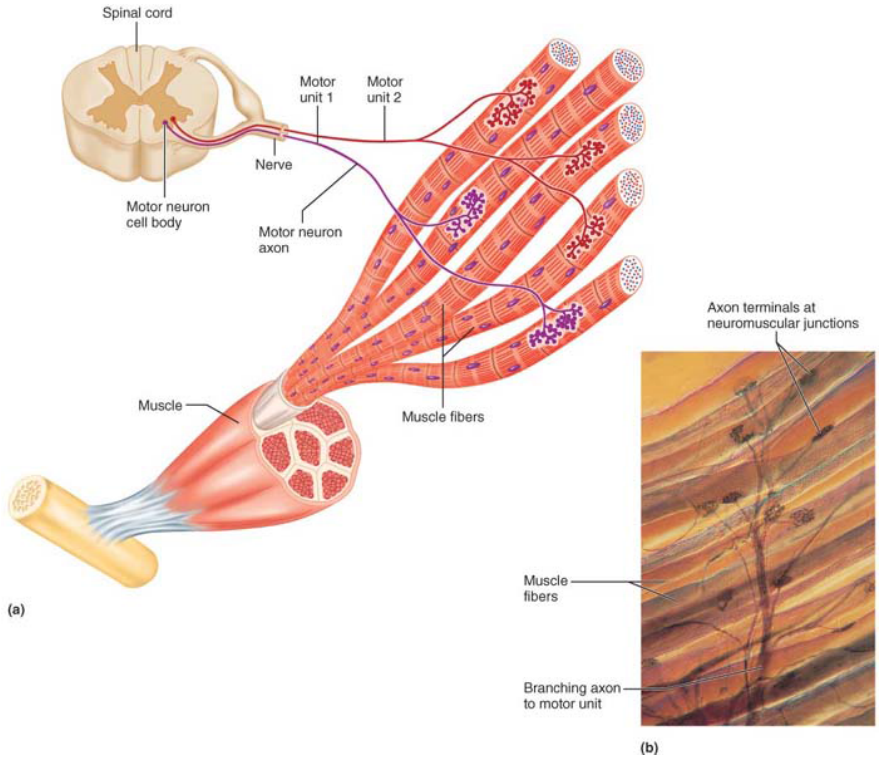

Figure 1.1: (a) Schematic view of two motor units: the cell body of the motor neurons reside in the spinal cord and their axons extend to the muscles, each axon divides into axon terminals witch innervate muscle fibers. (b) Photomicrograph of a portion of a motor unit (80×) [2].

The way the signals coming from the spinal cord and transmitted to the motoneurons are generated is still not fully known. The current idea is that motor control is structured on three levels: a low level control on the segmental level, an intermediate control on the projection level and a high level control on the precommand level.

The segmental level is the lowest level of the motor hierarchy and consists mainly of spinal cord circuits. Segmental circuits stimulate specific groups of muscles and some of them, called central pattern generators (CPGs), control locomotion and other oft-repeated motor activities. CPGs consist on networks of oscillating inhibitory and excitatory neurons, which set crude rhythms and alternating patterns of movements [2].

The projection level has direct control over the spinal cord. It consists of two systems, a direct (pyramidal) system and an indirect (multineuronal) system. The direct system is initiated by neurons of the motor cortex and is in charge of producing discrete voluntary movements of the skeletal muscles. Each skeletal muscle has a specific representation in the primary motor cortex: muscles of the left side in the right hemisphere and muscles of the right side in the left hemisphere. The size of the area that projects to a certain part of the body is proportional to how finely its movements can be controlled. The map of the projected body parts in the motor cortex is called the cortical homunculus (figure 1.2).

The indirect system on the other side is controlled by some areas of the brain stem and supervises the activity of the segmental apparatus, thereby influencing reflex and CPG-controlled motor actions. Information coming from the projection motor pathways in both transmitted to lower motoneurons and to higher command levels as an internal feedback. Even though direct and indirect systems provide separate and parallel pathways to control the spinal cord, they are interrelated at all levels.

The precommand level consists of two additional systems, located in the so called precommad areas, which control the outputs of the motor cortex and the brain stem. The cerebellum is responsible for an online sensorimotor integration

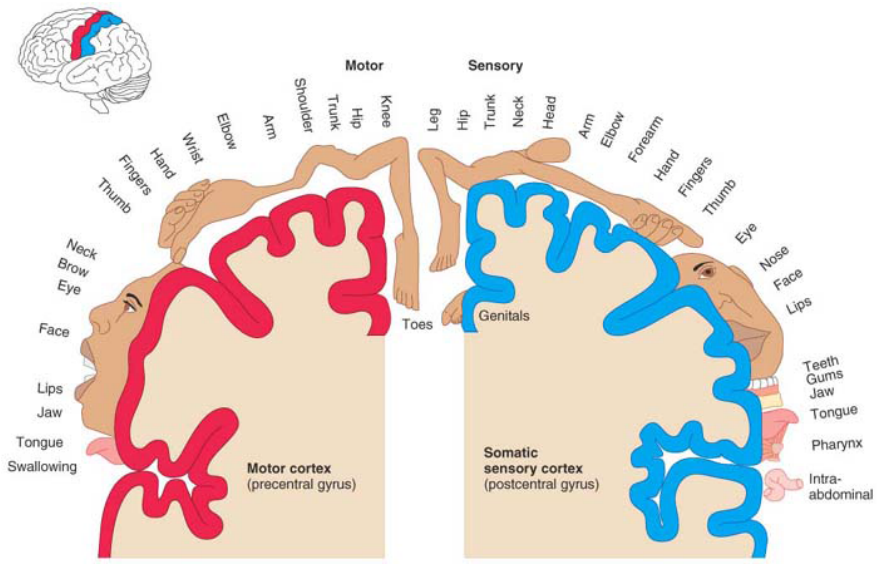

Figure 1.2: Motor and sensory areas of the cerebral cortex. The relative size of each body area in the drawing represents the relative amount of the cerebral cortex dedicated to that body area. The amount of the gyrus occupied by the body diagrams indicate the amount of cortical tissue assigned to that function.[2]

and control. It receives ascending proprioceptor, tactile, equilibrium and visual inputs, and information coming from the motor cortex and the brain stem. All this information is used to rapidly correct errors in motor activity and fine-tune movements. Even though it lacks a direct connection to the spinal cord, the cerebellum can act on motor pathways through the projection areas of the brain stem and the motor cortex via the thalamus.

The second system of the precommand level is located in the basal nuclei. Compared to the cerebellum, the basal nuclei seem to be involved in more complex aspects in motor control. They act primarily as a control system for the activity in the premotor cortical area, to which they are connected through the thalamus. The basal nuclei have two main functions, which happen unconsciously. The first is the inhibition of various motor centers of the brain under resting conditions. The second is the planning of complex motor tasks in advance of willed movements [2].

1.2 Overcoming the complexity of motor control

A central problem in motor physiology is how the activity of many muscles is coordinated to produce movement. To generate a purposeful behavior, the central nervous system has to coordinate the many degrees of freedom of the musculoskeletrical system [3]. Besides controlling the activity of a large amount of motor units, a challenging task by itself, the CNS has to take into account biomechanical constraints of the musculoskeletrical system, dynamic properties of the body, task-specific parameters such as movement kinematics, and many other factors which make the problem even more complex. In many circumstances, the CNS cannot rely on sensory feedback, but must use an open-loop control law to generate appropriate muscle patterns. Implementing such a controller, however, presents a great computational challenge because it requires mapping a potentially infinite number of different goals onto an infinite set of muscle patterns [4].

These remarks have led many authors to believe that the CNS adopts simplifying strategies to overcome the complexity of motor control.

In 1906 Sir Charles Sherrington published *The Integrative Action of the Nervous System*: here he introduced the concept of synapse and postulated that the reflex is the simplest unit of nervous integration. According to Sherrington, complex and unified behavior is enabled by the interaction of elementary reflexes [5].

Many years later, in 1981, Sten Grillner hypothesized the *unit burst generator model*. Unit burst generators are control elements that can produce rhythmic bursts of output at a single joint. Burst generators at adjacent joints are interconnected and can generate synergistic activation patterns: the unit burst generator at one joint can either excite or inhibit an adjacent generator, thereby producing complex biomechanical output [6, 7].

In 1990 Bizzi, Mussa-Ivaldi and Gistzer introduced a new theory: stimulation of specific areas of the spinal cord in spinalized frog suggested that the spinal neural circuits are organized in a modular way [8]. The force responses of microstimulation of the gray matter were summarized as force fields that converge to an equilibrium point, and the simultaneous excitation of two different areas

would result in a linear summation of the two respective force fields. The combination of these equilibrium paths could explain a large variety of motor behavior. They concluded that fixed-pattern force fields elicited in the spinal cord may be considered movement primitives [9, 10].

In the past decade a new and promising way to explain motor control has gained ground, claiming that the number of variables controlled by the CNS can be greatly reduced by a modular organization of muscles. Muscle modules, also called synergies by some authors, are groups of muscles that activate synchronously to produce a specific biomechanical output. Various studies have shown that a very limited number of such modules would be sufficient to describe the activity of many muscles, thereby effectively reducing the complexity of motor control. In fact, the CNS could only be in charge of coordinating the activation of a small set of modules, which in turn would be responsible of organizing the activity of all motor units involved in a specific task. It has been shown in literature that muscle modules can effectively describe muscle activation patterns in both animals and humans, and for both isometric force generation and dynamic tasks. However, it is not yet completely clear if modules represent actual neural structures, and at which level of the CNS they are positioned.

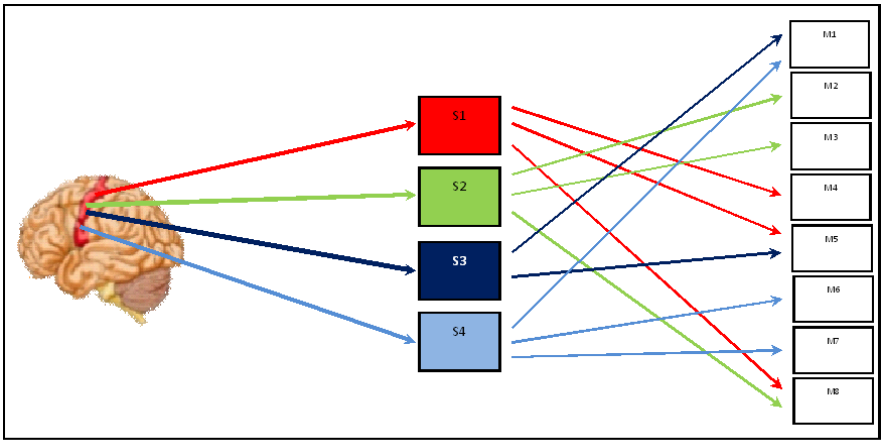

Figure 1.3: Schematic representation of the modular organization of muscles: the brain sends descending signals to a limited number of modules (S1 to S4), each of which controls multiple muscles. One specific muscle can be part of more than one module.

The first studies regarding motor modules were carried out on animals. Previous studies using intact or spinalized frogs suggested that coordinated movements can be generated by appropriated combinations of motor modules controlled by the central nervous system [11]. Ten spinalized frogs were chemically stimulated, the advantage was that the extract data would be task-independent. From the EMG data collection of 12 leg muscles, seven motor modules were found: these modules were similar among frogs and their linear combinations accounted for more than 91% of EMG data from all 10 frogs, giving strong evidence of the existence of modules [3].

Other authors sought to compare frogs behavior before and after certain spinal cord surgeries. Cheung at al. demonstrated that behaviors before and after deafferentation are primarily generated by the same motor modules and most of them are preserved after deafferentation [12]. EMG analysis on nine frogs before and after transection resulted in two types of modules: modules shared before and after transection and modules specific to individual states, demonstrating that motor behaviors may be constructed by motor modules organized within the brain stem and spinal cord and activated by descending commands from supraspinal areas [11]. Another study dealt with intact and unrestrained frogs during kicking in different directions. It was shown that: the variety of muscle activation patterns underlying the control of a natural behavior in an intact animal can be reconstructed as combinations of three time-varying modules, the modules extracted from each frog are very similar to each other and to those extracted from the pooled data, two of these modules are modulated in relation to the movement kinematics [4, 13]. Cheung et al. investigated the motor responses after an inertial load perturbation. The modules extracted from the EMG data of four frogs were robust across different dynamic conditions and immediate motor adjustment could be accomplished by modulating their activation coefficients [14].

In addition to frogs, other animals were used to study motor modules. EMG data was recorded from 8 to 15 hindlimb muscles of cats while the support surface was translated in 16 directions; results showed that as few as four modules could account for 95% of the automatic postural response across muscles and directions [15]. Overduin et al. applied microstimulations to motor cortical areas of

rhesus macaques to evoke hand movements. They inspected muscle data collected from two macaques while they performed a behavioral task prior to each of the intracortical microstimulation (ICMS) sessions. They found that ICMS can drive the hand towards particular postures and that ICMS-derived modules could be matched with a corresponding grasp-related module [16].

Regarding human subjects, the idea of the existence of motor modules was applied both to gait and upper limb analysis. In a recent study of 2009, authors analyzed data of 14 healthy adults walking for 30 seconds, identifying four modules that could describe most of the EMG variance: these were consistent across subjects in term of module weightings and timing profiles. The reconstruction of the EMG data obtained using these modules were able to account for more than 90% of the EMG variance for all muscles [17]. Two simulation studies attempted to provide further evidence to the existence of motor modules. Neptune et al. reconstructed recorded walking kinematics with a simulation software. An optimization algorithm was used to adapt the activation of previously identified muscle modules until the resulting kinematics would match the recorded ones. The authors showed that they could generate a good approximation of movement kinematics even by using only four modules, which proved that muscle modules are not only an artifact coming from EMG analysis, but that they can produce significant biomechanical output [17]. Other simulations were generated emulating human subjects during walking in four different conditions: normal, with added trunk loads, weight support, a combination of added trunk load and weight support (body weight and/or mass increased and decreased by 25%). It was found that a simple modular control scheme of five modules was able to reproduce well-coordinated walking even when the mechanical demands on the system were substantially altered by manipulations of body weight and body mass [18].

The theory of motor modules was also applied to the upper limb. This is a much more challenging area, as the upper limb has a wide variety of possible movements due to the degree of freedom of the shoulder, elbow and wrist joints. For this reason authors studied muscle activation patterns for many different tasks to investigate how the CNS controls the arm muscles. In one of the first studies EMG activity was recorded from 19 shoulder and arm muscles during

point-to-point reaching movements between a central location and 8 peripheral targets in the frontal and sagittal planes. In addition, these fast reaching movements were performed in different ways, changing the forearm starting position or adding a weight to the wrist. Four/five synergies were extracted from each of nine subjects involved in the study, and these were able to explain 73-82% of the data variation [19]. Another study demonstrated that the speed with which the tasks are executed doesn't affect the extracted modules: the complex changes observed in the muscles activation waveform of several shoulder and elbow muscles across movement directions and speeds were captured by scaling in time, scaling in amplitude, and shifting in time a few time-varying motor modules [20]. Ajiboye and Weier sought to understand if it is possible to exploit certain modules to reconstruct EMG data of a wide variety of hand movements. They recorded hand and forearm muscle activity form seven subjects while they were miming 33 posture of the ASL (American Sign Language alphabet). Modules were extracted from a subset of training postures: modules from 11 postures allowed for at least 90% prediction of the EMG patterns of all 33 postures [21]. Comparison between single and multi-joint movements was performed in reaching tasks in twelve different directions with the tested arm supported by a manipulandum. EMG signals were recorded from 12 muscles, both the single and the multi-joint modules provided a sufficient basis set to explain the variance in muscle activation patterns during planar reaching movements. However, while only three modules coming from multi-joint movements were sufficient to describe most of the EMG activity, at least four single-joint modules were needed to get comparable results [22]. This could indicate that complex movements are better suited for the purpose of module identification. Roh et al. evaluated motor modules of human arm muscles during three different isometric force generation protocols: a spatial protocol consisting in producing a certain force in a given direction, a load protocol requiring force generation on a broad range of load levels, and a position protocol on different hand positions that encompassed a substantial fraction of the arm's workspace. They proved that modules structures was conserved across the three experimental protocols and that module composition and tuning direction were consistent across all eight subjects in the study [23].

1.3 Effects of stroke on motor control

Every year, 15 million people worldwide suffer a stroke. Nearly six million die and another five million are left permanently disabled. Stroke is the second leading cause of disability, after dementia. Disability may include loss of vision and/or speech, paralysis and confusion. Globally, stroke is the second leading cause of death above the age of 60 years, and the fifth leading cause of death in people aged 15 to 59 years old [24]. In the elderly population of the 15-country Europe, estimates showed 2,700,000 prevalent cases, and 536,000 incident cases each year. Total number of stroke deaths in 48 European countries is currently estimated at 1,239,000 per year (508,000 per year in the 27 European Union members). Given that age is one of most substantiated risk factor for stroke, the ageing of the world population implies a growing number of persons at risk. Among EU members, for instance, Italy is the country with the highest percentage of people over the age of 65 years (19.9%). About 153,000 new stroke cases are expected each year in the Italian elderly population. Assuming stable incidence rates, a total of 195,000 new cases per year are expected in 2020, simply due to the ageing population. While stroke will firmly remain the second cause of death in the world by 2030, its ranking as a major cause of DALY (disability-adjusted life year) loss will increase during the same period. About half of stroke survivors are left with some degree of physical or cognitive impairment. The need of support for common daily activities directly impacts quality of life of patients and their relatives [25].

Stroke

Stroke is a clinical syndrome characterized by rapidly developing clinical symptoms and/or signs of focal, and at times global, loss of cerebral function, with symptoms lasting more than 24 hours or leading to death, with no apparent cause other than that of vascular origin [26].

The brain is an extremely complex organ that controls various body functions. When the blood flow to a certain area of the brain is disturbed, due either to an obstruction or to a hemorrhage, the functions associated with that specific area cease to work partially or completely.

The effects of a stroke depend on several factors, including the location of the obstruction/hemorrhage and how much brain tissue is affected.
If the stroke occurs in the brain's right side, the left side of the body will be affected, which could produce any or all of the following:

- Paralysis on the left side of the body
- Vision problems
- Quick, inquisitive behavioral style
- Memory loss

If the stroke occurs in the left side of the brain, the right side of the body will be affected, producing some or all of the following:

- Paralysis on the right side of the body
- Speech/language problems
- Slow, cautious behavioral style
- Memory loss

When stroke occurs in the brain stem, depending on the severity of the injury, it can affect both sides of the body and may leave someone in a "locked-in" state. When a locked-in state occurs, the patient is generally unable to speak or achieve any movement below the neck. There are three different types of stroke: There are three different types of stroke:

1. TIA (Transient Ischemic Attack)
2. Ischemic stroke
3. Hemorrhagic stroke

Transient Ischemic Attack (TIA) : it is characterized as a "warning stroke". It is caused by a clot; the only difference between a stroke and TIA is that with TIA the blockage is transient (temporary). TIA symptoms occur rapidly and last a relatively short time. Most TIAs last less than five minutes; the average is about a minute. Unlike a stroke, when a TIA is over, usually causes no permanent injury to the brain.

Ischemic Stroke (Clots) : it occur as a result of an obstruction within a blood vessel supplying blood to the brain. It accounts for 87% of all stroke cases. The underlying condition for this type of obstruction is the development of atherosclerosis, fatty deposits lining the vessel walls. These deposits can cause two types of obstruction:

- *Cerebral thrombosis* refers to a thrombus (blood clot) that develops at the clogged part of the vessel;
- *Cerebral embolism* refers generally to a blood clot that forms at another location in the circulatory system, usually the heart and large arteries of the upper chest and neck. A portion of the blood clot breaks loose, enters the bloodstream and travels through the brain's blood vessels until it reaches vessels too small to let it pass. A second important cause of embolism is an irregular heartbeat, known as atrial fibrillation. It creates conditions where clots can form in the heart, dislodge and travel to the brain.

Hemorrhagic Stroke (Bleeds) : it accounts for about 13% of stroke cases. It results from a weakened vessel that ruptures and bleeds into the surrounding brain. The blood accumulates and compresses the surrounding brain tissue. The two types of hemorrhagic strokes are intracerebral (within the brain) hemorrhage or subarachnoid hemorrhage. Two types of weakened blood vessels usually cause hemorrhagic stroke:

- *Aneurysm* is a ballooning of a weakened region of a blood vessel. If left untreated, the aneurysm continues to weaken until it ruptures and bleeds into the brain. The amount of damage is usually related to the amount of blood. Damage is due to the increased pressure and swelling from bleeding directly into the brain tissue, or from local cellular damage to brain tissue from irritation of blood in the space between the brain and the skull;
- *Arteriovenous Malformation (MAV)* is a cluster of abnormally formed blood vessels. Any one of these vessels can rupture, also causing bleeding into the brain.

If the stoke occurs in the motor cortex, it could affect motor control and cause movement dysfunctions like spasticity, muscular weakness and, above all, abnormal movement coordination [27].

Various researchers have studied the consequences of stroke on motor control, and recent work has attempted to explain the alterations in motor control through abnormal muscle coordination patterns, i.e. through changes in muscle modules or their activation. Recent studies have reported preservation of a low-dimesional modular organization of muscle coordination following stroke, claiming that reduced motor performance can be explained by alteration in the structure of modules. Although there are still many different opinions on this subject, and no unified theory, the views of the various authors can be classified into two main schools of thought: one asserts that changes in muscle activation patterns are due to alterations in the structures of modules, while the other states that the cause could be an abnormal activation of normal modules [28].

One example for the point of view of the authors belonging to the first group is the work done by Gizzi et al. in 2011. In this paper they analyzed the locomotion of 10 subacute stroke patients (within 20 weeks of the stroke), and compared it with that of healthy control subjects. They found that four modules where sufficient to explain the muscle activity of both groups, but that these modules where significantly different between affected and unaffected side and between stroke patients and healthy subjects. However they saw that even though the modules were different, the activation signals were very similar between the two groups and between the affected and unaffected side. Based on these observations, the authors claim that the activation signals are generated by central pattern generators and are then directed to motoneurons via a premotor network. Stroke might affect the behavior of the latter, which in turn might be visible as a change in muscle modules.

In another study, Roh et al. examined the spatial activation patterns of elbow and shoulder muscles in the affected arm of 10 stroke survivors and in both arms of 6 controls, using an isometric force matching protocol. In both groups four motor modules accounted for more than 90% of the total variance of muscle EMG patterns but are not comparable to each other, specially the two modules

dominated by activation of shoulder muscles were altered. They suggested that stroke induced abnormal coordination of muscle activation in severely impaired hemiparetic patients by altering the structure of motor modules [29].

Instead, many authors agree with the second approach. Cheung et al. recorded EMGs from 12-16 upper arm and shoulder muscles from both arms of stroke patients having moderate-to-severe unilateral ischemic lesion in the frontal motor cortical areas; in seven of eight patients the muscular compositions of the modules for both the affected and unaffected arms were strikingly similar to each other and concluded that modules were preserved and that the EMG differences may be described as differences in the spatiotemporal recruitment pattern of a few fixed modules [30]. Clark et al. examined the motor modules underlying gait in a group of 55 chronic stroke survivors and in 20 healthy control subjects. They identified four modules to account the variability of muscle activation in healthy subjects but fewer in stoke patients. They suggested that this reduction of the number of modules was due to a merging of the modules observed in healthy controls: stroke patients loose the independence of the activation timing profiles that led to the identification of merged modules [31]. In a subsequent study involving diverse subject groups, three different patterns of motor coordination were observed: in case of mild-to-moderate impairment (FM>30) modules in the affected and unaffected arms were similar even though the muscle activation patterns were different and the cause could be that the activation has faltered after stroke; in case of severe imparement (FM$\leq$30) in the affected arm multiple modules appeared to merge so the EMGs of the affected arm could be reconstructed with fewer modules; the third pattern is related with time passed after injury, a portion of the modules in the affected arm appeared to be fractionations of the modules observed in the unaffected arm and this fractionation process tended to increase the number of the modules required for adequate description of the affected-arm EMGs [32].

Chapter 2

Acquisition of electromyographic signals

The EMG signal is the electrical manifestation of the neuromuscular activation associated with a contracting muscle. The signal represents the current generated by the ionic flow across the membrane of the muscle fibers that propagate through the intervening tissue to reach the detection surface of an electrode located in the environment. This signal is affected by the anatomical and physiological properties of muscles and the control scheme of the nervous system, as well as the characteristics of the instrumentation used to detect and observe it. There are three classes of factors that influence the EMG signals:

- *Causative factors* have a basic or elemental effects on the signal;
- *Intermediate factors* represent physical and physiological phenomena that are influenced by one or more of the causative factors and in turn influence the deterministic factors;
- *Deterministic factors* represent physical characteristics of the action potentials.

2.1 Physiological aspects of the EMG signal

As already explained, muscles fibers are innervated in groups called motor units which, when activated, generate a motor unit action potential. The activation from the central nervous system is repeated continuously for as long as the muscle is required to generate force. This activation generates motor unit action potential trains and in turn these trains superimpose to form EMG signals.

2.1.1 Motor Unit Action Potential

The most fundamental functional unit of muscle is the motor unit. The electrical signal that emanates from the activation of the muscle fibers of a motor unit, that are in the detectable vicinity of an electrode, is called the motor unit action potential (MUAP). This constitutes the fundamental unit of the EMG signal. Many factors influence the shape of the MUAP:

- The relative geometrical relationship of the detection surfaces of the electrode and the muscles fibers of the motor unit in its vicinity;
- The relative position of the detection surfaces to the innervation zone;
- The size of the muscle fibers because the amplitude of the action potential is proportional to the diameter of the fiber;
- The number of muscle fibers in an individual motor unit in the detectable vicinity of the electrode.

2.1.2 Motor Unit Action Potential Train

The electrical manifestation of a MUAP is accompanied by a contractile twitch of the muscle fibers. To sustain a muscle contraction, the motor unit must be activated repeatedly. The resulting sequence of MUAPs is called a motor unit action potential train (MUAPT). The waveform of the MUAPs within a MUAPT will remain constant if the geometric relationship between the electrode and the active muscle fibers remains constant, if the properties of the recording electrode do not change, and if there are no significant biochemical changes in the muscle

tissue. Biochemical changes within the muscle can affect the conduction velocity of the muscle fiber and the filtering properties of the muscle tissue.

The MUAPT may be completely described by its interpulse intervals (the time between adjacent MUAPs) and the waveform of the MUAP. The interpulse intervals may be expressed as a sequence of Dirac delta impulses $\delta_i(t)$ convoluted with a filter $h(t)$ that represents the shape of the MUAP. It follows that the MUAPT, $u_i(t)$ can be expressed as:

$$u_i(t) = \sum_{k=1}^{n} h_i(t - t_k) \qquad \text{where} \qquad t_k = \sum_{l=1}^{k} x_l \quad \text{for} \quad k, l = 1, 2, 3, ..., n \tag{2.1}$$

t_k represents the time locations of the MUAPs, x represents the interpulse intervals, n is the total number of interpulse intervals in a MUAPT, and i, k, and l are integers that denote specific events.

The EMG signal may be synthesized by linearly summing the MUAPTs and mathematically corresponds to the equation:

$$m(t, F) = \sum_{i=1}^{p} u_i(t, F) \tag{2.2}$$

2.2 Electrodes

Two main types of electrodes are used to detect the EMG signal: surface (or skin) electrodes and inserted (wire or needle) electrodes.

Surface electrodes There are two categories of this kind of electrodes:

- *Passive electrodes*: they consist of one or two conductive detection surface that, when applied to the skin, measure the difference in voltage between one point and an electric reference, or between two points. The simplest form consists of silver disks that adhere to the skin. Electrical contact is greatly improved by introducing a conductive gel or paste between the electrode and skin;
- *Active electrodes*: they contain an high input impedance electronics amplifier in the same housing as the detection surface, they could be resistively or capacitively coupled to the skin.

The main disadvantages of surface electrodes are that they can be used effectively only with superficial muscles and that they cannot be used to detect signals selectively from small muscles or from single motor units (even though some computational decomposition techniques allow to infer the activity of the involved motor units from the EMG signal). Furthermore, due to the thickness of the tissue between electrode and muscle, and due to skin conductance, the electrode might pick up electric activity coming from adjacent muscles causing a phenomenon called "cross-talk".

Needle electrodes They are the most common indwelling electrode, in particular the "concentric" electrodes. This monopolar configuration contains one insulated wire in the cannula. The tip of the wire is bare and acts as a detection surface. The bipolar configuration contains a second detection surface. The single-fiber electrode consists of a thin, stiff, sharpened metal filament, usually made of tungsten. When inserted into a muscle it detects the action potentials of individual fibers. Needle electrodes have two main advantages:

- its relatively small pickup area enables the electrode to detect individual MUAPs during low force contractions;
- it may be conveniently repositioned within the muscle so that new tissue territories may be explore or the signal quality may be improved.

Wire electrodes These electrodes are constructed by inserting two insulated fine wires through the cannula of a hypodermic needle. They are extremely fine, easily implanted and withdrawn from skeletal muscles, and generally less pain full than needle electrodes whose cannula remains inserted in the muscles throughout the duration of the test. The extremity of the distal tips of the wire is deinsulated and bent to form two staggered hooks. The electrode is introduced into the muscles by inserting the hypodermic needle and then withdrawing it. The wires remain lodged in the muscle tissue, they may be removed by pulling them out, the hooks are pliable so they straighten out on retraction. A limitation of these electrodes is their tendency to migrate

after they have been inserted, however the migration usually stops after a few contractions.

Surface electrodes cannot detect deep muscles and signals from small muscles and they have the problem of "cross-talk". On the other side, even if the inserted electrodes can be used with deep muscles and allow to detect individual MUAPs, they represent an invasive method and for this reason a specialized personnel is required to insert them; besides, it could be hard to find subjects willing to give their informed consent to let the wire be introduced into their muscles [33].

2.3 Signal detection

The characteristics of the EMG signal are function of the apparatus used to acquire the signal as well as of the electrical current that is generated by the membrane of the muscles fibers. The electrical activity on the surface of the skin outside a muscle may be easily acquired by placing an electrode with only one detection surface and detecting the electrical potential that is point with respect to a reference electrode located in an environment that either is electrically quiet or contains electrical signals unrelated to those being detected. A surface electrode is commonly used as the reference electrode. In the bipolar detection configuration two surfaces are used to detect two potentials in the muscle tissue of interest each with respect to the reference electrode. The two signals are then fed to a differential amplifier which amplifies the difference of the two signals, thus eliminating any common mode components in the two signals. Signals emanating from the muscle tissue of interest near the detection surface will be dissimilar at each detection surface because of the localized electrochemical events occurring in the contracting muscle fibers, whereas "ac noise" signals originating from a more distance source and "dc noise" signals will be detected with an essentially similar amplitude at both detection surfaces. Therefore, they will be subtracted, but not necessarily nullified prior to being amplified.

2.4 Guidelines for setup and detection

The setup of the EMG acquisition system greatly influences the properties and the quality of the recorded signal. For this reason, the European Union and its Biomedical Health and Research Program (BIOMED II) have attempted to give some guidelines and to initiate a standardization process. The SENIAM project (surface EMG for non-invasive assessment of muscles) [34] provides some recommendations for the SEMG (Surface Electromyography) sensors geometry and construction, and for their placement.

SEMG sensors:

- *Electrode size*: it is defined as the size of the conductive area of a SEMG electrode, and has a significant influence on the recorded EMG. Upon an increase of the size in the direction of the muscle fibers, it can be shown that it has an integrative effect on the SEMG signal,increasing the detected amplitude and decreasing the high frequency contents. Circular electrodes with a diameter of 10mm are preferred most. For bipolar sensors the size of electrodes should be large enough to be able to record a reasonable pool of motor units, but small enough to avoid cross-talk from other muscles. It is recommended the use of bipolar sensors only with a maximum size of 10mm in the direction of the muscle fibers.
- *Intel electrode distance*: it is defined as the centre to centre distance between the conductive areas of two bipolar electrodes. It is recommended to apply the bipolar SEMG electrodes around the sensor location with an inter electrode distance of 20mm. When bipolar electrodes are being applied on relatively small muscles the inter electrode distance should not exceed 1/4 of the muscle fiber length. In this way unstable recordings, due to tendon and motor endplate effects can be avoided.

- *Electrode material*: the electrode material which forms the contact layer with the skin needs to create a good electrode skin contact, a low electrode-skin impedance and a 'stable' behavior in time (that is with respect to impedance and chemical reactions at the skin interface). It is recommended to use pre-gelled Ag/AgCl electrodes.
- *Sensor construction*: it is defined as the (mechanical) construction which is used to integrate the electrodes, the cables and (if applicable) the pre-amplifier. It is expected that the construction (and its mass) do not directly affect the SEMG characteristics. It is recommended a construction with fixed inter electrode distance, built from light weight material.A design with fixed inter electrode distance and using lightweight materials is recommended. Cables need to be fixed using (double sided) tape or elastic band in such a manner that pulling artifacts coming from pulling or from relative motion between sensor and skin can be avoided.

Sensor placement:

- *Preparation of the skin*: a good electrode-skin contact is important to obtain better SEMG-recordings (in terms of amplitude characteristics), fewer and smaller artefacts (electrical interference), less risk of imbalance between electrodes (smaller common mode disturbance signal) and less noise (better S/N ratio). It is recommended to shave the patient if the skin surface at which the electrodes have to be placed is covered with hair and, after that, to clean the skin with alcohol and allow the alcohol to vaporize so that the skin will be dry before the electrodes are placed.
- *Sensor location*: it is defined as the position of the center of 2 bipolar electrodes on the muscle. The location for the sensors is specific for individual muscles but it has to be based on two general recommendations: with respect to the longitudinal location of the sensor on the muscle, the sensor has to be placed halfway between the (most) distal motor endplate zone and the distal tendon.

With respect to the transversal location of the sensor on the muscle, the sensor has to be placed at the surface away from the 'edge' with other subdivisions or muscles so that the geometrical distance of the muscle to these subdivisions and other muscles is maximized.

- *Placement and fixation of the sensor*: when placing and fixing electrodes, the inter electrode distance, the orientation, the fixation method and the location of the reference electrode have to be chosen. Electrode orientation is defined as the orientation of the line between the 2 bipolar electrodes with respect to the direction of the muscle fibres; it is recommended that the bipolar SEMG electrodes should be placed around the recommended sensor location with the orientation parallel to the muscle fibers. It is recommended to use elastic band or (double sided) tape/rings for the fixation of the electrodes(construction) and cables to the skin in such a way that the electrodes are properly fixed to the skin, movement is not hindered and cables are not pulling the electrodes. Regarding the reference electrode, it need to be placed on electrical inactive tissue as the wrist or the ankle.
- *Testing of the connection*: it is recommended to perform a clinical test for each individual muscle. These tests are generally accepted muscle tests which guarantee (under normal circumstances) activity of the tested muscle, they are not 'selective' contractions in which only the desired muscle is active and all other muscles are inactive.

2.5 Experimental EMG setup

During our first training trials we used MA-411-003 active bipolar electrodes commercialized by Motion Lab System (see figure 2.1). They have two 12mm disks which function as sensor contacts and have a fixed inter electrode distance of 17 mm. In addition, there is a 13mm $\times$ 3mm bar as reference contact. Disks and reference contact are all made of Medical Grade Stainless Steel. Sensor contacts, reference bar and pre-amplifier are all enclosed in a rigid plastic case with a total body size of 38mm $\times$ 19mm $\times$ 8mm.

The electrodes are attached to the skin by using hypoallergenic tape. The main issue of this kind of electrodes was skin motion on the detection surface, especially in the recorded signals of the shoulder (Anterior Deltoid); moreover the setup was very long and complex and required frequent adjustments throughout the recording sessions due to electrode detachment.

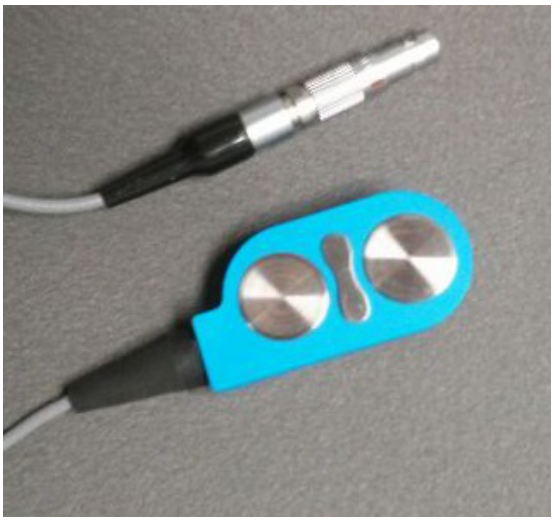

Figure 2.1: Active surface EMG electrode in bipolar configuration from Motion Lab System, model MA-411-003.

For these reasons these electrodes have been replaced with the MA-420-003 EMG preamplifier (figure 2.2) with the following features and specifications:

- Use disposable gel electrodes that can be applied to any muscle;

- The completely design works well under the most active situations eliminating problems with sweat and moisture on the skin surface;

- Gel electrodes are flexible enough to adapt to the shape of all measured muscles;

- Direct EMG pre-amplification close to the signal source provides the highest myoelectric signal quality for accurate, reliable EMG signal detection and reduces cable motion artifact from long signal cables;

- Internal RFI and ESD protection prevents radio frequency interference and static damage;

- The low-impedance output of the preamplifier eliminates cable noise and cable motion artifacts without requiring any additional signal processing within the preamplifier;

- An integral ground reference plane within the preamplifier provides immunity to electromagnetic environmental noise;

- All signal and power conductors in the preamplifier cable are enclosed inside an independent, isolated shield to eliminate interference from AC powerlines and other sources of interference;

- All subject contacts are via disposable gel electrode using standard snap electrodes;

- Moisture Proof construction using bio compatible housing materials to prevent allergic reactions;

- The sensor contacts are two standard snap connectors and the body size of the preamplifier is 25mm $\times$ 16mm $\times$ 10mm;

- Gain at 1kHz $\times$20 $\pm$1%;

- Input impedace $>$ 100000000 Ω;

- Noise $<$ 1,2 μV RMS;

- Signal Bandwidth - 10Hz to 2000Hz (-3dB).

The disposable gel electrodes are NOROTRODE 20 Bipolar SEMG Electrodes sold by Myotronics, INC.: they are silver-silver chloride electrodes for surface EMG applications. Contact surfaces are pre-jelled with hypoallergenic jel that is water soluble gel, mounted on hypoallergenic adhesive and have silver snap connectors. The distance between the two detected surfaces is 22mm, the diameter of the gel areas is 14mm and the one of the snaps is 10mm (figure 2.3).

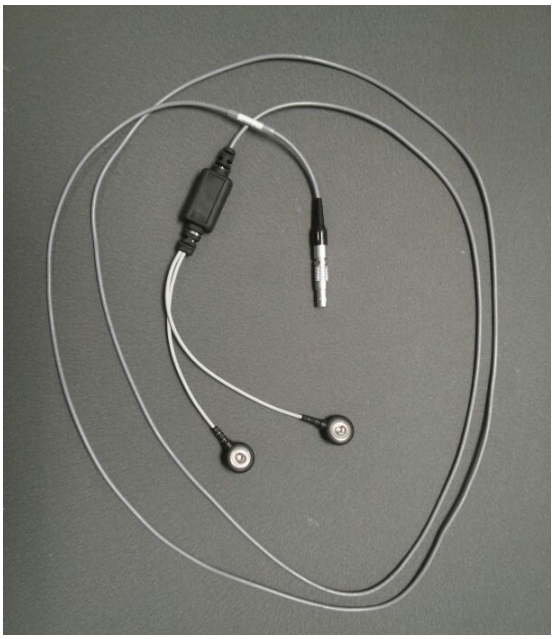

Figure 2.2: Preamplifier that uses disposable gel electrodes, it incorporates radio frequency interference (RFI) filters and electrostatic discharge (ESD) protection circuitry.

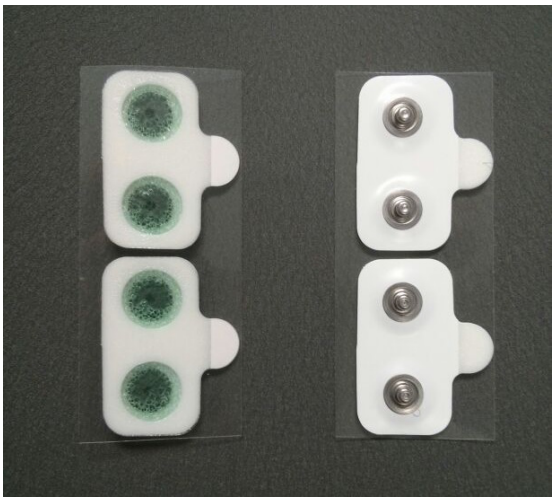

Figure 2.3: Norotrode Bipolar disposable electrodes for surface electromyography (SEMG). They have offset potential Max. 3.0 millivolt and Typ. 1.0 millivolt, impedance at 10Hz Max. 100 Ω and inter electrode spacing of 22$\pm$1mm.

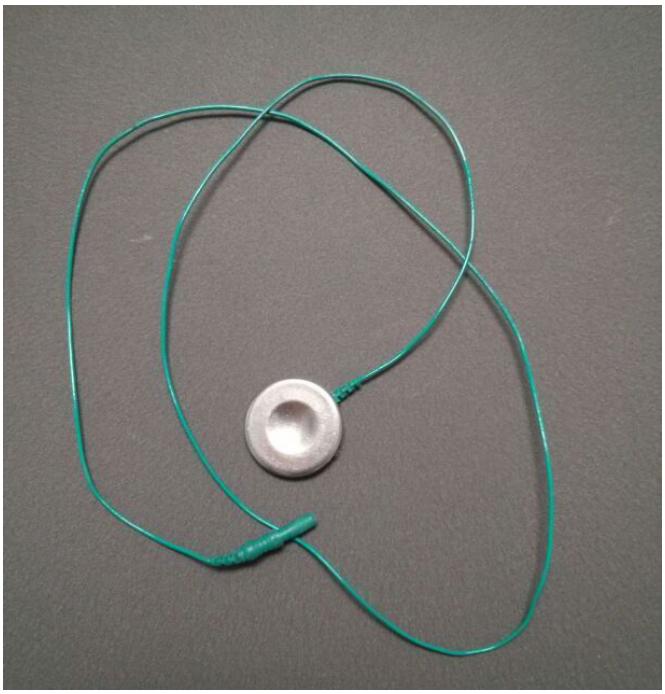

Figure 2.4: The ground electrode is crucial because it greatly reduces the background noise. It has to be placed on a body area in which there is a minimum thickness between the skin and the underlying bone.

The preamplifier cables are connected to the Motion Lab System EMG system backpack (see chapter 3) that offers 16 EMG channels and one for the ground electrode (figure 2.4), an individual gain control and signal level indicator for each EMG channel.

Chapter 3

Instrumentation and data acquisition

Data acquisitions were performed in the Upper Extremity Motor Function Laboratory at the Departement of Health Science and Research, College of Health Profession building C, of the Medical University of South Carolina, Charleston, SC, United States.

In order to run the clinical trials, it was necessary to get the approval of the IRB (Institutional Review Board), which assesses if the tests to be run are ethically acceptable and verifies that neither physical nor psychological harms will occur to the research subjects. This required to hand in various documents, including a detailed description of the study, the expected benefits and the risks, and the test protocol. Furthermore, before running a data collection, each subject was asked to read and sign a consent form containing an explanation of the study, of the type of collected data, of the information used for the study and for future publications and of the risk of disclosure of personal data.

The goal of this research is to study muscle coordination of the proximal upper limb and the shoulder during reaching tasks. As muscle modules define groups of muscles that activate together, we chose this approach to look at recurring patterns in muscle activation within the same subject and among different subjects.

For this purpose we recorded electromyographic activity of several muscles of the upper extremity and the shoulder. In addition, kinematics of the upper half of the body were collected through a motion capture system.

3.1 Instrumentation

The instrumentation in the Upper Extremity Motor Function Laboratory consists of various subsystems, which will be explained in detail in the next sections. The two most important systems are the EMG acquisition instrumentation, produced by Motion Lab Systems Inc., and a motion capture equipment developed by PhaseSpace Inc. These two instruments can work completely independently from each other, but for the purpose of this study kinematics and EMG data had to be precisely synchronized. This was achieved by using the OBSIS system integration software, developed by Orbis Inc., responsible for managing and synchronizing all the subsystems in the laboratory. In addition to the management of the data collection, the software provides tools for post-processing and data management.

3.1.1 300-XVI EMG system

The MA300-XVI Electromyography system produced by Motion Lab Systems is intended for use in the investigation of the physiological process involved in muscle contraction and can be used to record up to 16 EMG channels. It enables the user to observe the electromyographic signals that are produced when muscles activate, while maintaining the electrical isolation of the subject from any measuring or recording equipment that is attached to the system. The MA300 system consists of three main components:

- Electrodes and preamplifier cables attached to each measured muscle (see section 2.5);
- A backpack unit with connection ports for each EMG channel;
- A desktop unit connected to the backpack and responsible for providing power and for reading in all EMG channels.

Backpack The backpack is attached to the subject which during this study was accomplished by applying it to a Velcro belt at the subject's waist. The MA300-XVI system supports 16 EMG channels (figure 3.1 (a)) and features an adjustable gain switch for each channel that can be set to ten different values (see table 3.1). This guarantees that the MA300 EMG System has a precise gain setting at all times while allowing the user complete control of the output signal levels.

Gain switch	System gain	Maximum input level
0	350	$\pm 14,0mV$
1	2000	$\pm 2,50mV$
2	4000	$\pm 1,25mV$
3	5700	$\pm 875\mu V$
4	8000	$\pm 625\mu V$
5	9500	$\pm 525\mu V$
6	11500	$\pm 435\mu V$
7	13200	$\pm 375\mu V$
8	16600	$\pm 300\mu V$
9	18000	$\pm 275\mu V$

Table 3.1: Gain values to which it is possible to set the EMG channels to obtain a signal output between $\pm 5V$.

After reading in and amplifying the EMG signals, each channel runs into an AD converter with an input range of $\pm 5V$. It is important to set each gain properly, so that no analog signal is clipped during the digitalization. A blue LED next to the gain setting of each channel lights up every time its associated EMG input is within 5% of its maximum operating level, helping the user in preventing the collection of faulty data.

The backpack is connected to the desktop unit through a single multipolar cable, which carries both low-level DC power from and transmits the digital EMG data to the desktop unit. By digitizing all signals close to the subject, the MA300 guarantees a clean signal without any degradation and with a low noise level. The desktop interface samples each EMG channel at a rate of 5000Hz.

The backpack contains an adjustable anti-alias filter that allows to set the maximum EMG frequency that will be processed to avoid the possibility of recording signal aliasing errors. It passes all frequencies lower than the value selected and attenuate all analog signal components higher than the chosen value. The variable anti-alias filter provides seven different settings and is controlled by a rotary switch on the backpack unit. The choice of the filter frequency depends on the sampling rate of the customer-provided data collection system. According to the Nyquist theorem, the sampling rate must be at least twice as high as the highest frequency content of the signal.

The inclusion of high quality Bessel anti-alias filters for each EMG channel in the MA300 systems allows raw signals to be recorded at the full bandwidth of the analog recording system (see table 3.2). In our acquisition the filter is set to 4 with an EMG bandwidth of 1000Hz and a minimum sample rate of 2000 s/s.

The backpack also includes a recessed test button at the bottom of the backpack that allows to test each of the EMG channels by applying a 78Hz sine wave signal to all of the EMG channels. A single green power light on the front of the backpack indicates that the unit is receiving DC power from the desktop unit. The coaxial connector to the desktop interface cable is on the left side of the bottom of the unit while a green indifferent (or ground reference) connector is located on the bottom right side. This is a standard "TouchProof" DIN 42-802 connector that can be used to connect a ground reference electrode to the system that meets the performance standard for Electrode Lead Wires and Patient Cables, in Title 21 Code of Federal Regulations (CFR), part 898.

Filter switch	EMG bandwidth	Minimum sample rate
0	2000 Hz	4000 s/s
1	1750 Hz	3500 s/s
2	1500 Hz	3000 s/s
3	1250 Hz	2500 s/s
4	1000 Hz	2000 s/s
5	750 Hz	1500 s/s
6	500 Hz	1000 s/s
7	350 Hz	700 s/s

Table 3.2: Different setting of the anti-alias filter. The high quality Bessel anti-alias filters for each EMG channel allows raw signals to be recorded at the full bandwidth of analog recording system.

(a) (b)

Figure 3.1: The Motion Lab System MA300-XVI: the backpack (a) and the desk-top interface unit (b).

Desktop interface unit The desktop unit contains the isolated electrical interface to the subject unit. It supplies isolated, low-level, DC power to the backpack unit and converts the digitized EMG signals to analog signals suitable for connection to any data collection system (figure 3.1 (b)). Front panel status lights show the DC power status and provide fault detection (No Signal) plus an indication of signal quality (the CRC light).

The analog signals coming from the desktop unit are then read through a National Instruments PCI-6225 multifunction data acquisition card and sampled at 2000Hz. The DAQ card has the following specifications:

Form Factor	PCI
Measurement type	Quadrature encoder, Digital, Voltage, Frequency
Analog input channels	80 single-ended, 40 differential
ADC resolution	16 bits
Analog sample rate	250 kS/s
Max voltage range	$\pm 10V$
Analog output channels	two 16 bit channels updated at 833 kS/s
Digital I/O	24 bidirectional channels
Counters/Timers	two 32 bit counters, max frequency of 80MHz

Table 3.3: Specifications of the NI PCI-6225 multifunction data acquisition card.

3.1.2 PhaseSpace

The PhaseSpace Impulse system is able to capture motion in real time using an LED-tracking technology. Motion capture is accomplished by placing several PhaseSpace cameras around the capture volume, and moving objects with LEDs attached to them. The information coming from all cameras is transmitted to a central computer that processes the data and calculates the position of each marker. These positions are then available for further processing by client systems in a client-server environment.

The PhaseSpace system available at the Upper Extremity Motor Function Laboratory consists of:

- 8 cameras
- LED base station
- 2 LED driver units
- Active LEDs
- A HUB into which the cameras and the LED Base Station connect
- A server computer which runs Linux and communicates with the HUB
- A calibration wand that serves as the principal tool to accurately calibrate the system
- Server and client software

The PhaseSpace Impulse system has four primary components. LEDs are affixed to the target at predetermined positions. These LEDs are detected by the cameras, which then transmit data to the HUB. The HUB collates the information from multiple cameras and relays it to the server computer. The server can perform some further processing, like calculating position and orientation of certain pre-programmed objects, and makes the information available to all connected clients in the form of a TCP data stream. In addition, there is a calibration object that is required for camera calibration (mainly the extrinsic parameters).

Cameras : the system uses high-speed, high-resolution linear CCD cameras to triangulate the position of LED markers in real time. Each PhaseSpace camera has two detectors (figure 3.2). Each detector consists of a semi-cylindrical lens and a linear CCD at the focal distance of the lens and perpendicular to the axis of the lens. The cameras can be easily mounted on typical camera tripods or attached to walls or other permanent fixtures. A standard ethernet cable is necessary to connect each camera.

On the front of each camera are two apertures, behind each of which are the lens assembly and the CCD detector. On the side of each camera are two ethernet ports that are used to connect the camera to the HUB. Each camera achieves an optical resolution of 3600×3600 (12Megapixel) using two linear detectors with 16-bit dynamic range. Onboard processors can produce a subpixel resolution of 30000×30000 at 960Hz.

Figure 3.2: : 8 cameras are mounted to the walls of the Upper Extremity Motor Function Laboratory cameras and placed in a circular configuration with the field of view being in the center of the room.

LED Base Station : it functions as the primary link between the PhaseSpace HUB and the LED system. The base station is connected to the HUB by connecting one end of an ethernet cable to a port on the HUB and connecting the other end of the cable into the ethernet port on the base station. The LED base station has the function of transmitting a timing signal to the LED driver units, and can also be used for programming the LED drivers. The transmission of the timing signal occurs once per frame and happens wirelessly through RF antennae, or directly through a 6-pin connection. The base station also has the capability to drive LED strings independently.

LED Driver Unit : it is the driver of the LED modules (figure 3.3). The unit consists of a battery pack as well as an RF receiver, which receives a timing signal from the LED base station. A total of six LED strings can be connected to the 14-pin connector using a six-wire breakout adaptor or a six-port breakout box.

Figure 3.3: LED Driver Unit: it allows to connect up to six LED strings through the 14-pin connector.

LED string : it consists of the LED cable and the LED cable connectors (figure 3.4 (a)). The LED cable consists of two wires, one of which is colored. The connector has two sockets, one for each wire of the LED cable. A total of six LED strings can be attached to a single 14-pin connector, which connects to the 14-pin LED string port on the LED driver unit. Each LED string is capable of having up to 12 LED modules attached to it using the proper LED connectors. Each LED module on a particular LED string must have a unique LED designation, i.e. two LEDs with the same designation should not be connected to the same string.

LEDs : LED modules contain the actual light sources that are tracked by the PhaseSpace cameras. Along with the light source is a microprocessor that controls the modulation of the LED's pulse duration and amplitude. Each LED has one of 12 LED designations (labeled A through L, figure 3.4 (b)). This designation along with the identifier of the LED driver gives each LED a unique identifier, each LED is modulated at a unique frequency. This unique identification of each marker is one of the big advantages that the PhaseSpace system has with respect to other motion capture systems. In fact, other systems (such as the widespread Vicon system) rely on passive markers. This requires the operator to label each marker during the post-processing phase, which is a very time-consuming process, and can lead to problems when marker drop-out occurs (e.g. when a marker is covered during part of the data collection).

The position of all LED markers can be recorded at various frequencies, ranging from 120Hz to 480Hz. During this study kinematic data was captured at 240Hz.

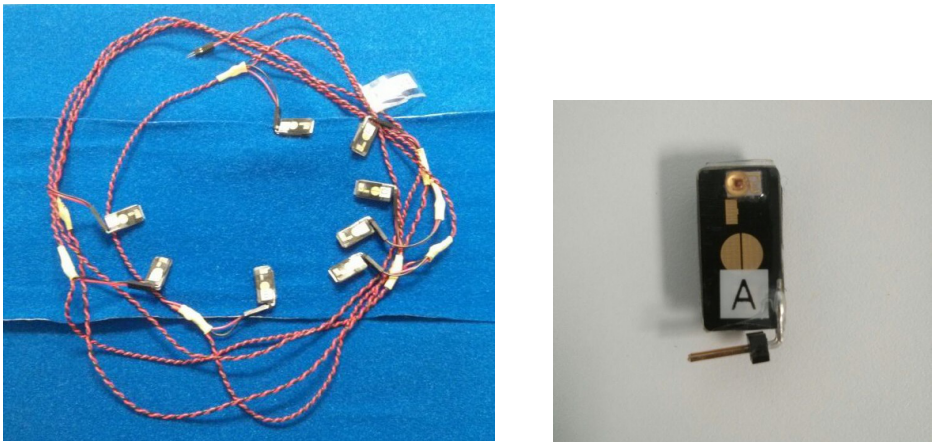

(a) (b)

Figure 3.4: LED string connects 8 LEDs used to track arm and forearm movements (a) and a single LED (b).

3.1.3 OBSIS (Orbis Biomechanical System Integration Suite)

Figure 3.5: Orbis Biomechanical System Integration Suite.

OBSIS is a system integration software package designed to be upgraded in order to incorporate custom and novel measurement equipment, and synchronize the resulting data with PhaseSpace motion capture systems. Because PhaseSpace motion capture systems utilize wireless active markers, OBSIS provides instantaneous biomechanical model preview and immediate data quality analysis in real time. The off-the-shelf OBSIS package synchronizes the data of up to 40 differential analog voltage signals from a National Instruments (NI) USB data acquisition system with the PhaseSpace motion capture system; although the version used for this study was slightly modified to use the NI PCI-6225 DAQ card.

EMG data : the number of collected channels depends solely on the properties of the EMG acquisition system and of the DAQ card. Each channel can be labeled and previewed during the data collection. The tools available to the user in the post-processing give the user the possibility to apply various signal-processing techniques and filters.

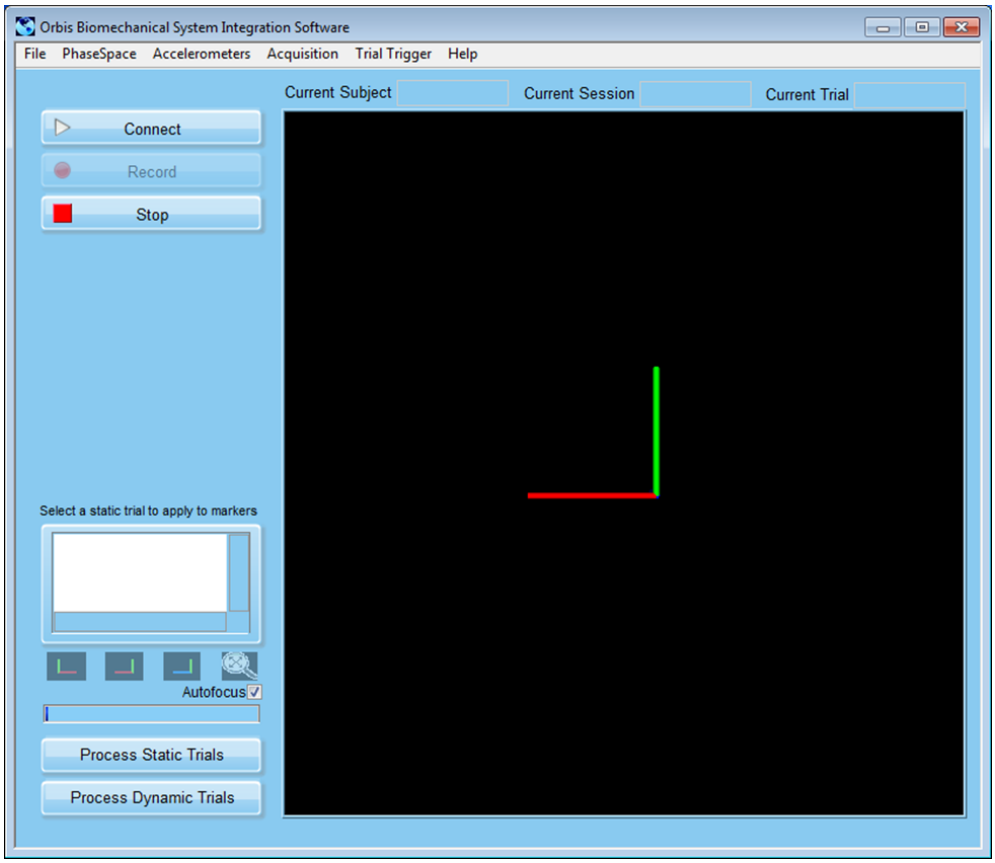

Figure 3.6: OBSIS main window.

Force plate data : the analog signals coming from force plates can be collected synchronously with EMG and kinematic data. Various filters can be applied to process the recorded forces at the end of the collection.

Kinematic data : besides logging the raw marker position coming from the PhaseSpace system, OBSIS allows to define a kinematic model of the subject (which can also be only a partial model, e.g. only the upper half of the body). This requires the user to record a static trial at the beginning of the data collection, which is then used to fit the kinematic model to the subject-specific marker positions. After this step is completed, the software can compute the position and orientation of different segments of the body, such as trunk, head, humerus, forearm, hand, etc.

Using these locations, the OBSIS calculates inverse kinematics and provides the user with information such as joint angles, joint angular velocities and angular accelerations. The kinematic model can be customized in order to modify the tracked segments, the respective reference frames and the definition of the joint angles. In the post-processing phase, the user can use kinematic data to define specific phases of the movement. For example, in this study we used the magnitude of the wrist velocity to identify movement onset and end times. These events can then be used to identify only the important chunks of EMG and force plate data, and to associate them with a specific phase of the movement.

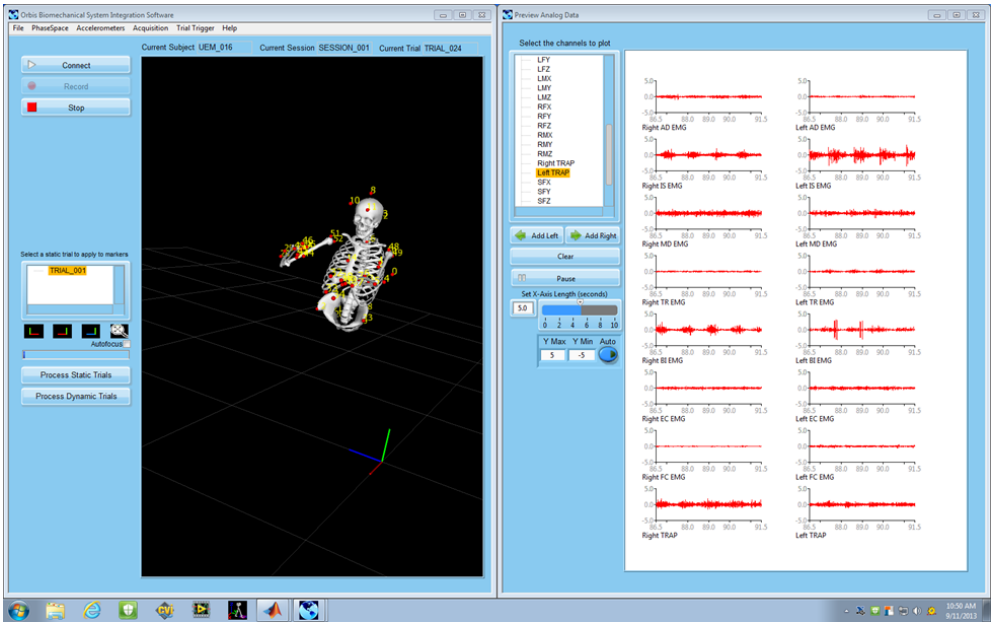

Figure 3.7: OBSIS preview of the kinematic model (left) and of the recorded EMG data (right)

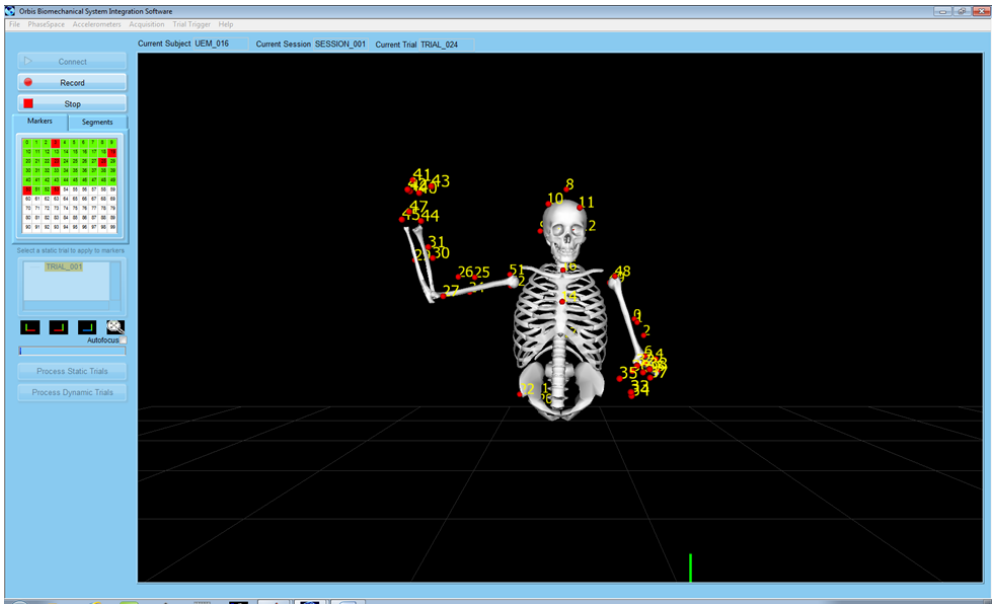

Figure 3.8: Recording of a trial. The preview window provides a 3D view of all tracked markers and of the kinematic model. The box in the left upper section of the window provides information on each marker: green squares indicate that the respective marker is visible by the system, while red squares signal that the marker cannot be located by the PhaseSpace system

3.2 Data acquisition

Participants in this study included 15 healthy adults (9 males and 6 females, age: 47,8 ± 15,9 years, see table 3.4), selected according to age and gender in order to have a sample that could be compared to the stroke population. Furthermore the study includes 15 hemiparetic patients, even though this thesis will focus only on the first 5 (3 males and 2 females, age: 66,11 ± 7,9 years, see table 3.5). Every subject provided informed consent in accordance with the Declaration of Helsinki. Stroke patients were asked to undergo some clinical assessments (Fugl-Meyer Assessment, Activity Card Sort, Stroke Impact Scale) to evaluate their motor behavior and to have a preliminary idea of the level of impairment of the hemiparetic arm. The motor ability of all stroke subjects ranged from mildly to moderately impaired.

The first part of the data collection consisted of a setup phase, which took about 45 minutes on average. The subjects were asked to sit on a bench placed in the center of the room, which was adjusted to their height. After cleaning the skin with alcohol, surface EMG electrodes were applied to muscles of the proximal upper extremity or trunk in accordance with standardized SENIAM procedures: activity of 16 muscles was acquired through the multi-channel surface EMG system and sampled at 2 kHz. Electrodes were placed at 8 muscles per side (table 3.6):

- Anterior deltoid(AD)
- Infraspinatus(IS)
- Middle deltoid(MD)
- Triceps(TR)
- Biceps(BI)
- Serratus anterior(SA)
- Pectoralis major(PM)
- Trapezius(TP).

Subject	Age	Gender	Dominant side
UBC_001	22,76	F	R
UBC_002	30,87	F	R
UBC_003	77,05	M	R
UBC_004	56,81	M	R
UBC_005	56,23	M	R
UBC_006	68,07	M	R
UBC_007	52,74	F	L
UBC_008	59,25	F	L
UBC_009	52,02	M	R
UBC_010	44,95	F	R
UBC_011	20,13	M	R
UBC_013	44,39	M	R
UBC_014	56,93	F	R
UBC_015	47,98	M	L
UBC_016	26,86	M	R

Table 3.4: Clinical data for healthy subjects (subject UBC_012 is not included because his session was aborted for technical problems).

Subject	Age	Gender	Dominant side	Affected side	Time since incident	Impairment
UBH_001	69,67	F	R	R	3,69	mild
UBH_002	61,11	F	R	L	0,86	mild
UBH_003	54,46	M	R	R	0,87	mild
UBH_004	67,38	M	R	R	1,13	moderate
UBH_005	77,82	M	R	R	6,11	moderate

Table 3.5: Clinical data for stroke patients.

Channel	Side	Muscles
1	Right	Anterior deltoid
2	Left	Anterior deltoid
3	Right	Infraspinatus
4	Left	Infraspinatus
5	Right	Middle deltoid
6	Left	Middle deltoid
7	Right	Triceps
8	Left	Triceps
9	Right	Biceps
10	Left	Biceps
11	Right	Serratus anterior
12	Left	Serratus anterior
13	Right	Pectoralis major
14	Left	Pectoralis major
15	Right	Trapezius
16	Left	Trapezius

Table 3.6: Each EMG cable is connected to a specific channel of the backpack: the odd channels are connected the right side of the body, the even channels the left side.

After connecting the cables to the EMG backpack, the gains needed to be adjust: the subjects were asked to contract the recorded muscles one at a time by performing specific movements, and in the meantime the signal of each muscle was displayed on a monitor (figure 3.9). The gain of the selected muscle was turned up or down from 0 to 9 in order to have an adequate amplitude of the signal without seeing clipping phenomena.

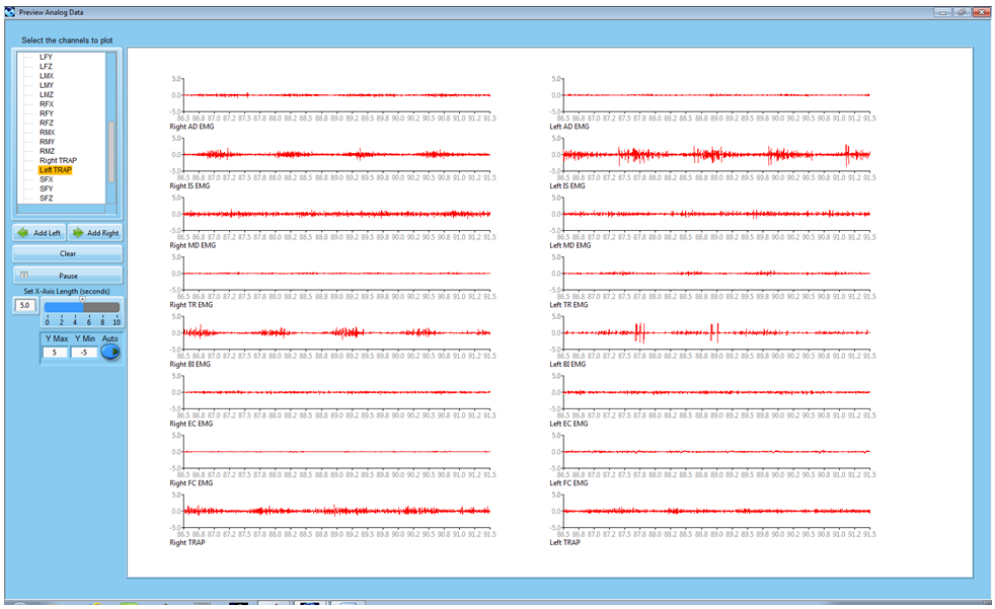

Figure 3.9: Obsis interface showing the EMG signals, on the left side of the display there are the muscles of the right side of the body and on the right side of the display the muscles of the left side of the body. During the setup procedure it was necessary to adjust the gains of each channel, and by looking at this graphics it was possible to understand if the signal of a specific muscle (during contraction) was in the range of ± 5V.

The next step was the placement of the PhaseSpace markers. Kinematic data was recorded with a 8-camera motion analysis system using 54 active markers sampled at 240Hz. The tracked body segments are head, pelvis, trunk, scapula, arm, forearm, hand and fingers. Each marker was placed in a pre-determined position (table 3.7) using velcro tape and velcro straps (markers of the scapula were placed on an appropriate rigid support).

ID	LED string	Position	Cluster
0 A	left arm	arm	arm
1 B			
2 C			
3 D		medial epicondyle	elbow
4 E		lateral epicondyle	
5 F		forearm	forearm
6 G			
7 H			
8 A	head	top of the head	head
9 B		back of the head	
10 C		forehead	
11 D		forehead	
12 E		back of the head	
13 F		not used	-
14 G		sternum	trunk
15 H		not used	-
16 A	pelvis	cervical v. (C7)	trunk
17 B		thorax v. (T12)	trunk
18 C		back of the pelvis	pelvis
19 D			
20 E			
21 F			
22 G		front of the pelvis	
23 H			
24 A	right arm	arm	arm
25 B			
26 C			

ID	LED string	Position	Cluster
27 D	right arm	medial epicondyle	elbow
28 E		lateral epicondyle	
29 F		forearm	forearm
30 G			
31 H			
32 E	left hand	index knuckle	fingers
33 F		index nail	
34 G		middle nail	
35 H		thumb nail	
36 I		radial styloid	wrist
37 J		ulnar styloid	
38 K		middle knuckle	fingers
39 L		back of the hand	wrist
40 E	right hand	index knuckle	fingers
41 F		index nail	
42 G		middle nail	
43 H		thumb nail	
44 I		radial styloid	wrist
45 J		ulnar styloid	
46 K		middle knuckle	fingers
47 L		back of the hand	wrist
48 E	scapula	left scapula	left scapula
49 F			
50 G			
51 H		right scapula	right scapula
52 I			
53 J			

Table 3.7: Marker set used during the data acquisition. Seven LED strings were used to track the body segments. Each LED has a specific ID that consists of a number ad a label (a letter) for each LED string.

Before starting the recording of the reaching tasks it was necessary to take a static trial of the subject. This required the subjects to move to a position where all markers were visible by the PhaseSpace system and to maintain this position for a few seconds. This static trial was used to fit the kinematic model to the subject a and to adapt it to the subject's anatomy (figure 3.10).

After the setup phase we could proceed to the actual data collection. The test consisted of 6 different tasks, which were designed so as to cover a wide variety of movements in the subject's workspace.

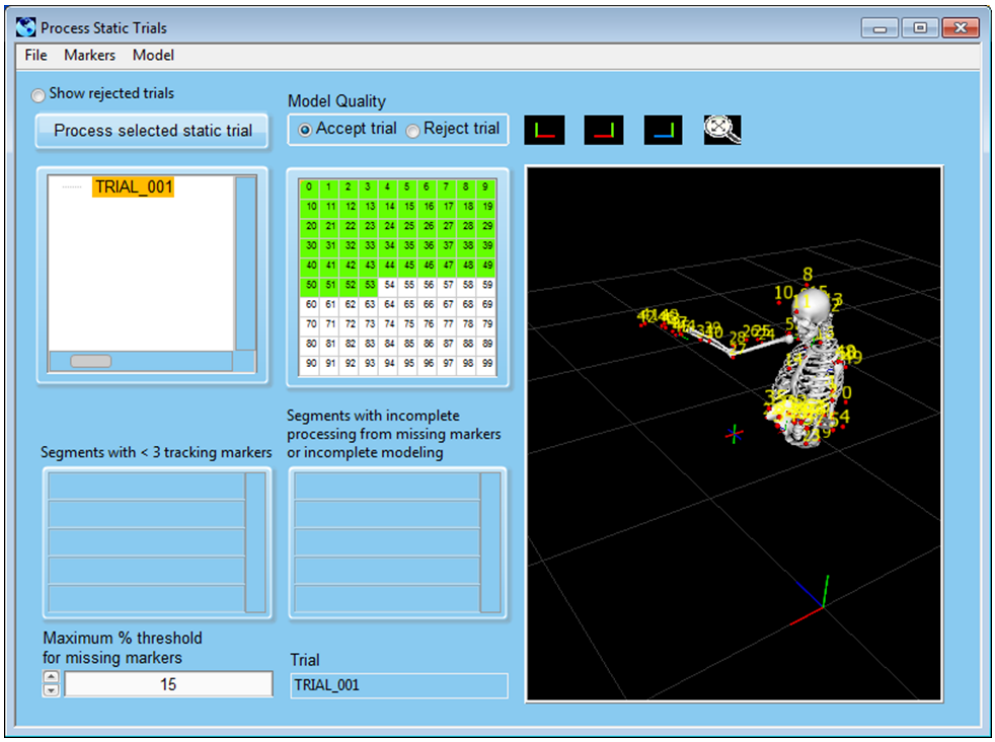

Figure 3.10: OBSIS interface allows to select the recorded static trial. The green lights represent the markers: all the markers were visible at least during more than 85% of the acquisition time. In this case the trial can be accepted for applying the model (otherwise it will be rejected): the skeleton represents the model adapted to the subject and the markers are visible directly on the skeleton (the numbers represent the marker IDs). Every movement of the subject will correspond to a movement of the skeleton and is displayed in real time.

This is one of the main novelties of this study, as previous work mostly focuses on a single task or on a more limited set of movements. The reason for this wide variety of tasks is that we wanted to find coordination patterns that could explain motor control of the upper extremity in many different situations, and not just for a very specific task. As a matter of fact, motor modules extracted from a single task could be biased by the constraints introduced by that task, and might not provide useful information about motor control.

Each task, except for the last, was repeated 6 times with both left and right arm. This is not a random number, preliminary tests revealed that 6 repetitions are good to obtain a meaningful average and, if necessary, allows to reject one bad repetition. Furthermore, 6 repetitions is a good compromise between statistical significance and subject effort. For each task, subjects were asked to perform movements as fast as possible.

The tasks will be described below. The subject was sitting on a bench with the hands positioned near the legs resting on the bench or, for tasks 4 and 5, with the hands on a table in front of them.

Task 1 (MD) : the subjects had to reach towards different heights (90°, 100° and 110° of shoulder elevation) and in three different directions (45°, 90° and 120° of horizontal shoulder adduction). Each target was positioned at a distance of 90% of the subject arm length from his acromion. The targets were green LEDs which turned on one at a time in a random sequence. When the first LED lit up the subject had to reach as fast as possible towards the target, hold the position until the LED went off and reach as fast as possible back to the starting position (hand on the seating plane). When the hand was at the starting position the next LED lit up and the subject had to perform the next reach. The status of the LEDs was regulated by the velocity of a hand marker and not by the position of the hand, so that the task was adaptable to the motor abilities of all subjects, even to those not able to reach completely to the target. Before starting the trial, 5 test movements were performed to allow the subject to familiarize with the system.

Task 2 (FF) : movements began and ended with hand on the seating plane. Subjects were asked to bring their fingers to the forehead, hold the position for a second and go back to the starting position as fast as possible and repeat this for 6 times.

Task 3 (GR) : the subjects had to grasp a rope positioned on the coronal plane on the tested side; the grasping height corresponded to a shoulder elevation

of 110°. The subjects had to reach for 6 times as fast as possible to the marked height, grasp the rope, pause and go back to the initial position.

Task 4 (BB1) : for this task and the following an adjustable table was placed in front of the subjects. This task consisted in moving bean bags along the sagittal plane by bringing them from the table to a basket in the back on the tested side, starting with the hand in the back over the basket. The bean bags were placed on the table, one at a time, at a distance of 90% of the arm length from the sternum.

Task 5 (BB2) : the subjects had to move bean bags performing a horizontal adduction/abduction of the arm, starting with the hand leaning on the table. If the task was performed with the right hand, the subjects had to bring the bag from the left side of the table to the right side, stop for a moment, go back to the left to pick the next bag. The sequence was repeated 6 times and all movement were performed as fast as possible.

Task 6 : a hand cycle was positioned on the table in front of the subjects. The distance was chosen in order to reach 90% of the arm length at maximum extension and the center of rotation was about at shoulder height. The hand cycle had a break which was adjusted such that it provided a low level of resistance, but still high enough to avoid free spinning. The subjects were asked to cycle for about 20 seconds at a constant speed of 50rpm, and only the best 5 cycles were chosen.

Chapter 4

Processing of EMG data

Compared to movement kinematics, muscle coordination and muscle force generation, the frequency content of EMG signals is higher by at least one order of magnitude. It is therefore common practice to perform a number of processing steps in order to get, from the raw EMG data to a low-frequency, signal that still represents muscle activity, but is easier to read and to relate to movement kinematics. Furthermore, since data is usually collected for a longer time than the actual duration of a task, it is important to identify the time frame that is relevant to the movement. This requires the selection of the time instant of movement onset and of movement end; all data outside of these two events can be disregarded. This chapter covers the details of how kinematic events were defined and the techniques used for processing EMG signals, and explains how modules were extracted from the processed data.

4.1 Selection of kinematic events

All tasks analyzed in this study have in common that the hand position at the beginning of the task coincides with the end position. Therefore we could detect two different phases:

- *Reaching movement*: the part of the task where the subject brings the hand from the starting position to the target position.

- *Return movement*: the part of the task where the subject moves the hand from the target position back to the start position.

The implicit assumption when separating the task into two distinct movements is that muscle coordination might be different between reach and return.

The events relative to the two movements were defined by looking at the kinematic data of the wrist. More specifically, we looked at the velocity magnitude of one of the three wrist markers (due to marker drop out we could not always use the same one). The time of movement onset was defined as the instant in which the marker velocity increased over 5% of the maximum velocity, while the time of movement end corresponded to the instant in which the velocity decreased under 5% of the maximum value. These steps were performed using the processing tools provided by OBSIS (figures 4.1, 4.2 and 4.3).

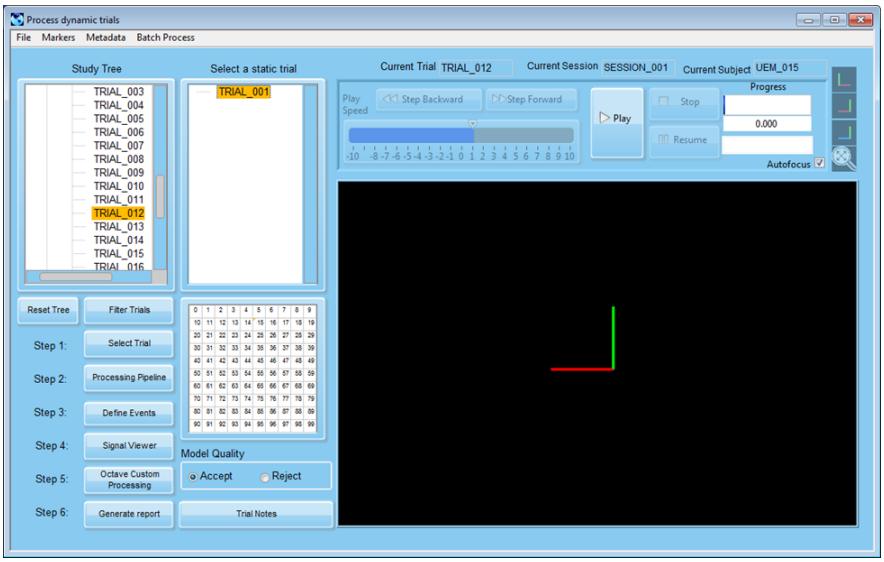

Figure 4.1: For each subject OBSIS allows to select the trial for which events have to be defined.

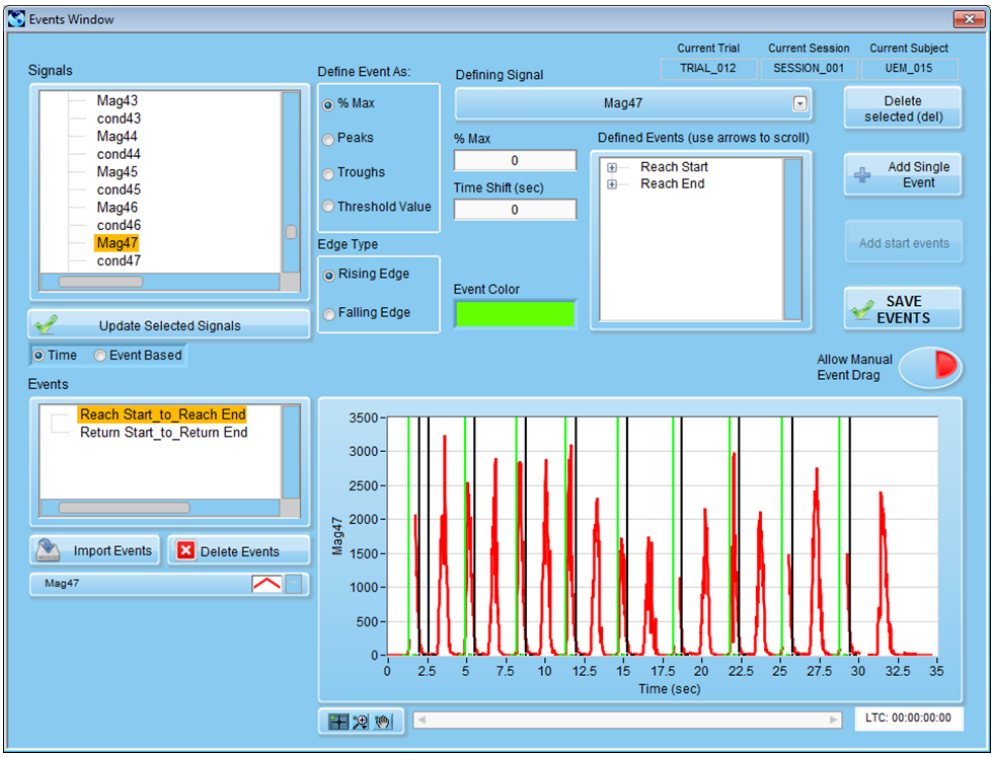

Figure 4.2: This interface allows to define the events. The operator can choose the kinematic variable (x,y,z position, velocity, acceleration) which will be used to define the events. For this study we used the velocity magnitude of one of the three wrist markers. The following parameters can be set: the ID of the marker that will be visualized in the plot; the type of edge (rising for movement start, falling for movement end); the threshold value to define each event, usually at 5% of the maximum velocity; the type of event (reach start, reach end, return start, return end); the color used to identify the edges in the plot. In the plot: in red the velocity magnitude of marker 47 (back of the right hand). Green edges identified reaching start events, black ones reaching end events.

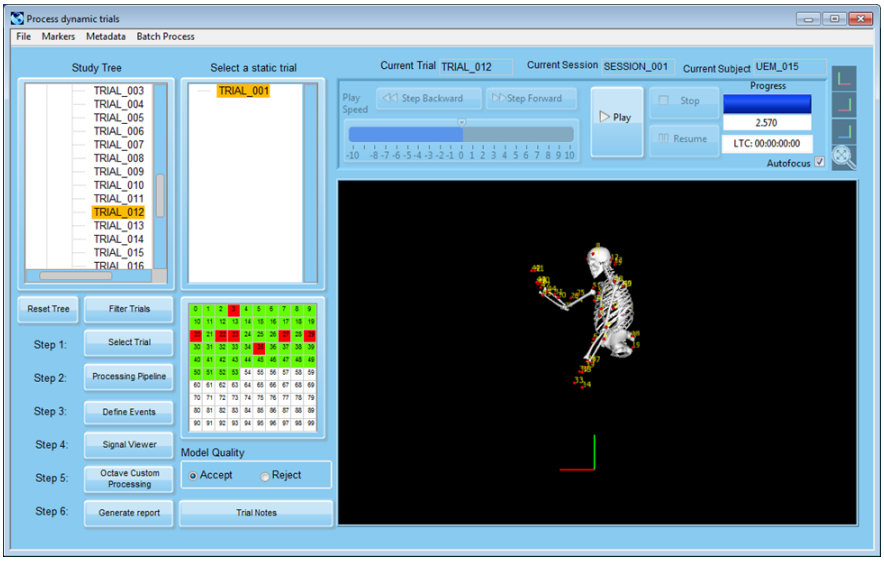

Figure 4.3: During the definition of the events it is possible to replay the recorded trial: the skeleton model is displayed and repeats exactly the movements performed by the subject during the acquisition. This feature is useful when it is hard to identify the events by just looking at hand velocity profile.

4.2 EMG post-processing

The purpose of the following steps is to start from the high-frequency raw EMG signal and to obtain a so called linear envelope for each EMG channel, i.e. a low-frequency signal whose amplitude represents how much a muscle is active.

The first step is to remove artifacts introduced by the heartbeat. In fact, heartbeat can have a significant impact on certain EMG channels, especially on those of the left-hand side of the subject's trunk (e.g. pectoralis major, see figure 4.4 (a)). A common technique found in literature to remove this artifact is to high pass filter the raw EMG sighal at around 30Hz. We used a high-pass 4^{th} order Butterworth filter with zero lag and with a 30Hz cutoff frequency.

The next step consists in demeaning and rectifying the signal: its average is subtracted from the signal and the absolute value (full way rectify) is applied to it to have only positive values (figure 4.4 (c)).

After applying these first three processing techniques, the signal still has a high frequency content. In order to obtain the linear envelope of each EMG channel, we applied a zero-lag 4^{th} order low-pass Butterworth filter with a cutoff frequency of approximately 5Hz. The actual value of the filter frequency was chosen on a case by case basis so as to adapt it to the speed with which the subject executed the movement (figure 4.4 (d)). More precisely, we calculated the average duration of all events defined for a specific trial. We then chose the frequency as a function of this average duration, in order to filter all signal features that lasted less than one third of the length of the movement. Having a variable cutoff frequency allowed us to reduce the effect of movement speed on the linear EMG envelopes.

As was explained in chapter 2, the amplitude of the EMG signal depends on the properties of the electrodes and on their placing. It follows that the amplitude of raw data cannot be compared among different EMG channels. In order to accomplish that, each channel has to be normalized with a biomechanically significant value. In preliminary tests we tried to use the maximum voluntary contraction (MVC), but this procedure turned out to be very time consuming. Moreover, it would be difficult (if not impossible) and tiring for stroke patients to contract all tested muscles one at a time.

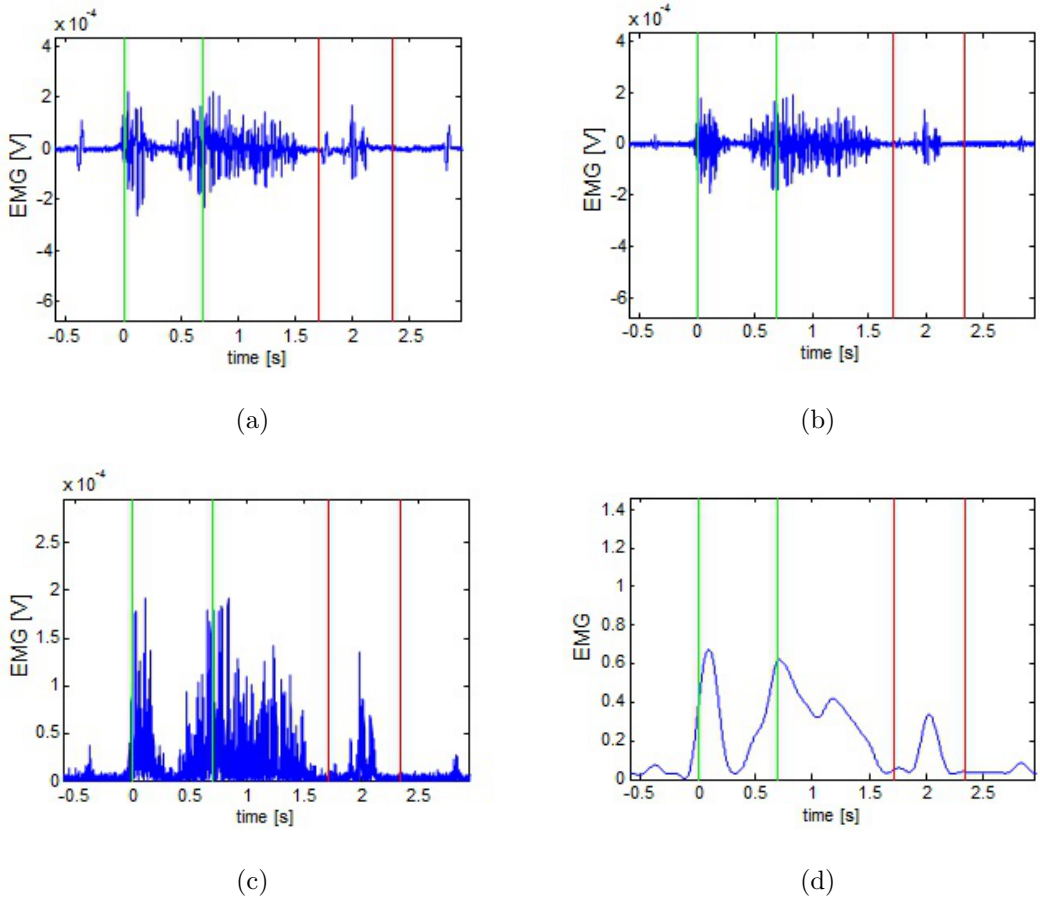

Figure 4.4: EMG data processing. The plots show an example for the three processing steps and represent EMG data of the pectoralis major. The green and red lines identify the reach and return intervals, respectively. (a)The raw EMG data. (b)Data filtered with a Butterworth high-pass filter at 30Hz, effectively removing heartbeat artifacts. (c)Demeaned and rectified signal. (d)EMG signal after filtering with a Butterworth low-pass filter and after normalization.

Therefore we used another method to derive the normalization coefficients for every muscle:

- we took the raw EMG signals of each reach and return movement;
- for each muscle, all 16 EMG channels from all trials were concatenated, demeaned and rectified;
- we measured the average activation of each muscle over a biomechanically significant time interval, i.e. we calculated a moving average over a 90ms window and took its maximum value for each EMG channel. This maximum average activation was then used as a normalization coefficient.

4.3 Extraction of muscle modules

Starting from the hypothesis that the CNS simplifies motor control through a modular organization of muscles, we looked for algorithms that could identify such muscle groups. The underlying idea is to search for common activation patterns among EMG signals, as muscles with similar EMG profiles are likely to be part of the same module.

A simple but powerful model adopted by many authors describes EMG signals as linear combinations of a limited number of activation signals. These so-called activation coefficients could potentially represent the descending neuronal signals that originate in the brain. Each activation coefficient is linked with a module containing all muscles controlled by that signal. Furthermore, each muscle is associated with a weight that determines how much the muscle participates in the overall activity of the module. Due to neuronal interconnectivity muscles might be part of more than one module, and it is not uncommon to find a muscle with non-zero weights in two or more modules. From a mathematical point of view, each weight inside a module represents the multiplicative coefficient associated with an activation coefficient. According to this model, the total EMG activity of a muscle is given by the sum of all activation coefficients, each multiplied by the respective weight.

In order to apply the aforementioned model to the collected EMG data, the recorded channels have to be organized into a $[n \times m]$ matrix V.

Inside this matrix, each of the m columns represents an EMG channel (since we mainly studied unilateral movements, our V matrix had eight columns), and each of the n rows represents a sample. The model can then be written as:

$$V \approx WH \tag{4.1}$$

W is a $[n \times r]$ matrix of activation coefficients (each column represents the activation coefficient of one module) and H is a $[r \times m]$ matrix of modules (each row represents the muscle weightings inside a module). The rank r is chosen to be smaller than m so that the W and H are smaller than the original matrix V. This results in a compressed version of the original data matrix.

There are several algorithms that could be used to obtain such a factorization. These algorithms have been applied to a wide variety of problems, ranging from image processing to text recognition, and they mainly differ from each other in their different constraints imposed on two matrices W and H. Some of the most common factorization algorithms are:

- Principal Component Analysis (PCA)
- Factor Analysis (FA)
- Vector Quantization (VQ)
- Independent Component Analysis (ICA)
- Non-negative Matrix Factorization (NMF)

Many authors sought to assess the performances of these algorithms. Tresh et al. compared PCA, FA, ICA and NMF in extracting motor modules from simulated experimental data sets. Despite the differences in evaluating the basis vectors (modules) and activation coefficients, the similarity of the modules identified by the different algorithms suggests that these analysis do not produce arbitrary fits to the data but capture features underlying muscle activation patterns. The authors suggest that factorization algorithms for the identification of the motor modules are useful tools for examining the organization of motor behaviors [35].

Lee and Seung explained more in detail VQ, PCA and NMF [36]. In VQ each column of H is constrained to be a unary vector, i.e. with only one element equal to one and all others equal to zero.

Therefore every column of V is approximated by a single column of W (the authors use face recognition as an example; here every column of W would represent an eigenface). PCA constrains the columns of W to be orthonormal and the rows of H to be orthogonal to each other. This allows a distributed representation in which each column of V is approximated by a linear combination of all columns of W, but W and H can have an arbitrary sign. NMF does not allow negative entries in the matrix factors W and H. These non-negativity constraints permit the combination of multiple columns of W but only additive combinations are allowed because all the non-zero elements are positive. As muscle activity can only be described by non-negative signals, NMF is the algorithm that is most commonly used to study muscle modules.

4.3.1 Non-negative Matrix Factorization

Given an $[n \times m]$ data matrix V with $V_{ij} \geq 0$ and a pre-determined positive integer $r < min(n, m)$, NMF finds two non-negative matrices $W \in R^{n \times r}$ and $H \in R^{r \times m}$ so that equation 4.1 is satisfied. Since the algorithm cannot automatically detect the number of modules needed to optimally describe the EMG signals, the value of r must be provided manually. The selection of the optimal value of r will be described in the following paragraphs.

Although NMF can be implemented in many different ways, the two most popular methods are the Alternating Least Squares (ALS) technique and the Multiplicative Update Rules.

ALS finds the two non-negative matrices by minimizing the squared error $||V - WH||^2$. At each iteration of the algorithm W and H are updated in two steps: at first the W matrix is held constant and the minimization is implemented by modifying only the H matrix, while in the second step H is held constant and the error is minimized by acting on W. Negative elements in the two matrices are forced to be equal to zero. The advantages of the ALS algorithm are: the elements set to zero in H and W aren't locked, i.e. zero elements at one iteration will not necessarily be equal to zero at the next iteration, only $W^{(0)}$ has to be initialized and in most cases the algorithm converges rapidly to a local minimum.

However non-negativity is not inherent in the algorithm but has to be enforced, and there is no convergence theory.

On the other side, the multiplicative update method acts on both W and H at the same time. It can be shown that this method is a special case of the gradient descend method. Lee ad Seung [37] developed two different update rules, whose main difference is the cost function that is to be optimized. One very important feature of this technique is that, although the two cost functions are convex either in W only or in H only but not in both at the same time, the update rules guarantee convergence at least to a local minimum.

The two cost functions considered by the authors are the Euclidean distance between V and (WH) (4.2) and the divergence of V from (WH) (4.3):

$$\| V - WH \|^2 = \sum_{i,j=1}^{n,m} (V_{ij} - (WH)_{ij})^2 \tag{4.2}$$

$$D(V \parallel WH) = \sum_{i,j=1}^{n,m} (V_{ij} log \frac{V_{ij}}{(WH)_{ij}} - V_{ij} + (WH)_{ij}) \tag{4.3}$$

Both Euclidean distance and divergence are lower bounded by zero, and vanish if and only if $V = WH$. These cost functions can be optimized through specific update rules, but since we chose to use the Euclidean distance, only the update rules for this cost function are shown:

$$H_{bj}^{k+1} \leftarrow H_{bj}^{k} \frac{((W^k)^T V)_{bj}}{((W^k)^T W^k H^k)_{bj}}, \qquad \forall\, b, j \tag{4.4}$$

$$W_{ia}^{k+1} \leftarrow W_{ia}^{k} \frac{(V(H^{k+1})^T)_{ia}}{(W^k H^{k+1} (H^{k+1})^T)_{ia}}, \qquad \forall\, i, a \tag{4.5}$$

The results given by the algorithm depend heavily on the starting values of $W^{(0)}$ and $H^{(0)}$, which are usually initialized with random values. As a consequence, the optimization has to be repeated multiple times, starting from different initial solutions, in order to reach convergence to a good local minimum.

The advantages of the multiplicative update rules are the very easy implementation of the method and the existence of a convergence theory. On the other side, the algorithm converges rather slowly, requires a good initialization of both W and H and locks zero-elements for all the following iterations.

We used Matlab's implementation of the NMF algorithm ('nnmf' function) with the following setting:

- multiplicative update algorithm
- the mean square error of the Euclidean distance as cost function
- 100 iteration (multiplicative updates) to reach convergence
- 500 repetition of the optimization: for each V matrix the algorithm repeats 500 times the extraction changing the $W^{(0)}$ and $H^{(0)}$.

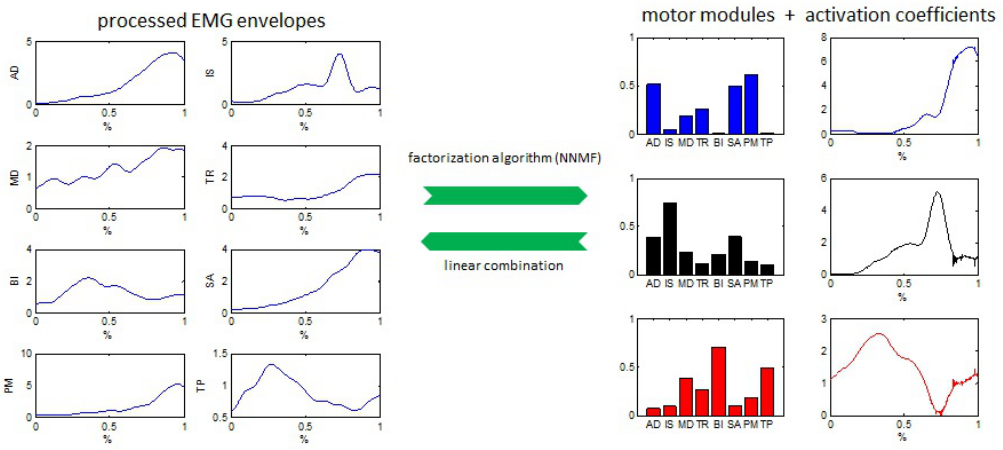

Figure 4.5: Starting from the processed EMG evelopes (on the left) the NMF algorithm extracted three motor modules with their corresponding activation coefficients (on the left). Looking at the activation coefficients we can understand when the corresponding modules are active during the movement: in this case, the third module is active in the first part, the second in the middle and the first module at the end of the movement. A linear combination of motor modules and activation coefficients gives the reconstruct EMG signals.

The rank r represents the number of modules that can be extracted: it can assume value from 1 to m, where m corresponds to the number of recorded muscles. Since we had no a priori knowledge of the correct number of modules, we performed the extraction for each r value in the range from 1 to m.

In a second step we chose the number of modules based on the Variance Accounted For (VAF) between the original EMG (V) and the reconstructed EMG (WH) evaluated for each extraction (all r values):

$$VAF = 1 - \frac{\sum_{i=1}^{n}\sum_{j=1}^{m}(V - WH)^2}{\sum_{i=1}^{n}\sum_{j=1}^{m}V^2} \tag{4.6}$$

Modules extraction was performed in two phases. In the first phase we used the NMF algorithm to obtain modules from the pooled EMG data recorded during all tasks. More precisely, we considered only the transport phase of each task, i.e. the movement where the subject moves the hand towards a target. As a consequence, we analyzed only the reach movements of all tasks, in addition to the return movements of task 4 and task 5. Task 6 was excluded from the analyses adopted for this thesis work. For each movement we selected the best 5 repetitions, we selected those repetitions with the most similar kinematic data. These EMG recordings were concatenated in a matrix in which each column represents a muscle. We applied the NMF algorithm to extract the modules for all values of r. The VAF was calculated for each extraction, and we chose the number of modules equal to the first value of r whose VAF was higher than 95%. This first step gave us a set of modules that could explain most of the EMG variance of all tasks.

Extracting modules from all tasks gave us a good general idea of how muscles are coordinated. However, when looking at how well individual tasks were reconstructed, we noticed that modules extracted on a global level could not explain all the variance in a single task. Therefore we formulated the hypothesis that although modules could be structures that are common between tasks, the muscle weights within a module could show a slight variation from task to task. To verify this hypothesis, we extracted modules from each individual task and tried to compare them to modules extracted from all tasks. During this second phase, we had to modify our criterion to determine the correct number of modules, as not all muscles necessarily participate to all movements. Therefore we changed our algorithm so as to consider the variance only for those muscles that are active.

We neglected all muscles that contributed less than 8% to the EMG variance of a specific movement and then selected the number of modules that:

- guaranteed a VAF of at least 90% for each individual muscle;
- identified an area of the VAF curve with a small slope, i.e. the VAF of each muscle would change by less than 5% when adding another module;
- guaranteed a VAF of at least 95% for all muscles.

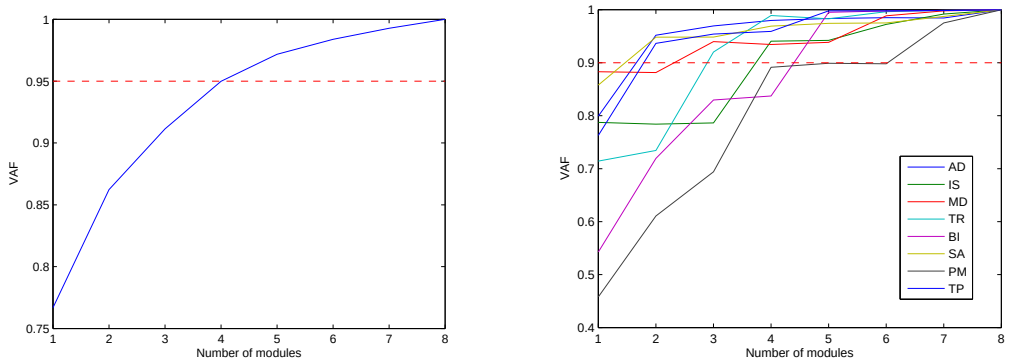

(a) (b)

Figure 4.6: (a) VAF of all muscles with the threshold at 95%: it suggest 4 modules for a well reconstruction of the EMG signals. (b) VAF of single muscles: five modules are necessary to reconstruct at least the 90% of the original signals.

Chapter 5

Results

We recorded EMG signals from 16 muscles, 8 per side. Data relative to the left and right side was processed separately, and therefore the module decomposition was performed on 8 signals at a time. Accordingly, the matrix V containing the filtered EMG signals had eight columns and we could set the NMF algorithm to extract from one to eight modules. The extraction of just one module represents the case in which muscles are all synchronized; 8 modules is the case in which each muscle is activated independently form the others and all modules feature just the activation of one muscle. The numbers of rows in the matrix V depends solely on how many samples are considered.

First, we tried to understand how muscle coordination patterns can be described on a global level, i. e. for all tasks combined. EMG data of the following tasks was concatenated:

- Task 1 (reaching movements)
- Task 2 (reaching movements)
- Task 3 (reaching movements)
- Task 4 (reaching and return movements)
- Task 5 (reaching and return movements)

The number of modules extracted are summarized in the tables (5.1) and (5.2).

Subject	Dominant side	Modules			
		Left	Right	Dominant	Non Dominant
UBC_001	R	4	5	5	4
UBC_002	R	5	5	5	5
UBC_003	R	4	5	5	4
UBC_004	R	5	3	3	5
UBC_005	R	5	5	5	5
UBC_006	R	6	5	5	6
UBC_007	L	3	4	3	4
UBC_008	L	3	4	3	4
UBC_009	R	5	4	4	5
UBC_010	R	4	4	4	4
UBC_011	R	4	4	4	4
UBC_013	R	4	4	4	4
UBC_014	R	3	4	4	3
UBC_015	L	4	4	4	4
UBC_016	R	5	5	5	5

Table 5.1: Summary of the modules extracted for all healthy subjects. Modules were extracted separately form left and right side, and dominant and non dominant side were compared.

Looking at these results we can assert that:

- on average of 4.3 modules per arm are sufficient to reconstruct all the EMG signals;
- there are no significant differences between the number of modules of left and right arm;
- even considering the comparison between dominant and non-dominant side there are no significant differences.

In a second step, we proceeded analyzing the modules. To compare modules correlation coefficient was used:

$$R(i,j) = \frac{C(i,j)}{\sigma_i \sigma_j} \tag{5.1}$$

where $C(i,j)$ is the covariance between module i and module j and σ_i and σ_j the standard deviations of modules i and j. Two modules were considered comparable if their correlation was greater than 0.6. We paired modules of both sides starting by the ones with the highest correlation and kept iterating until no more modules were left or until all remaining pairs had a correlation lower than the threshold. The results of this comparison are summarized in tables (5.2) and (5.3).

	Number of Modules				
	Dominant	**Non Dominat**	**Shared**	**Specific D**	**Specific ND**
Mean	4,2	4,4	3,3	1,07	1,2
STD	0,75	0,71	1,15	0,78	0,99
Min	3	3	1	0	0
Max	5	6	5	3	3

Table 5.2: Comparison between modules of dominant and non-dominant side.

On average, 3.3 modules are shared between dominant and non dominant side and just 1 is specific for one side: we can assert that not only the number but also the configuration of the modules is comparable between the two arms.

Subject	Dominant side	Number of Modules				
		Shared	Specific			
			L	R	D	ND
UBC_001	R	4	0	1	1	0
UBC_002	R	4	1	1	1	1
UBC_003	R	4	0	1	1	0
UBC_004	R	2	3	1	1	3
UBC_005	R	5	0	0	0	0
UBC_006	R	4	2	1	1	2
UBC_007	L	2	1	2	1	2
UBC_008	L	2	1	2	1	2
UBC_009	R	4	1	0	0	1
UBC_010	R	1	3	3	3	3
UBC_011	R	4	0	0	0	0
UBC_013	R	2	2	2	2	2
UBC_014	R	2	1	2	2	1
UBC_015	L	3	1	1	1	1
UBC_016	R	4	1	1	1	1

Table 5.3: Modules of dominant and non dominant side were compared: in the table for each subjects the number of modules shared and specific are summarized.

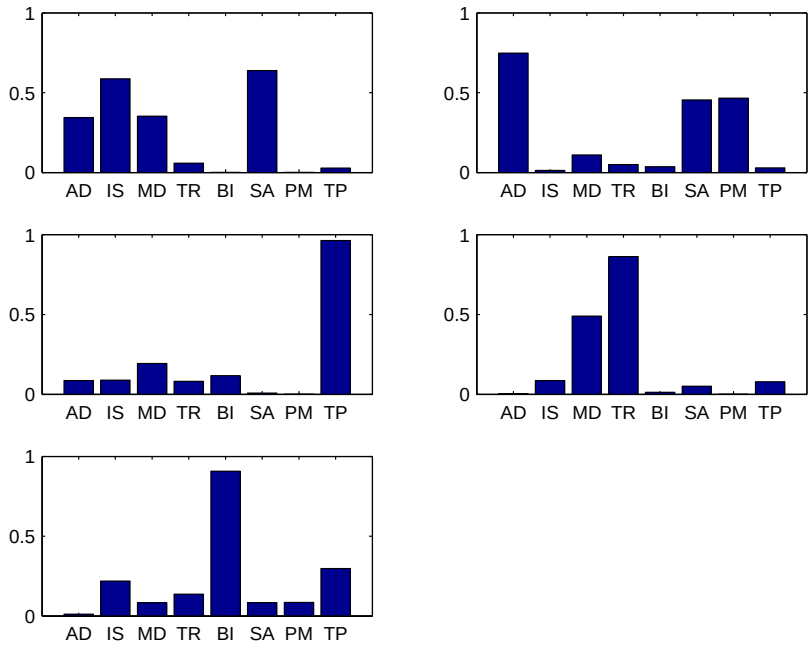

(a)

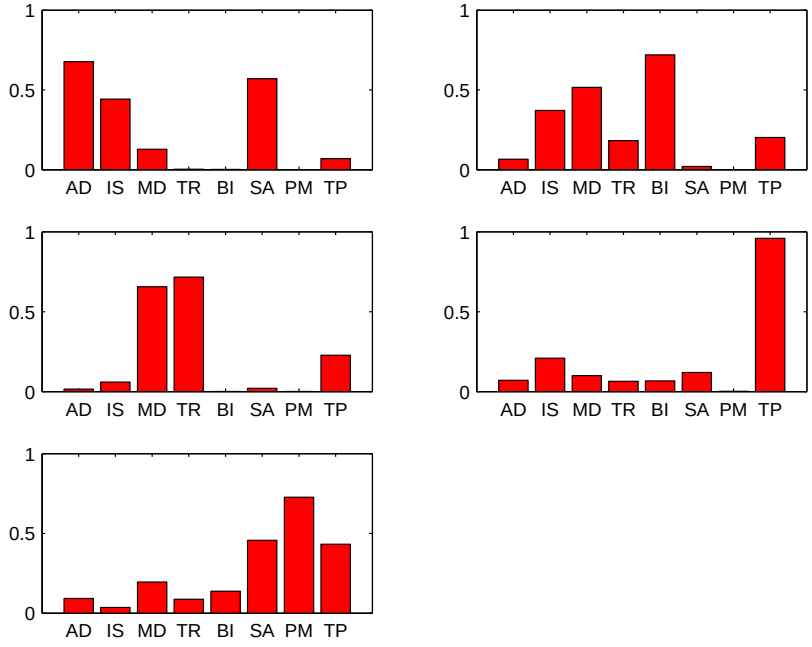

(b)

Figure 5.1: Example of modules extracted from dominant (a) and non dominant side (b) of a subject.

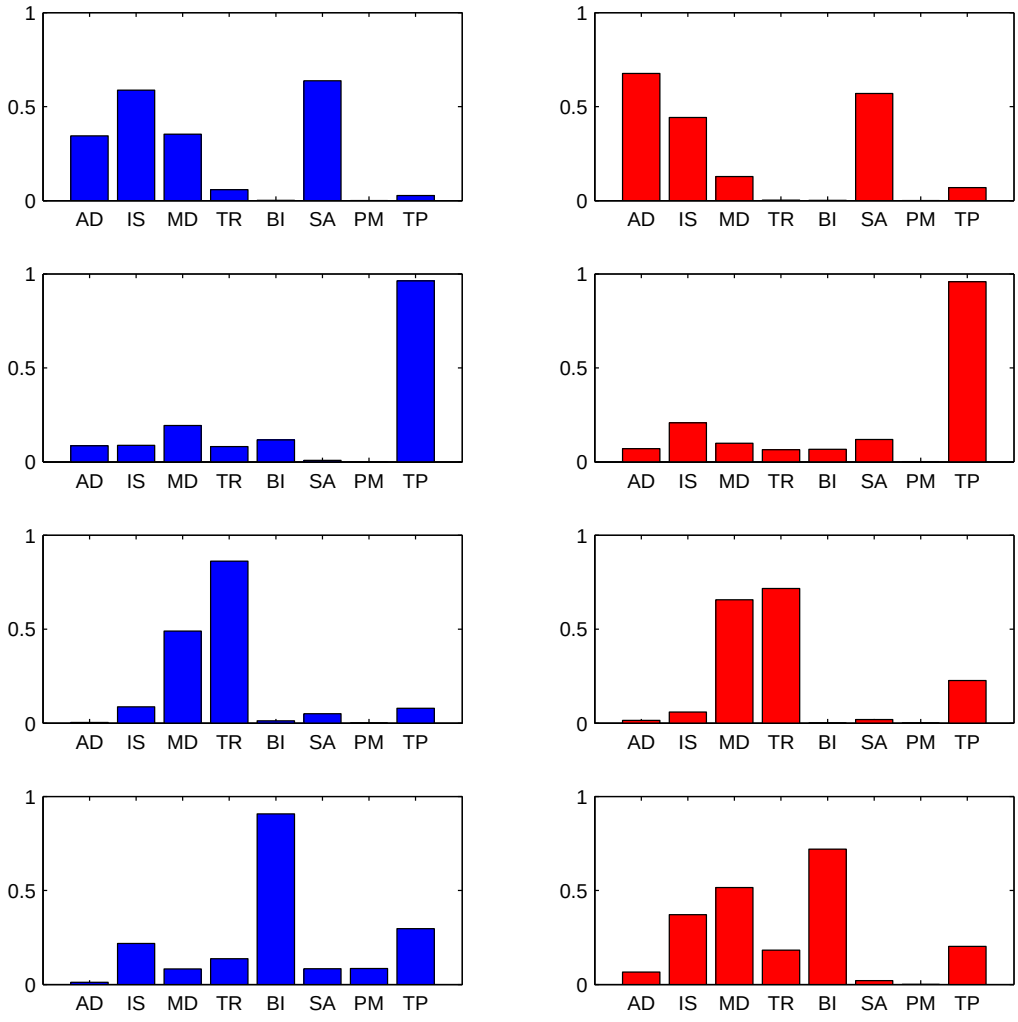

Figure 5.2: Comparison between modules of the previous figure (5.1): similar modules from dominant (blue) and non dominant side (red) were coupled, four modules result comparable.

The next step consisted in comparing modules between all subjects to understand if there are some in common. In order to get there, we used a cluster analysis based on the k-means algorithm: this procedure was repeated varying the input number of clusters and choosing the solution so that had the lowest number of clusters and had an intra-cluster correlation at least 0.6. For each side all modules can be grouped into 8 clusters of which at lest three are shared between most subjects (figure 5.3).

This is a very encouraging result as it shows that most subjects share similar coordination strategies. Furthermore, finding similar modules in all subjects indicates that these modules are not only a random result coming from a fitting algorithm, but that they might represent actual coordination patterns.

So far we assessed the quality of signal reconstruction of all combined tasks, obtaining overall good results when using only an average of four modules. The next step is looking at how well muscle activity of each individual task can be reconstructed, and how well each EMG channel is captured.

To assess how well the extracted modules captured finer task specific details, we looked at the quality of reconstruction for each movement. This was done by calculating the VAF relative to each individual movement. We also looked at how well the activity of each single muscle was reconstructed, both on a global level (all movements) and on a movement specific level. As shown in figure (5.4 on the left) the values of the overall VAF (of all muscles) reveal for each individual movement that the reconstruction of the single movements is not always good: on average the VAF is comparable to that of all tasks but, looking at the worst case, the VAF lowers up to 0.78. If we consider the VAF calculated for each muscle the results are even worse (figure 5.4 on the right): the VAF of the reconstruction of all tasks is between 0.5 and 0.9, the VAF of the single movement is even lower than 0.4 in the worst case. Modules extracted form all task give an overall idea of how the muscles are coordinated but they are not able to describe specific movements. It follows that we did a second factorization: modules from each movement were extracted separately for each subject. In this case we factorized matrices V that contained samples from only one movement and got specific modules from it.

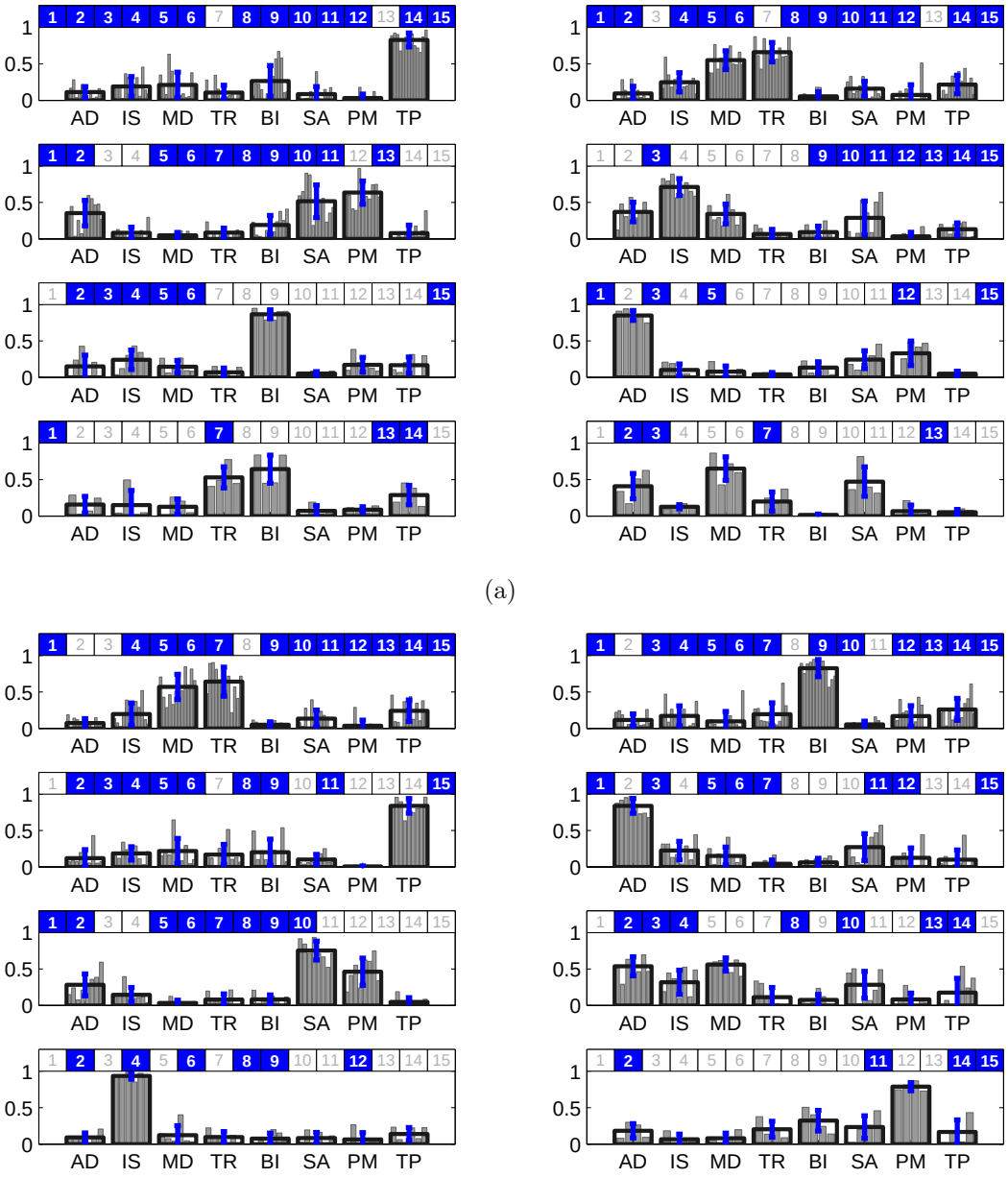

(a)

(b)

Figure 5.3: These plots summarize all the module extracted from each subject((a) dominant side, (b) non dominant side). In each plot the empty bars represent the average module and the blue error bars represent the standard deviation of each muscle weight. The grey columns represent subject-specific modules. At the top of each plot, the blue squares point out in which subject that modules exist.

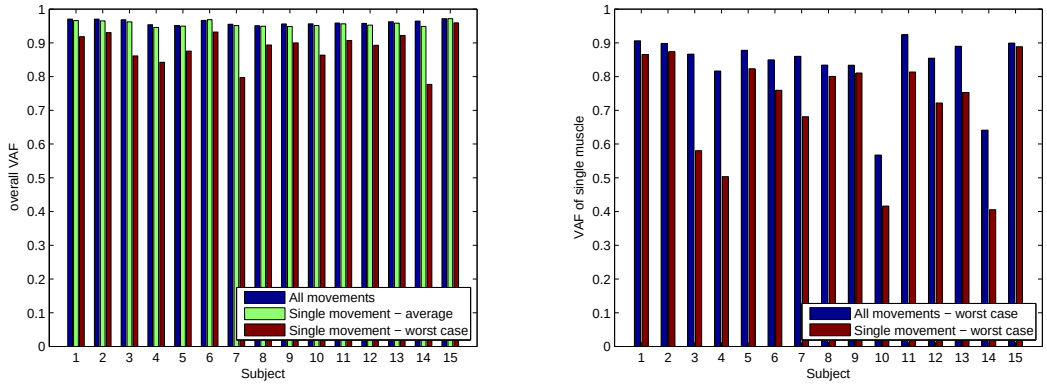

(a)

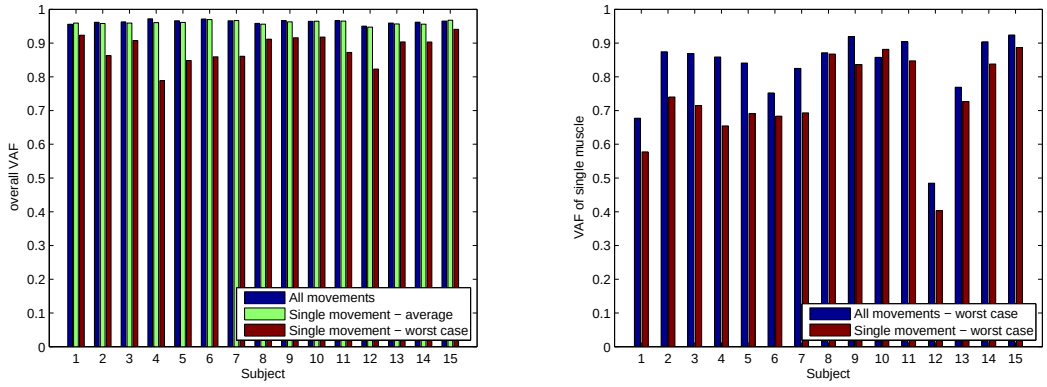

(b)

Figure 5.4: The plots represent the overall reconstruction quality and the reconstruction quality of a single channel for dominant (a) and non dominant side (b). In the plots on the left the overall VAF: blue bars are the VAF values got from the reconstruction of the entire EMG signals, the green bars are, on average, the VAF got from the reconstruction of the EMG of the single movements, in red the worst case. In the plots on the right the VAF of single muscle is shown, this VAF was calculated only for the muscles that resulted active during the movements (contribute more than 8% to the EMG variance of the movement). The blue bars are the worst VAF value got from the reconstruction of the entire signals, the red ones represents the VAF of the worst reconstruction of the single movement.

Calculating again the VAF with these new modules, we can see that the reconstruction is more reliable (compare figure (5.4) and figure (5.5)): all the VAF values are over 0.9, even in the worst case.

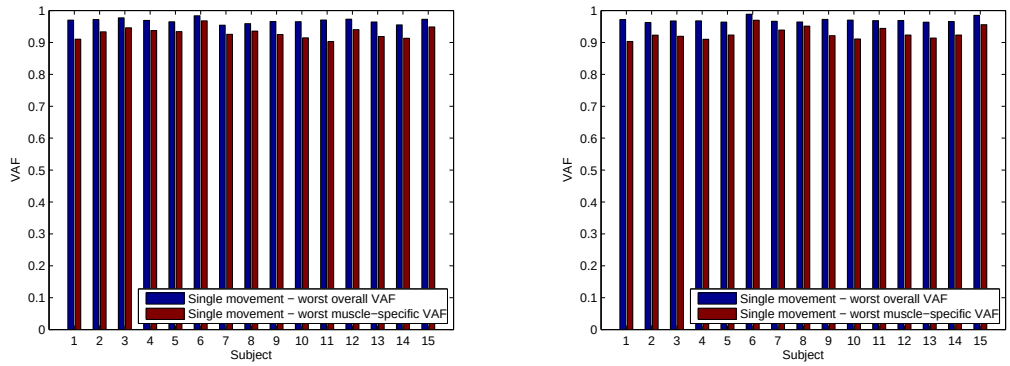

(a) (b)

Figure 5.5: The blue bars represents the worst overall VAF and the red ones the worst VAF of single muscle got using the specific modules for the reconstruction (dominant side (a) non dominant side (b)).

The result of the new factorization is a large number of modules. To understand if these task specific modules are comparable to those modules extracted from all tasks we paired modules that had a correlation higher than 0.6, starting from the pair with the highest correlation. We found that most task-specific modules can be associated to a generic module, but not all of them. We performed a cluster analysis on the modules that could not be paired, finding that an average of 4.1 clusters is sufficient to group all the remaining modules. For this cluster analysis we required a intra-cluster correlation of at least 0.6. We think that those modules that could not be associated with the general ones represent coordination patterns that are specific for certain tasks and are not of fundamental importance on a larger scale. They could also represent noise components of the signal or artifacts introduced by the factorization algorithm. In fact, applying NMF to a multitude of tasks lead to more stable results then applying it only to a single task.

For the remainder of this analysis we focused on those modules that could be associated with those extracted from all tasks.

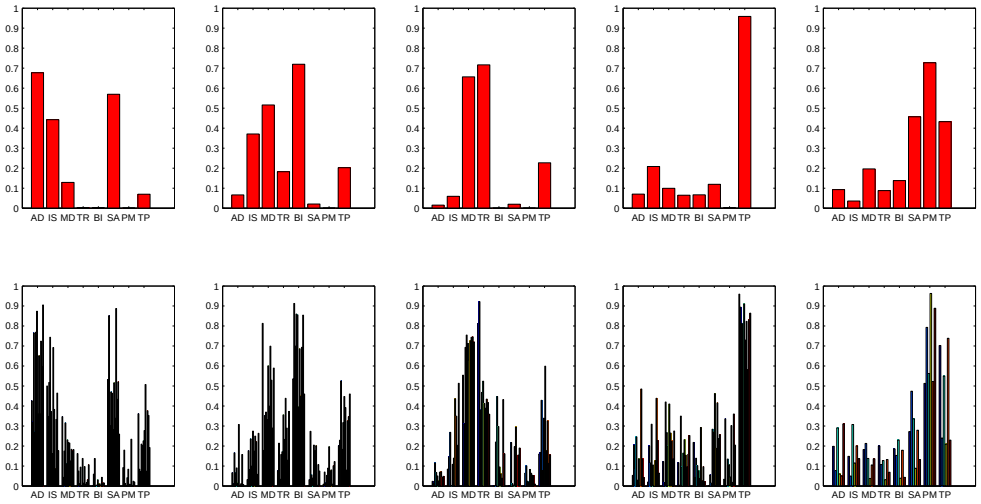

(a)

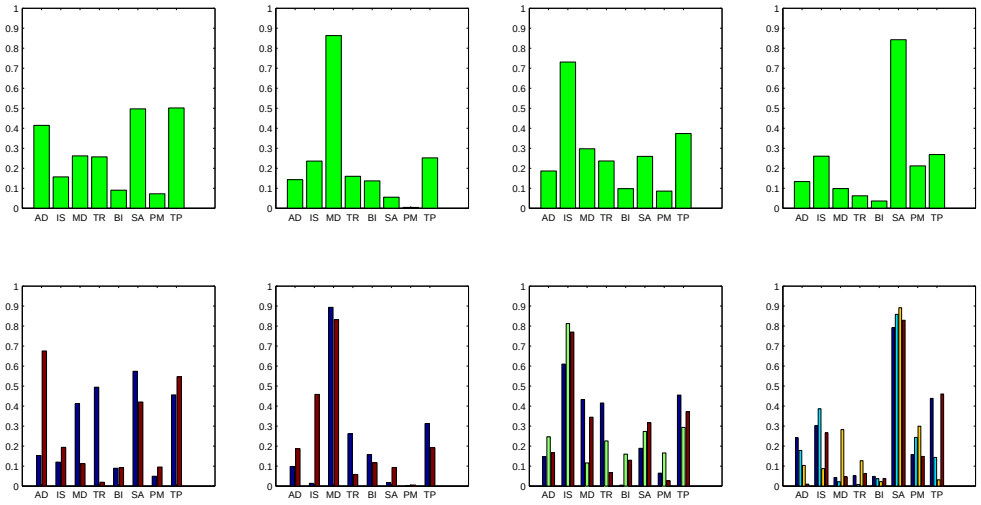

(b)

Figure 5.6: (a) Red bars represents the overall modules of a subjects, at the bottom his modules task specific associated. (b) Specific modules that cannot be comparable with the overall ones, in green the new specific modules result from a cluster analysis of the previous ones.

Exploiting this association between overall modules and movement specific ones, now we were able to find out how these overall modules are distributed in the specific movements and quantify how much they change in different tasks.

We looked at those overall modules shared by most subjects and group the modules of all subjects that could be associated with one of the shared modules,

we did this on a task-by-task basis. Therefore, for each module shared by more than one subject, we could see how it changed from task to task and from subject to subject. For each task the average module over all subjects and the standard deviations of each module weight were calculated: by looking at these values, we observed how a module might be adapted to task-specific demands.

Considering the first shared module of the non dominant side, we can notice that the modules that it represents, even if with small alteration, are present in all tasks. In figure (5.7), we can see an example of how a module changes from task to task: in each plot, the gray bars represent the modules of all subjects of that movements, the back empty bars are the average of all modules with their standard deviation in blue. These modules are very similar to each other, we can notice only small alterations. This changes are more evident if we look at the trend of the single muscle weights through the different movements (figure 5.9): in the plot the blue line is the weight of a specific task in each movement with its respective standard deviation (black bar), in cyan the average weight of that muscles in all tasks. Looking at the figure of the activation coefficients (5.8) we can understand when these modules are active during each movements: the black curves are the averages of the coefficients, in blue their standard deviations.

Thanks to this representation it is possible to give a biomechanical explanation of these modules. We proceeded analyzing the modules shares by most subjects one by one.

Module 1 (non dominant side) : the trapezius is dominant compared to the other, the function associated is shoulder elevation. The trend of the weights is quite regular except in some cases: the triceps is higher in movement 1 (External Rotation reach) because the subject had to lift up the arm to move it from back to the table; middle deltoid is lower in movement 2 (External Rotation return) and 3 (Ab-Adduction reach). Regarding the activation coefficients, this module results more active at the beginning and at the end of the movements, in particular for the multidirectional reaching movements.

Module 2 (non dominant side) : middle deltoid and triceps are the most active muscles, the function correlated is the arm elbow extension and shoulder abduction. Looking at the muscle weights: the anterior deltoid is more active in movement 6 (grasping a rope) because an higher elevation of the shoulder is required, the middle deltoid is lower in movement 3 ad 4 (Ab-Adduction) because the movements occurred in front of the subjects, triceps is more active in movements 1 and 2 (External Rotation) because the arm moves from the front to the back, the pectoralis major is higher in the fourth (Finger to Forehead) because it helps to move up the arm. This module is active in different moments during the different movements: i.e. in the first movement is active at the beginning and in the end, in the multidirectional movements is active mostly in the middle.

Module 3 (non dominant side) : the biceps is the muscle more active, the correspondent function could be elbow flexion in the frontal plane. This is confirmed looking at the weight values of the biceps in each movemets: in movements 5 in which the subject had to reach his forehead with the hand, the biceps is higher than in the other. Trapezius and serratus are higher in 3 (Ab-Adduction reach) because subjects had to lift up the shoulder to execute the movement. The activation coefficients show that these modules are active mainly at the beginning of the movements, that corresponds to the moment in which the subjects had to lift the arm from the starting position.

The same observation can be made for the cluster of the dominant side. More interesting is that we can notice similarity between the modules of the two side:

- the first module of dominant and non dominant side are comparable. There are just few difference: in Ab-Adduction reach the infraspinatus is more active in the dominant side, in the movement of grasping a rope the serratus anterior is lower in the non dominant side; in all multidirectional reaching movements the serratus anterior is higher in the dominant side, in most of them even the anterior deltoid. The activation coefficietns have the same trend in dominant and non dominant side.

- the second module of the non dominant side is associated with the second module of the dominant side. There are some differences in the Ab-Adduction reaching movement: in the dominant side middle deltoid, triceps and serratus anterior are higher; in the non dominant side triceps is more active in the execution of the External Rotation reaching movement. The activation coefficients are almost the same, except for the Ab-Adduction reach in which its coefficient is slightly more active in the end of the movement in the dominant side.

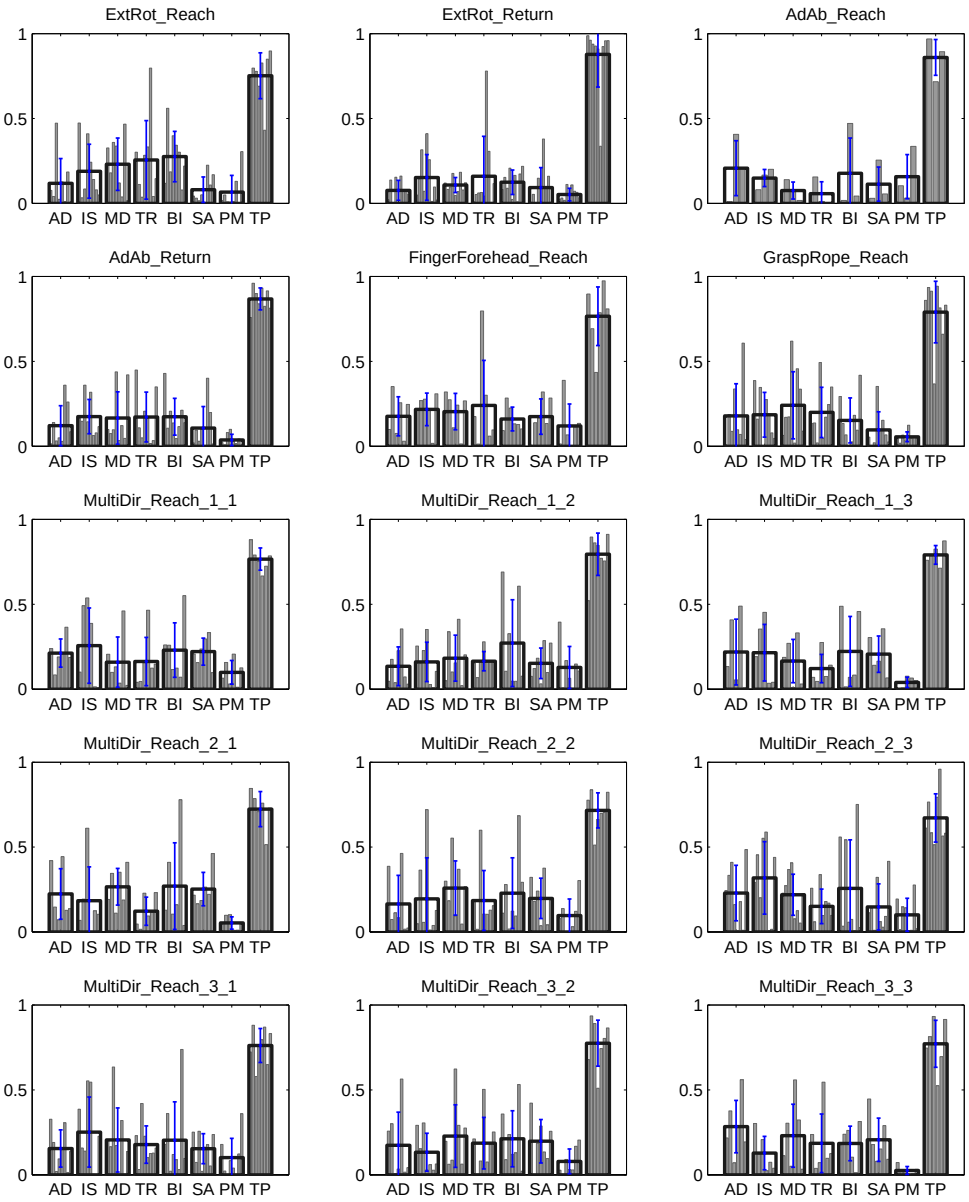

Figure 5.7: Shared module 1 - Non Dominant side: modules from all tasks associated with the first shared module and grouped by different movements (the empty black bars represents the average modules with their SDTs (in blue) for each movement, the gray bars are the subjects specific modules for each movement.)

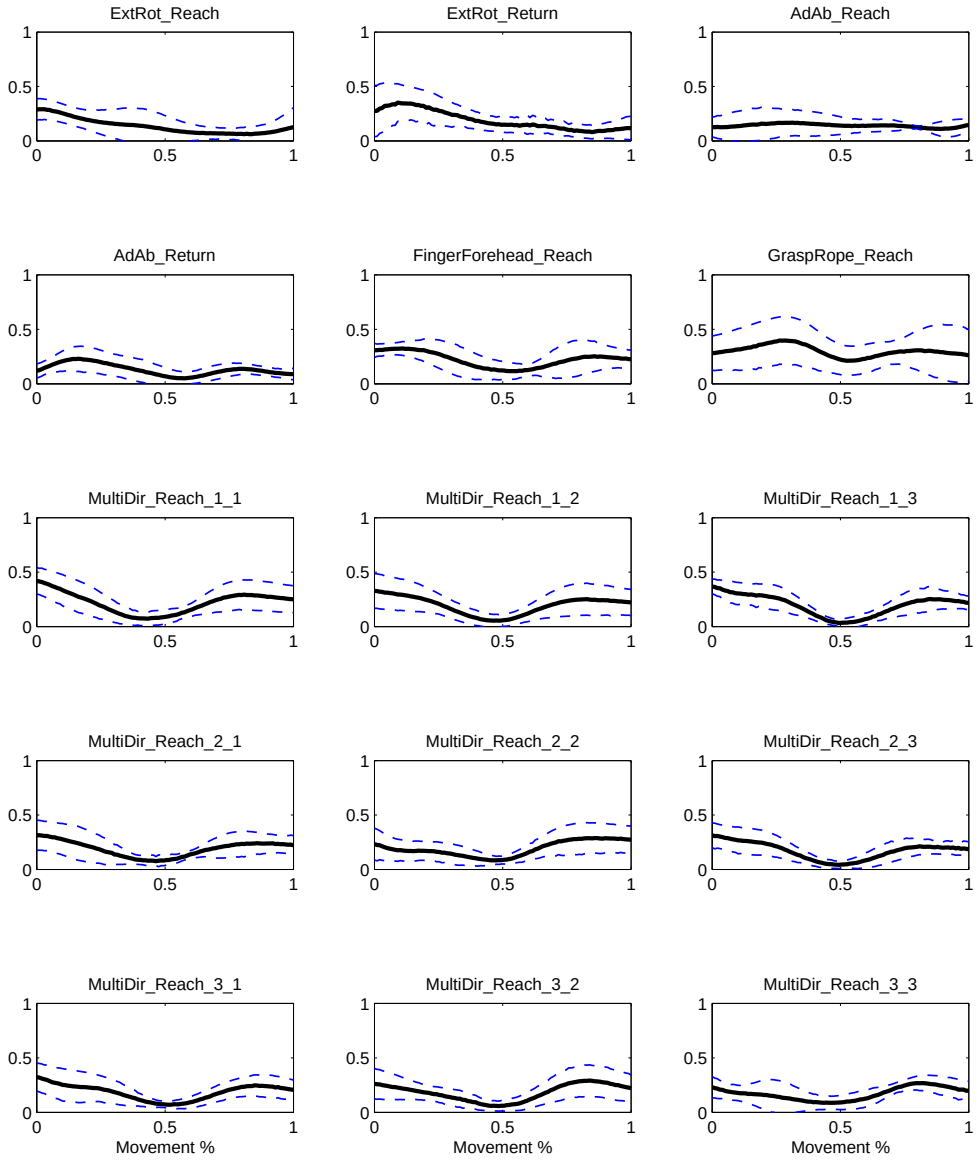

Figure 5.8: Shared module 1 - Non Dominant side: activation coefficients of the modules belonging the first shared module for each movement (in black the averages, in blue the standard deviations).

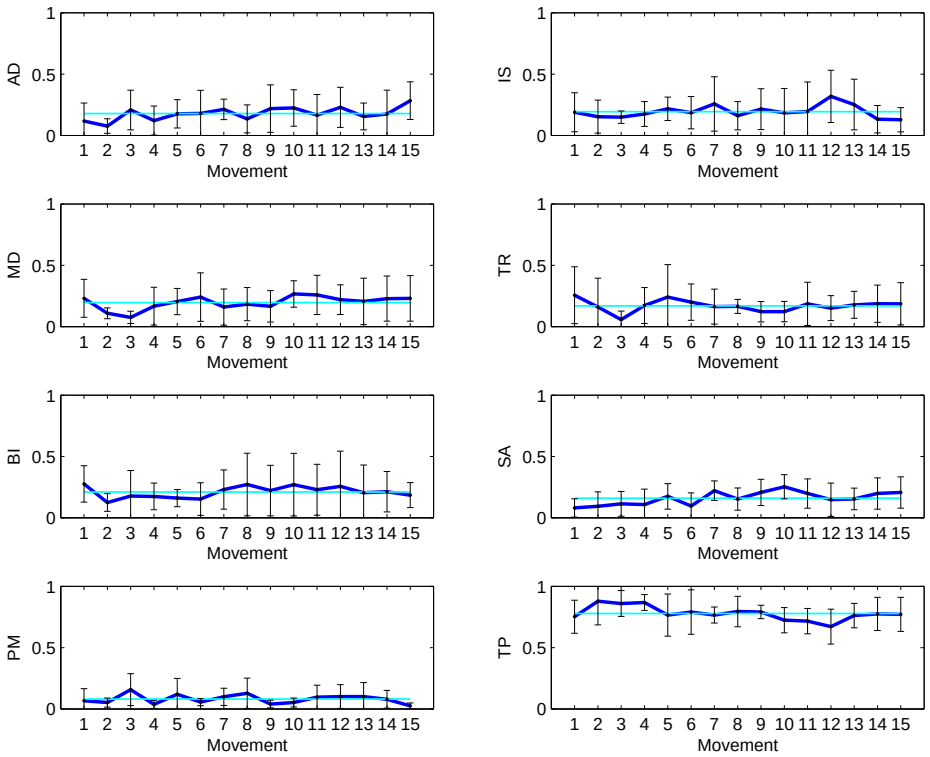

Figure 5.9: Shared module 1 - Non Dominant side: weights of the modules associated to the first shared module. In each plot in blue the trend of the weights through the different movements with their STDs and in cyan the average weights.

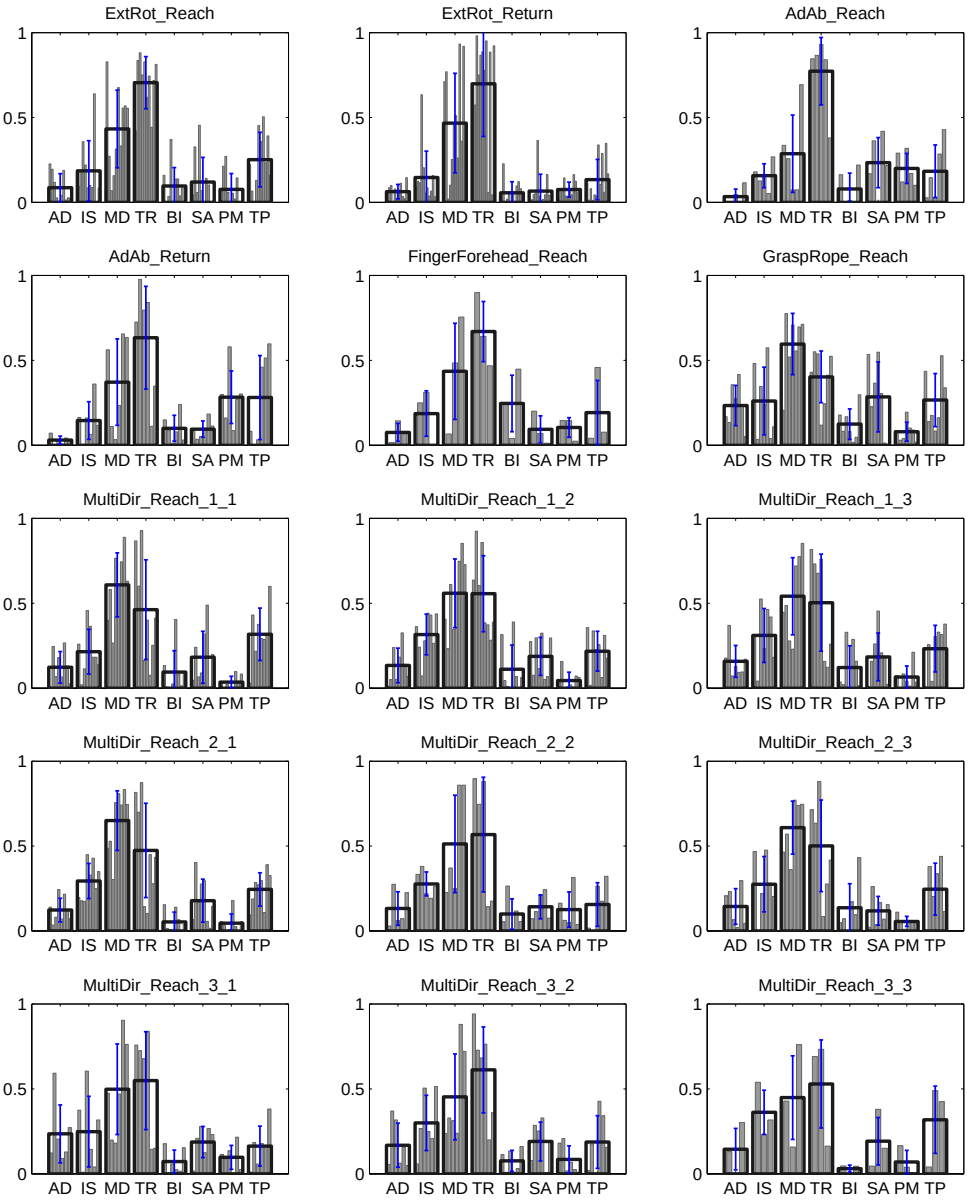

Figure 5.10: Shared module 2 - Non Dominant side: modules from all tasks associated with the second shared module and grouped by different movements (the empty black bars represents the average modules with their SDTs (in blue) for each movement, the gray bars are the subjects specific modules for each movement.

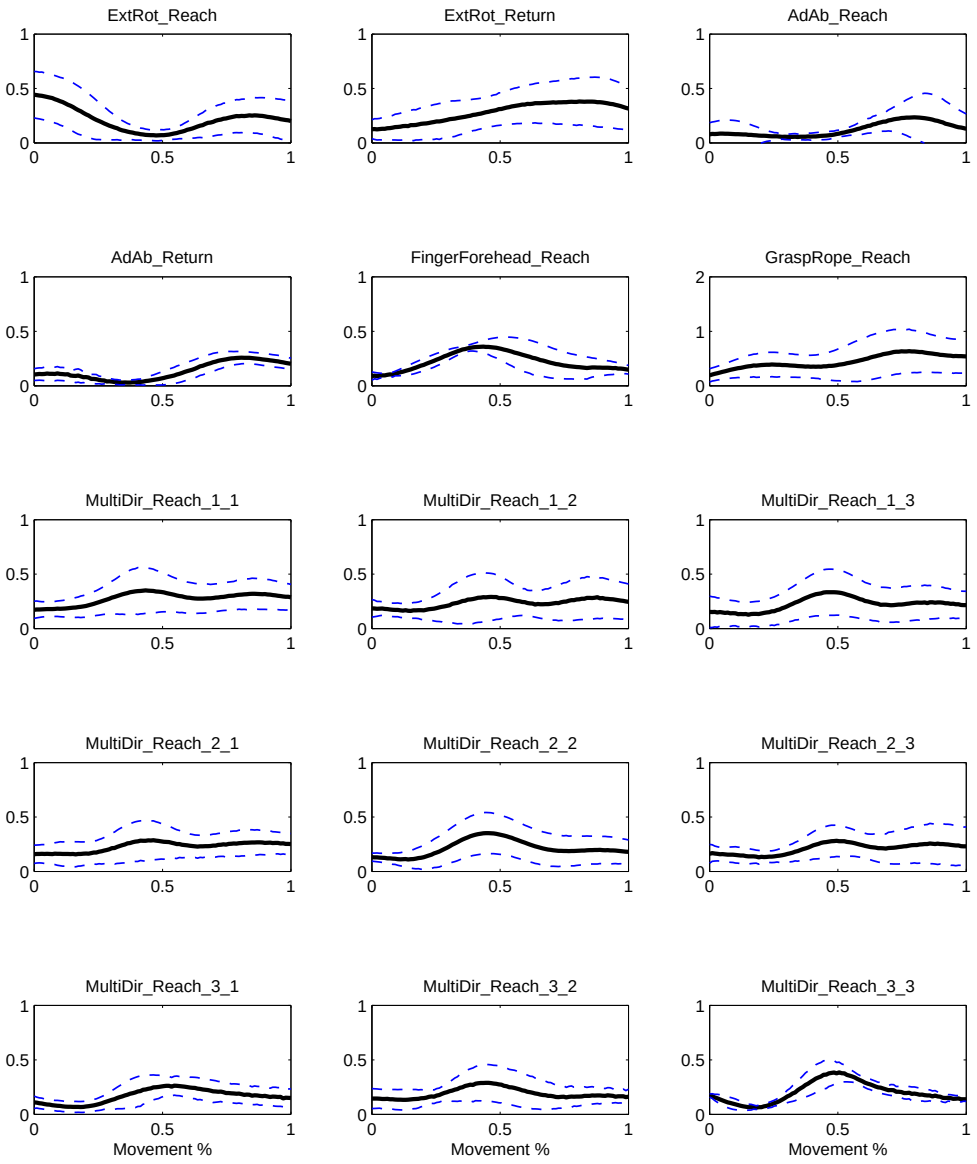

Figure 5.11: Shared module 2 - Non Dominant side: activation coefficients of the modules belonging the second shared module for each movement (in black the averages, in blue the standard deviations).

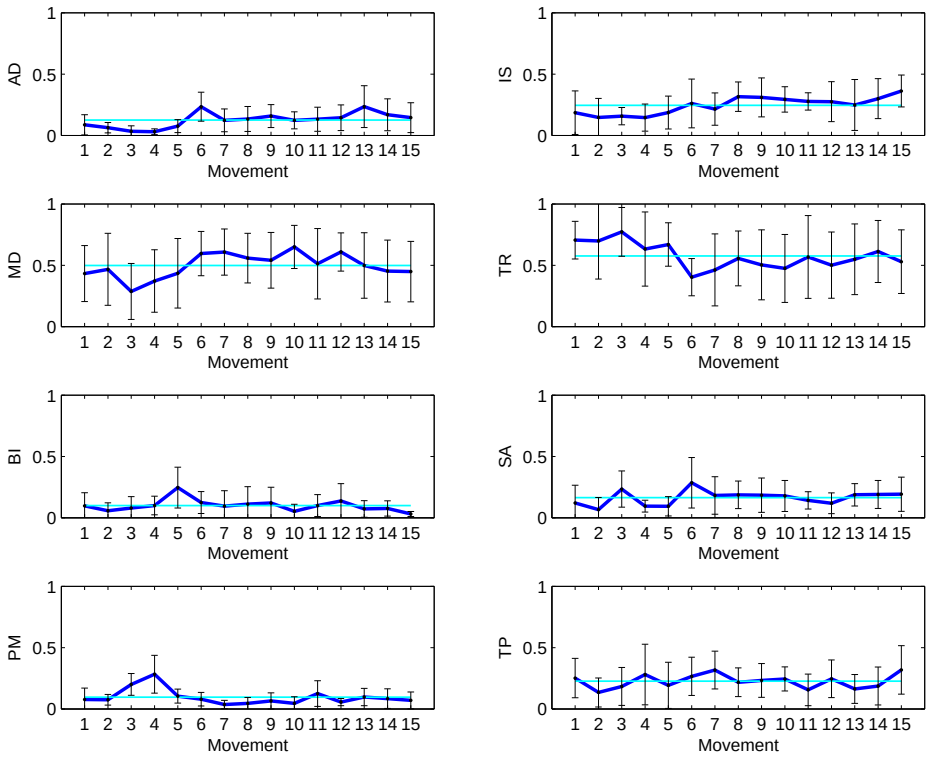

Figure 5.12: Shared module 2 - Non Dominant side: weights of the modules associated to the second shared module. In each plot in blue the trend of the weights through the different movements with their STDs and in cyan the average weights.

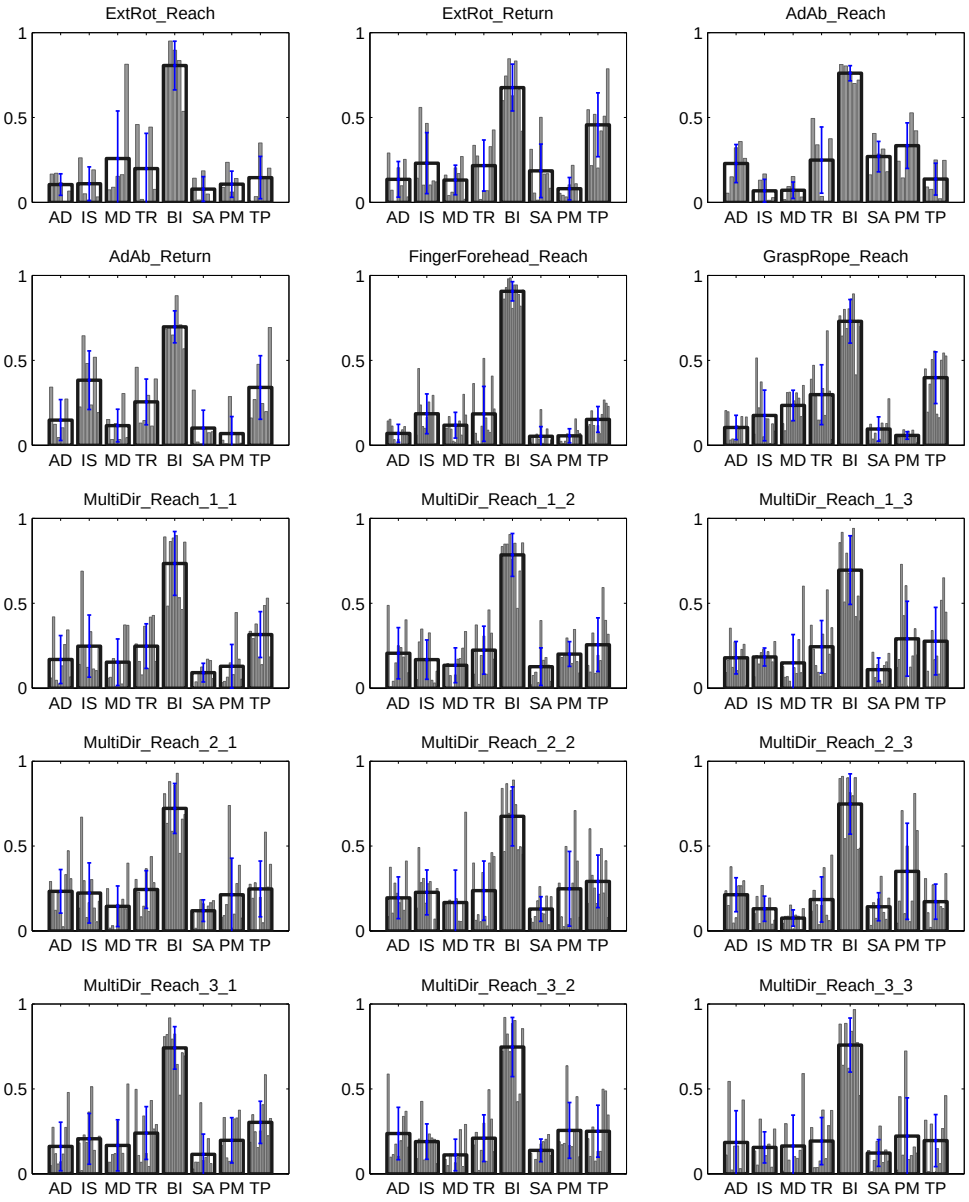

Figure 5.13: Shared module 3 - Non Dominant side: modules from all tasks associated with the third shared module and grouped by different movements (the empty black bars represents the average modules with their SDTs (in blue) for each movement, the gray bars are the subjects specific modules for each movement.

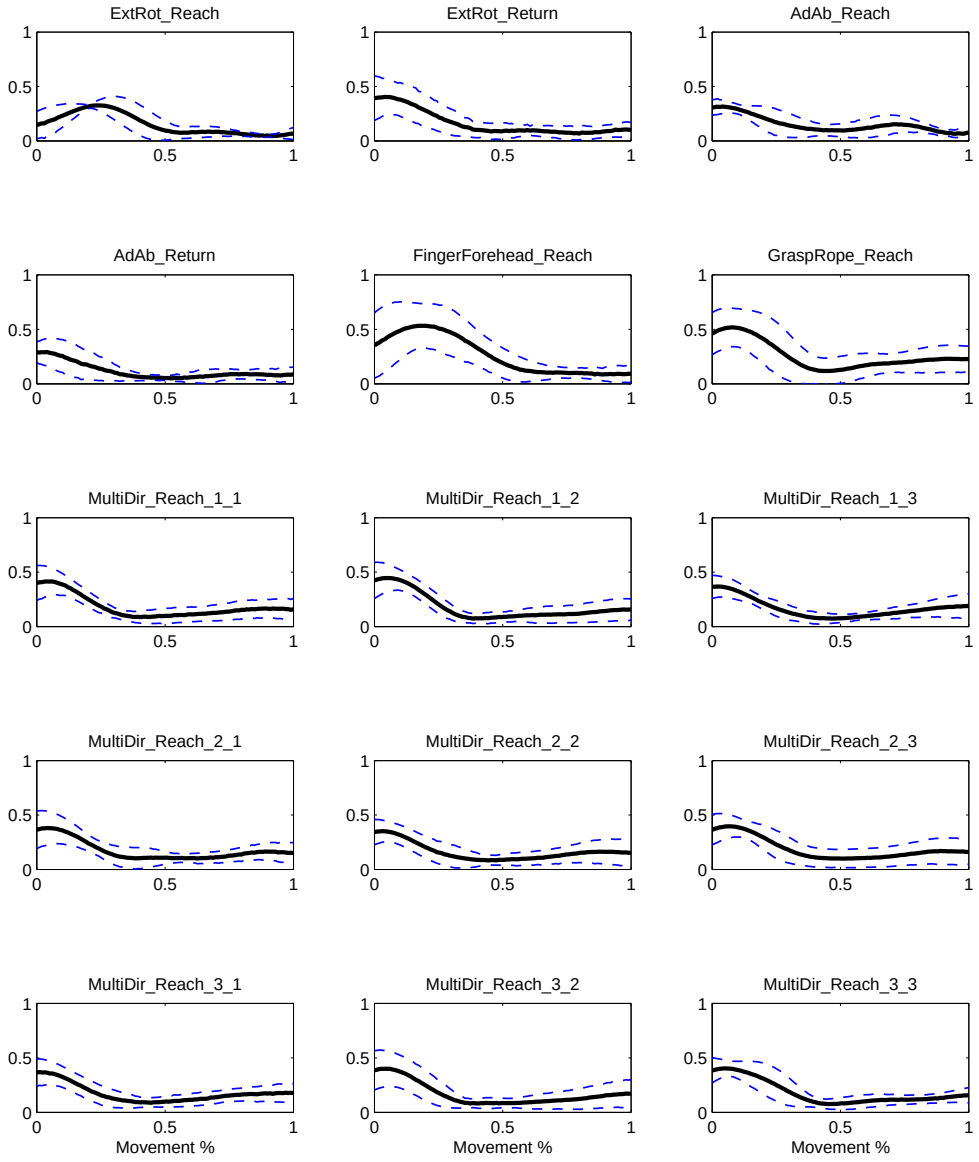

Figure 5.14: Shared module 3 - Non Dominant side: activation coefficients of the modules belonging the third shared module for each movement (in black the averages, in blue the standard deviations).

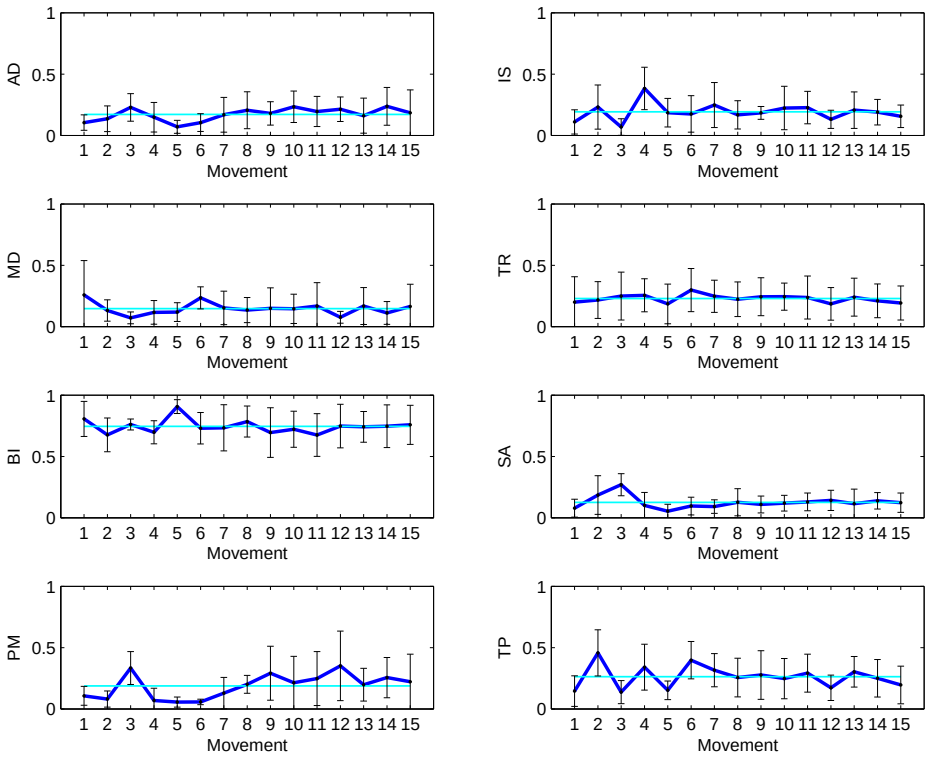

Figure 5.15: Shared module 3 - Non Dominant side: weights of the modules associated to the third shared module. In each plot in blue the trend of the weights through the different movements with their STDs and in cyan the average weights.

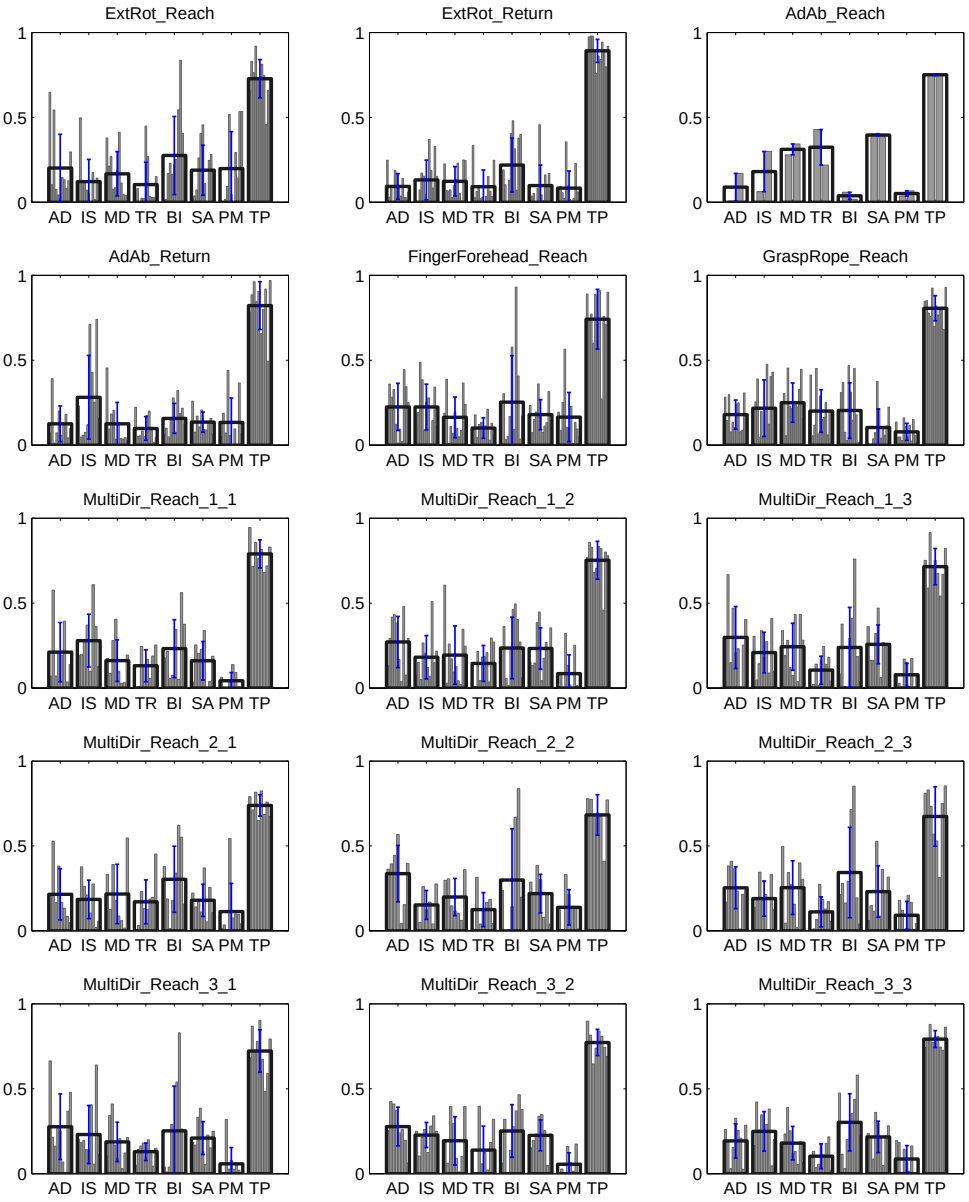

Figure 5.16: Shared module 1 - Dominant side: modules from all tasks associated with the first shared module and grouped by different movements (the empty black bars represents the average modules with their SDTs (in blue) for each movement, the gray bars are the subjects specific modules for each movement.

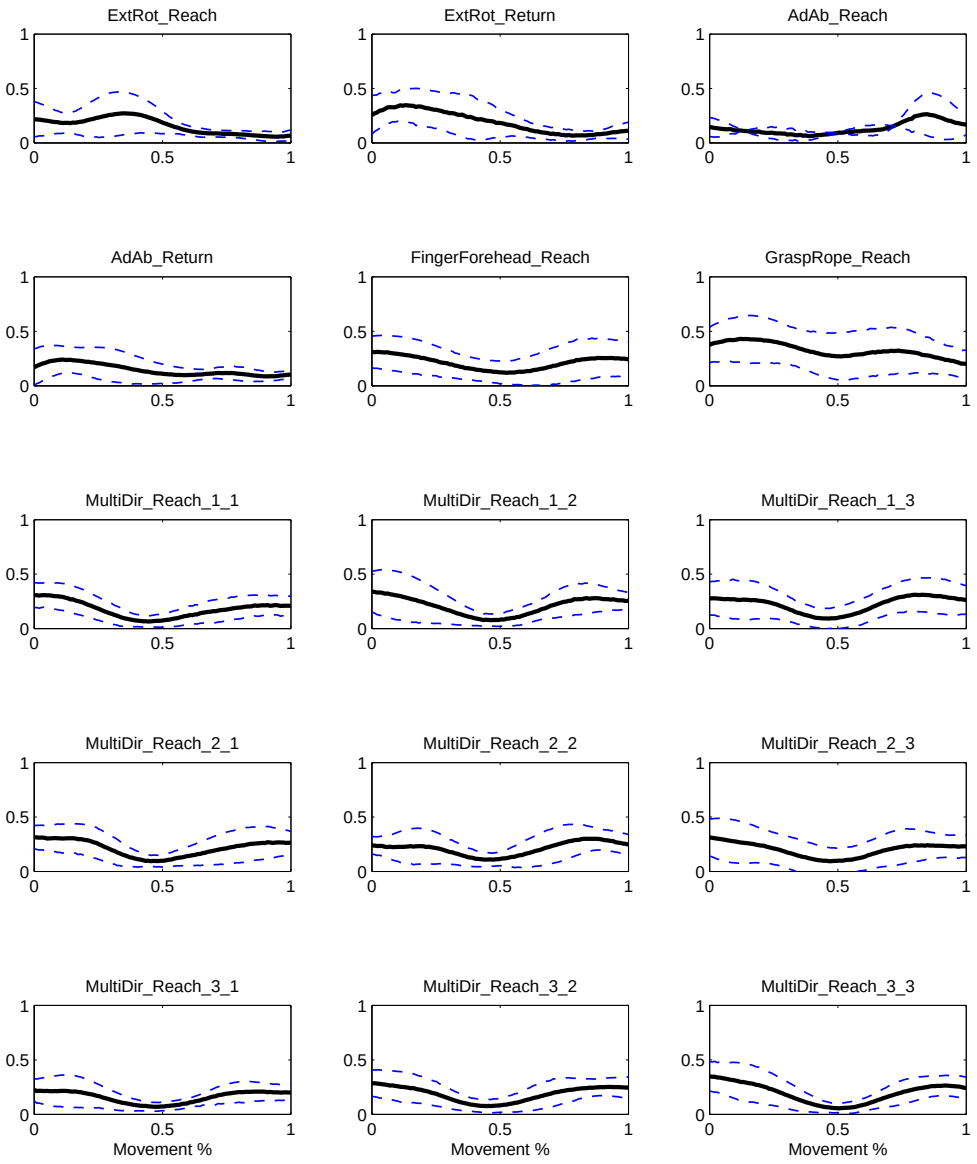

Figure 5.17: Shared module 1 - Dominant side: activation coefficients of the modules belonging the first shared module for each movement (in black the averages, in blue the standard deviations).

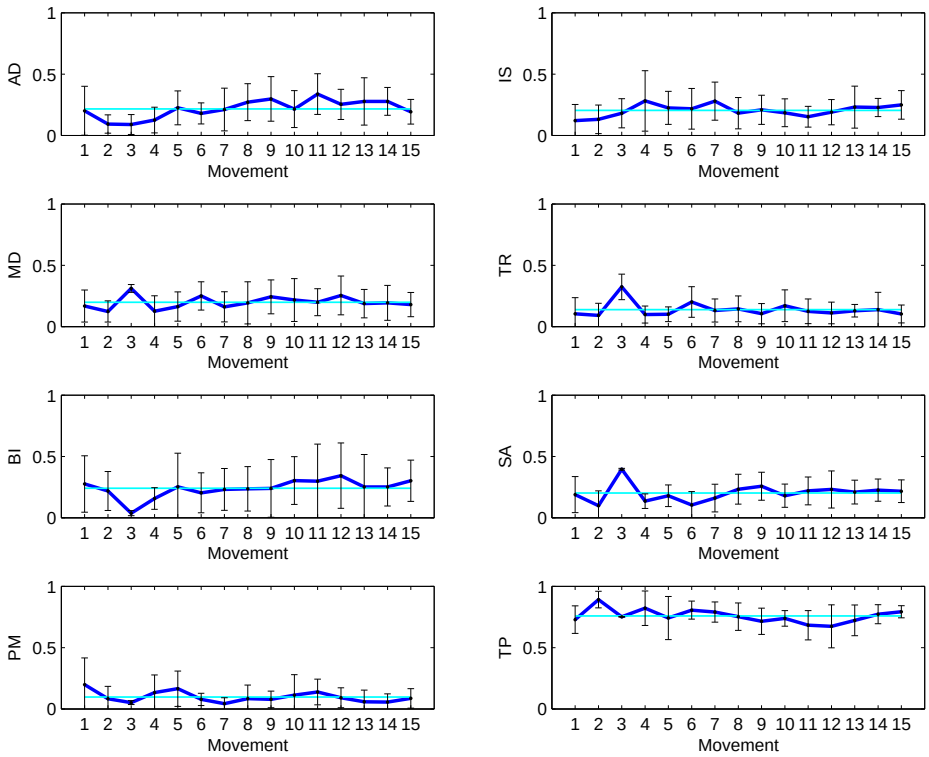

Figure 5.18: Shared module 1 - Dominant side: weights of the modules associated to the first shared module. In each plot in blue the trend of the weights through the different movements with their STDs and in cyan the average weights.

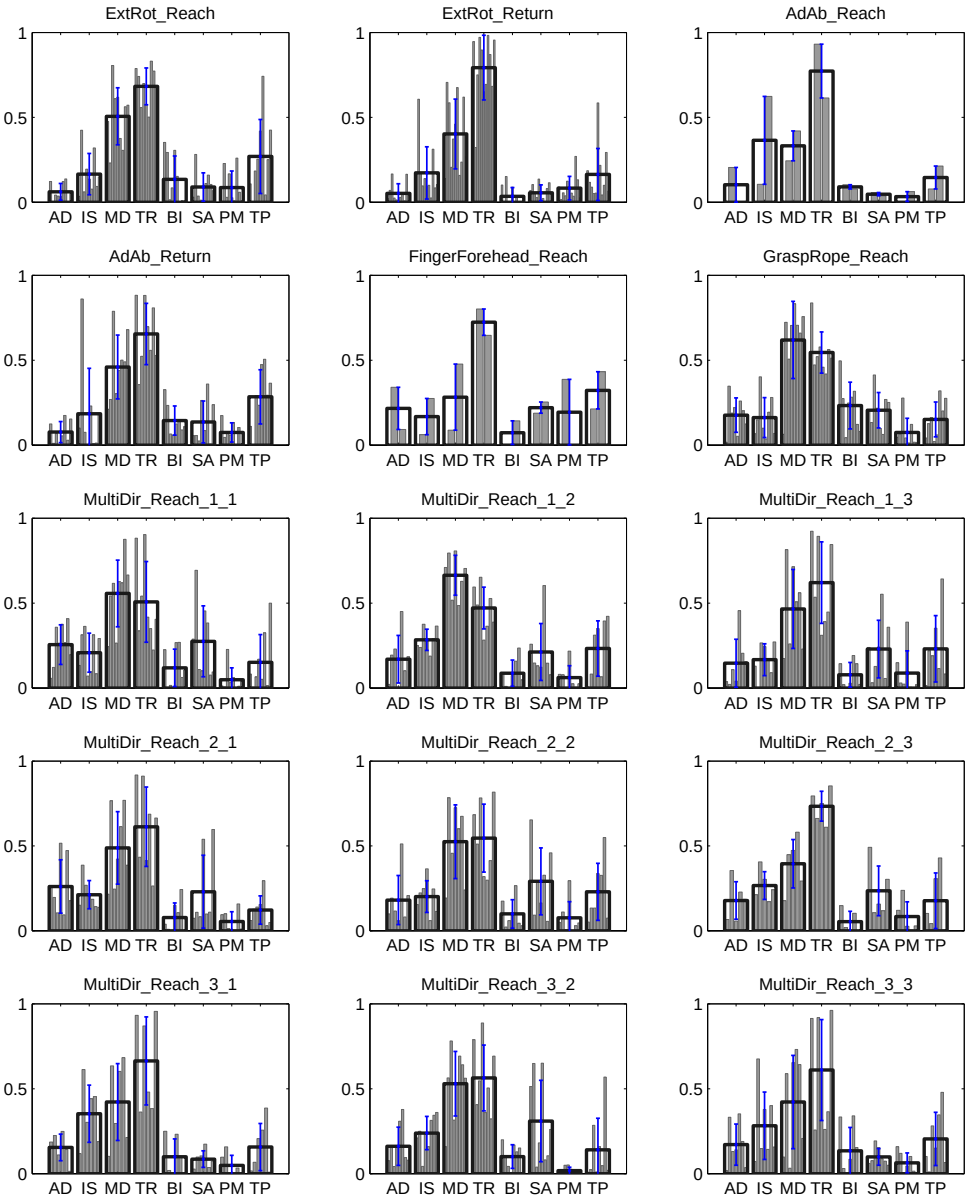

Figure 5.19: Shared module 2 - Dominant side: modules from all tasks associated with the second shared module and grouped by different movements (the empty black bars represents the average modules with their SDTs (in blue) for each movement, the gray bars are the subjects specific modules for each movement.

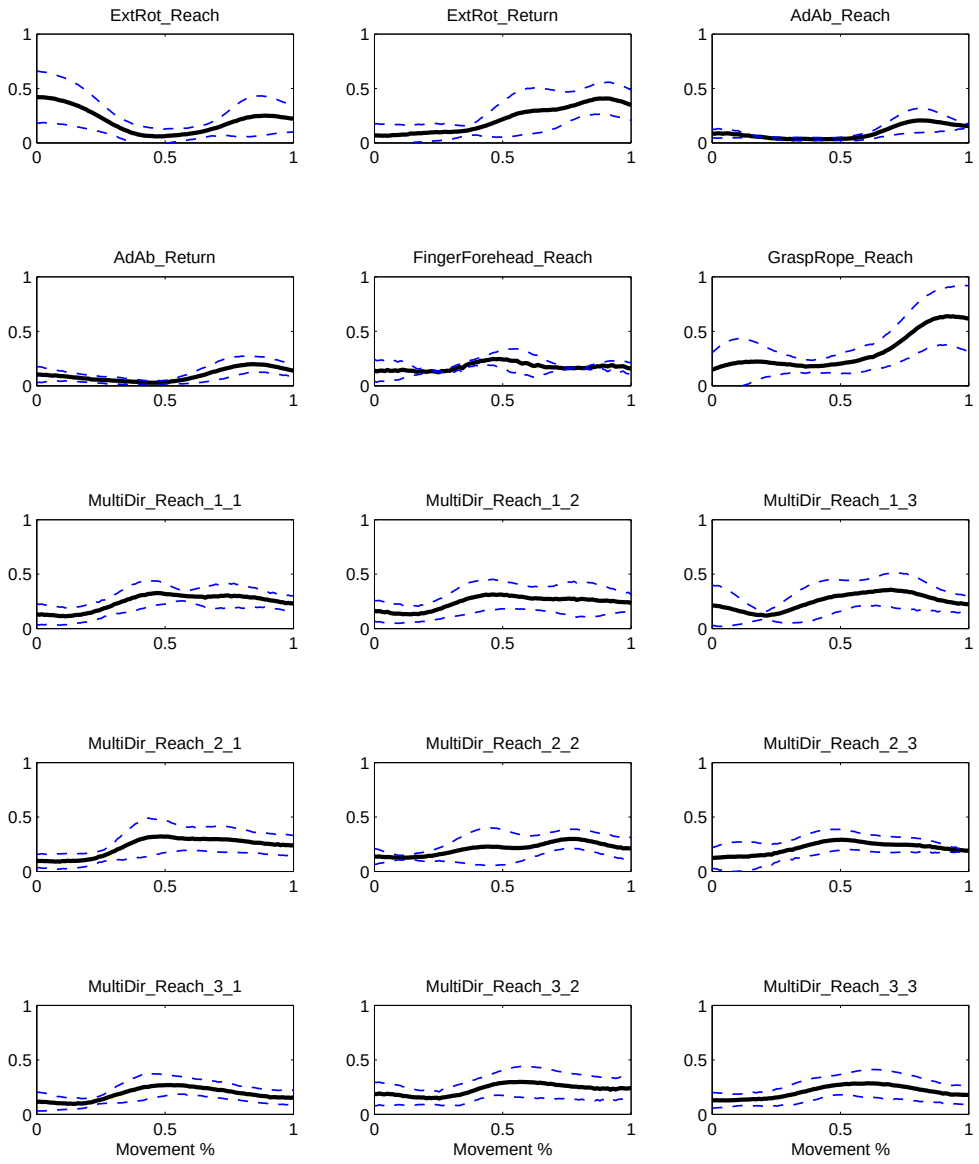

Figure 5.20: Shared module 2 - Dominant side: activation coefficients of the modules belonging the second shared module for each movement (in black the averages, in blue the standard deviations).

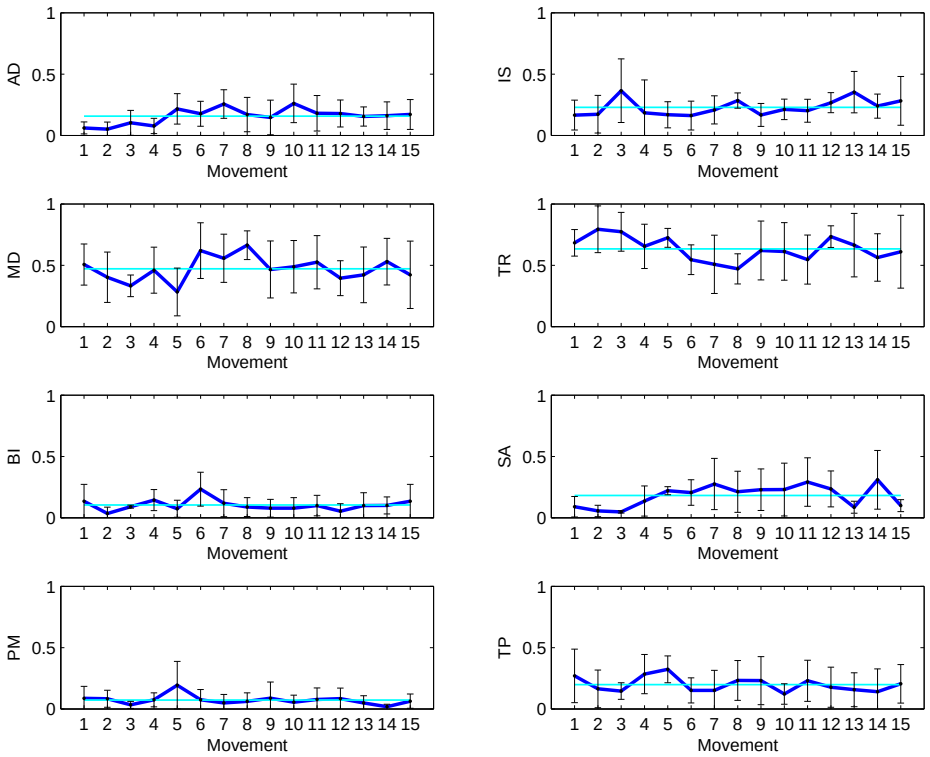

Figure 5.21: Shared module 2 - Dominant side: weights of the modules associated to the second shared module. In each plot in blue the trend of the weights through the different movements with their STDs and in cyan the average weights.

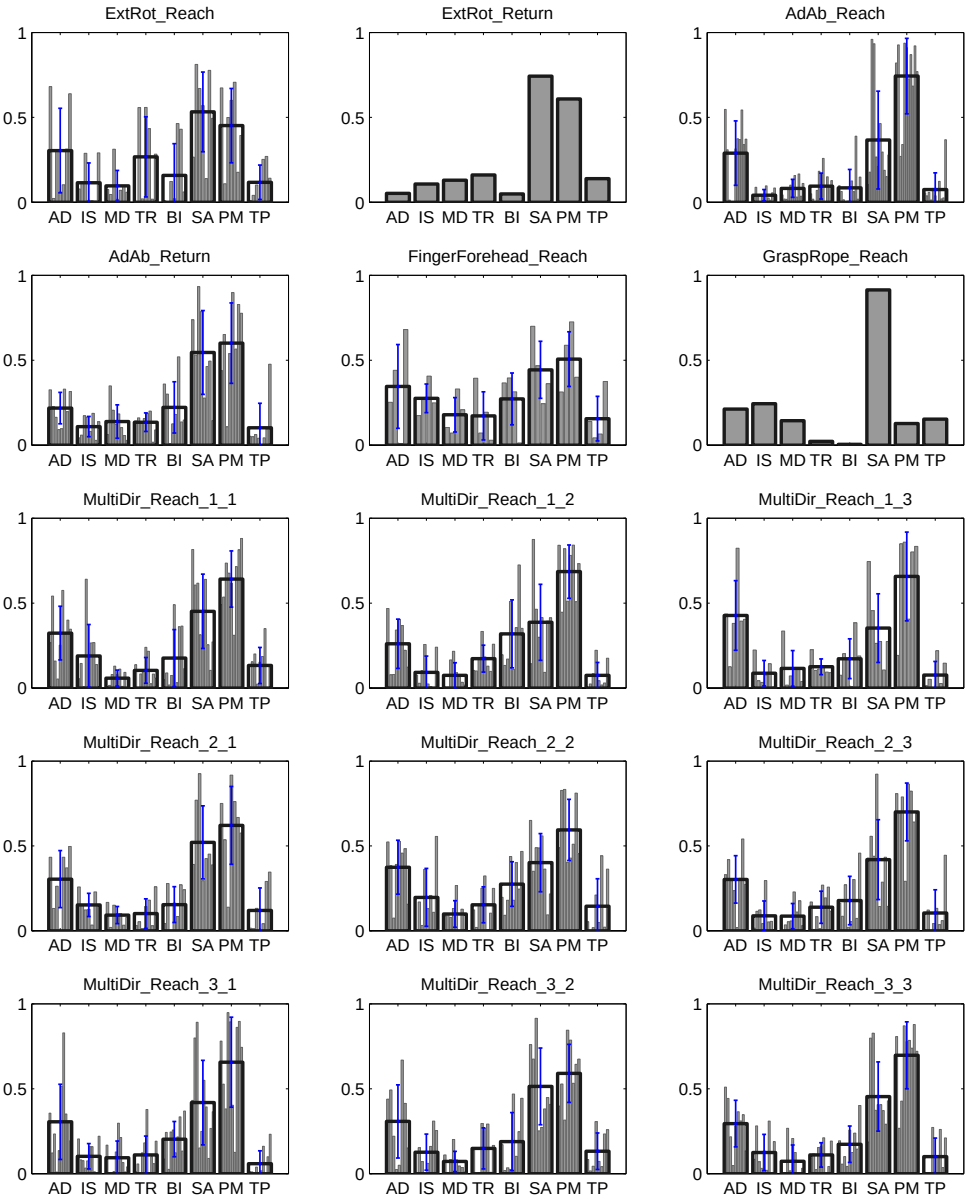

Figure 5.22: Shared module 3 - Dominant side: modules from all tasks associated with the third shared module and grouped by different movements (the empty black bars represents the average modules with their SDTs (in blue) for each movement, the gray bars are the subjects specific modules for each movement.

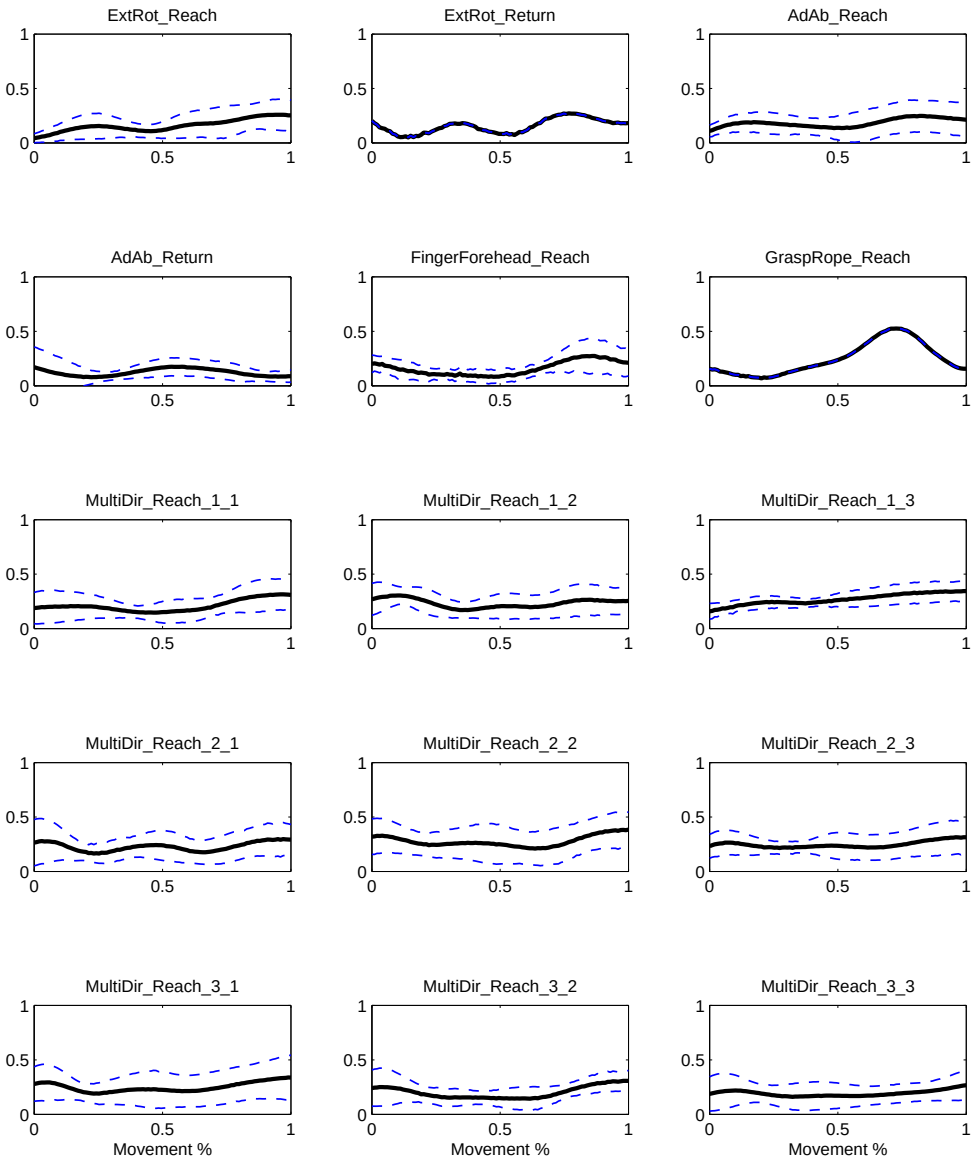

Figure 5.23: Shared module 3 - Dominant side: activation coefficients of the modules belonging the third shared module for each movement (in black the averages, in blue the standard deviations).

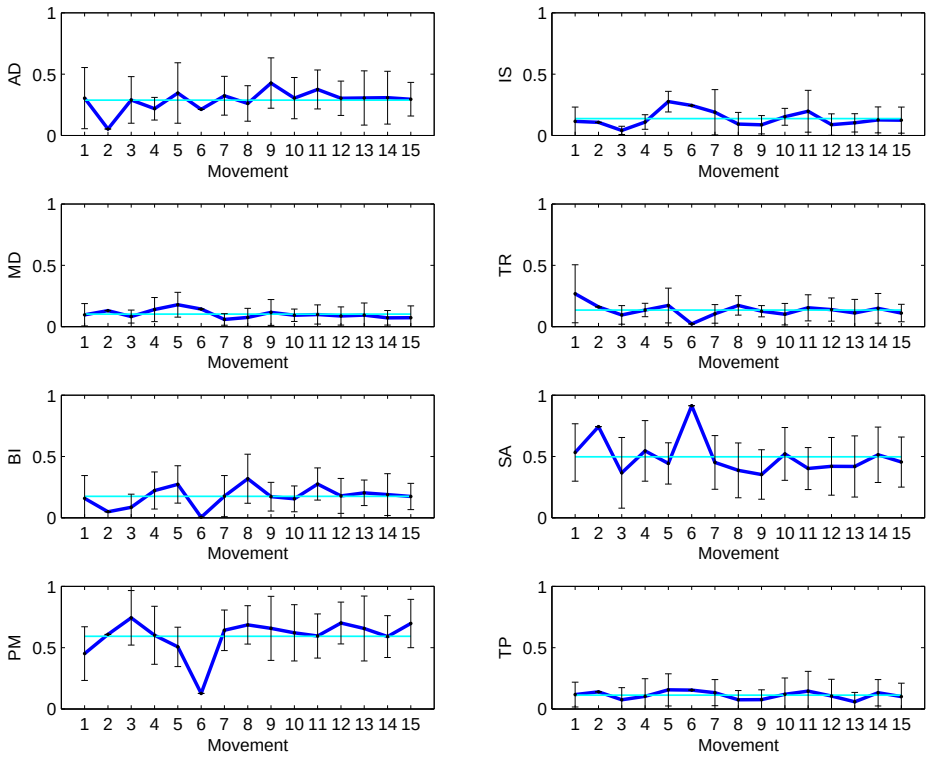

Figure 5.24: Shared module 3 - Dominant side: weights of the modules associated to the third shared module. In each plot in blue the trend of the weights through the different movements with their STDs and in cyan the average weights.

5.1 Upper extremity modules after stroke: first results

Regarding stroke patients, a preliminary investigation was carried out. As with healthy subjects, we concatenated the same tasks data and extracted modules (table 5.4).

Subject	Dominant	Affected	Number of Modules					
			Left	Right	Dom.	ND	Aff.	NA
UBH_001	R	R	1	2	2	1	2	1
UBH_002	R	L	2	3	3	2	2	3
UBH_003	R	R	3	3	3	3	3	3
UBH_004	R	R	2	2	2	2	2	2
UBH_005	R	R	3	2	2	3	2	3

Table 5.4: Summary of the modules extracted from the first five stroke patients. Modules were extracted separately form left and right side and affected and non affected side were compared.

	Affected	Non Affected	Dominant	Non Dominant
Mean	2,2	2,4	2,4	2,2
STD	0,4	0,8	0,5	0,7
Min	2	1	2	1
Max	3	3	3	3

Table 5.5: Comparison between modules of affected and non-affected side of stroke patients.

On average, 2.3 modules are necessary to reconstruct the EMG signals with a minimum value of 1 and a maximum of 3. From these result we can assess that:

- modules extracted are significantly less than in healthy subjects (4.3 on average);

- if we consider just the unaffected side the number of modules extracted are low (2.4);

- there are not so evident differences between affected (2.2 $\pm$ 0.4 modules) and non affected side (2.4 $\pm$ 0.8 modules).

The decrease of the number of modules in the unaffected side confirms the theory according to which when a brain injury occurs, not only the controlateral side is affected but there is also an influence on the ipsilateral side; that could lead to a decrease on the number of motor modules of the unaffected side. Then, if we compare the number of modules of the affected side with the modules extract from healthy subjects there are significant difference, changing from 2,4 to 4,3 modules on average. This is in agreement with what is reported in literature. However, these are just preliminary results, further investigations on a larger sample of subjects are needed.

Conclusion

Evidence collected during this study supports the hypothesis that muscle modules could be an effective way to simplify motor control. We found that an average of 4 modules could be enough to explain most movements. We think that these modules represent general structures that could describe muscle coordination from a global point of view, but we saw that they are not able to capture finer movement-specific aspects.

We also found that dominant and non-dominant side share about 3 modules on average, which means that the majority of modules are common between the two sides and that there is a smaller number of modules that are specific for one side. Furthermore, many subjects share similar modules. Although not all subjects use the same coordination patterns, a very limited number of modules could describe muscle activation of all 15 healthy subjects. In fact, we could group all modules of the dominant side into eight clusters, and all modules of the non-dominant side into another eight clusters. All of these clustered modules could be associated with a biomechanical function, which is of fundamental importance if we want to attempt to use modules as a tool for describing motor coordination. Additionally we could associate each module with a specific phase during a movement by looking at its activation coefficient.

When looking at each movement individually, we found that modules extracted from all pooled movements were not able to describe certain details. However, we found significant similarities between modules extracted from a single movement and modules extracted from all movements.

This suggests that those structures found when pooling all movements together are still valid on a movement-specific basis, and that their individual weights can be tweaked in order to adapt to the performance requirements of a certain movement.

This study provided us with a basic understanding of how muscle coordination might be achieved in healthy people. We also started to look at the changes happening after stroke. In accordance with the literature, we found that the number of modules of the affected side decreases. However, we also saw a significant reduction in the number of modules on the unaffected side. Due to the very limited number of stroke subjects these results are certainly not statistically significant, and they might change once the data for all subjects is processed. If confirmed though, this would be a novel result that would agree with recent discoveries in rehabilitation science, which claim that also movement of the ipsilateral side is affected by stroke.

Bibliography

[1] V. Brooks, "Motor Control How Posture and Movements are Governed," *Physical Therapy*, pp. 664–673, 1983. [Online]. Available: http://physther.org/content/63/5/664.short

[2] E. N. Marieb and K. Hoehn, *Human Anatomy & Physiology*, 7th ed. Benjamin Cummings, 2006.

[3] P. Saltiel, K. Wyler-Duda, A. D'Avella, M. C. Tresch, and E. Bizzi, "Muscle synergies encoded within the spinal cord: evidence from focal intraspinal NMDA iontophoresis in the frog." *Journal of neurophysiology*, vol. 85, no. 2, pp. 605–19, Feb. 2001. [Online]. Available: http://www.ncbi.nlm.nih.gov/pubmed/11160497

[4] A. D'Avella, P. Saltiel, and E. Bizzi, "Combinations of muscle synergies in the construction of a natural motor behavior." *Nature neuroscience*, vol. 6, no. 3, pp. 300–8, Mar. 2003. [Online]. Available: http://www.ncbi.nlm.nih.gov/pubmed/12563264

[5] D. N. Levine, "Sherrington's "The Integrative action of the nervous system": a centennial appraisal." *Journal of the neurological sciences*, vol. 253, no. 1-2, pp. 1–6, Feb. 2007. [Online]. Available: http://www.ncbi.nlm.nih.gov/pubmed/17223135

[6] S. Grillner, "Control of locomotion in bipeds, tetrapods and fish," in *Handbook of Physiology. The Nervous System, Motor Control. Vol. 2*, V. B. Brooks, Ed., 1981, pp. 1179–1236.

[7] P. S. Stein, S. Grillner, A. I. Selverston, and D. G. Stuart, Eds., *Neurons, Networks, and Motor Behavior*, 1999.

[8] F. A. Mussa-Ivaldi, S. F. Giszter, and E. Bizzi, "Linear combinations of primitives in vertebrate motor control." *Proceedings of the National Academy of Sciences of the United States of America*, vol. 91, no. 16, pp. 7534–8, Aug. 1994. [Online]. Available: http://www.pnas.org/content/91/16/7534.shorthttp://www.pubmedcentral.nih.gov/articlerender.fcgi?artid=44436&tool=pmcentrez&rendertype=abstract

[9] S. F. Giszter, F. A. Mussa-Ivaldi, and E. Bizzi, "Convergent force fields organized in the frog's spinal cord." *The Journal of neuroscience : the official journal of the Society for Neuroscience*, vol. 13, no. 2, pp. 467–91, Feb. 1993. [Online]. Available: http://www.jneurosci.org/content/13/2/467.shorthttp://www.ncbi.nlm.nih.gov/pubmed/8426224

[10] E. Bizzi, F. A. Mussa-Ivaldi, and S. Giszter, "Computations underlying the execution of movement: a biological perspective." *Science (New York, N.Y.)*, vol. 253, no. 5017, pp. 287–91, July 1991. [Online]. Available: http://www.ncbi.nlm.nih.gov/pubmed/1857964

[11] J. Roh, V. C. K. Cheung, and E. Bizzi, "Modules in the brain stem and spinal cord underlying motor behaviors." *Journal of neurophysiology*, vol. 106, no. 3, pp. 1363–78, Sept. 2011. [Online]. Available: http://www.pubmedcentral.nih.gov/articlerender.fcgi?artid=3174810&tool=pmcentrez&rendertype=abstract

[12] V. C. K. Cheung, A. D'Avella, M. C. Tresch, and E. Bizzi, "Central and sensory contributions to the activation and organization of muscle synergies during natural motor behaviors." *The Journal of neuroscience : the official journal of the Society for Neuroscience*, vol. 25, no. 27, pp. 6419–34, July 2005. [Online]. Available: http://www.ncbi.nlm.nih.gov/pubmed/16000633

[13] A. D'Avella and E. Bizzi, "Shared and specific muscle synergies in natural motor behaviors." *Proceedings of the National Academy of Sciences of*

the United States of America, vol. 102, no. 8, pp. 3076–81, Feb. 2005. [Online]. Available: http://www.pubmedcentral.nih.gov/articlerender.fcgi?artid=549495&tool=pmcentrez&rendertype=abstract

[14] V. C. K. Cheung, A. D'Avella, and E. Bizzi, "Adjustments of motor pattern for load compensation via modulated activations of muscle synergies during natural behaviors." *Journal of neurophysiology*, vol. 101, no. 3, pp. 1235–57, Mar. 2008. [Online]. Available: http://www.pubmedcentral.nih.gov/articlerender.fcgi?artid=2666413&tool=pmcentrez&rendertype=abstract

[15] L. H. Ting and J. M. Macpherson, "A limited set of muscle synergies for force control during a postural task." *Journal of neurophysiology*, vol. 93, no. 1, pp. 609–13, Jan. 2005. [Online]. Available: http://www.ncbi.nlm.nih.gov/pubmed/15342720

[16] S. a. Overduin, A. D'Avella, J. M. Carmena, and E. Bizzi, "Microstimulation activates a handful of muscle synergies." *Neuron*, vol. 76, no. 6, pp. 1071–7, Dec. 2012. [Online]. Available: http://www.ncbi.nlm.nih.gov/pubmed/23259944

[17] R. Neptune, D. Clark, and S. Kautz, "Modular control of human walking: a simulation study," *Journal of biomechanics*, vol. 42, no. 9, pp. 1282–1287, 2009. [Online]. Available: http://www.sciencedirect.com/science/article/pii/S0021929009001389

[18] C. P. McGowan, R. R. Neptune, D. J. Clark, and S. a. Kautz, "Modular control of human walking: Adaptations to altered mechanical demands." *Journal of biomechanics*, vol. 43, no. 3, pp. 412–9, Feb. 2010. [Online]. Available: http://www.pubmedcentral.nih.gov/articlerender.fcgi?artid=2813323&tool=pmcentrez&rendertype=abstract

[19] A. D'Avella, A. Portone, L. Fernandez, and F. Lacquaniti, "Control of fast-reaching movements by muscle synergy combinations." *The Journal of neuroscience : the official journal of the Society for Neuroscience*, vol. 26, no. 30, pp. 7791–810, July 2006. [Online]. Available: http://www.ncbi.nlm.nih.gov/pubmed/16870725

[20] A. D'Avella, L. Fernandez, A. Portone, and F. Lacquaniti, "Modulation of phasic and tonic muscle synergies with reaching direction and speed." *Journal of neurophysiology*, vol. 100, no. 3, pp. 1433–54, Sept. 2008. [Online]. Available: http://www.ncbi.nlm.nih.gov/pubmed/18596190

[21] A. Ajiboye and R. Weir, "Muscle synergies as a predictive framework for the EMG patterns of new hand postures," *Journal of neural engineering*, vol. 6, no. 3, 2009. [Online]. Available: http://iopscience.iop.org/1741-2552/6/3/036004

[22] S. Muceli, A. T. l. Boye, A. D'Avella, and D. Farina, "Identifying representative synergy matrices for describing muscular activation patterns during multidirectional reaching in the horizontal plane." *Journal of neurophysiology*, vol. 103, no. 3, pp. 1532–42, Mar. 2010. [Online]. Available: http://www.ncbi.nlm.nih.gov/pubmed/20071634

[23] J. Roh, W. Z. Rymer, and R. F. Beer, "Robustness of muscle synergies underlying three-dimensional force generation at the hand in healthy humans." *Journal of neurophysiology*, vol. 107, no. 8, pp. 2123–42, Apr. 2012. [Online]. Available: http://www.ncbi.nlm.nih.gov/pubmed/22279190

[24] "world heart federation," http://www.world-heart-federation.org/cardiovascular-health/stroke/.

[25] A. Di Carlo, "Human and economic burden of stroke." *Age and ageing*, vol. 38, no. 1, pp. 4–5, Jan. 2009. [Online]. Available: http://www.ncbi.nlm.nih.gov/pubmed/19141505

[26] "stroke association," http://www.strokeassociation.org/.

[27] J. P. Dewald, V. Sheshadri, M. L. Dawson, and R. F. Beer, "Upper-limb discoordination in hemiparetic stroke: implications for neurorehabilitation." pp. 1–12, Jan. 2001. [Online]. Available: http://www.ncbi.nlm.nih.gov/pubmed/14523747

[28] L. Gizzi, J. r. F. k. Nielsen, F. Felici, Y. P. Ivanenko, and D. Farina, "Impulses of activation but not motor modules are preserved in the

locomotion of subacute stroke patients." *Journal of neurophysiology*, vol. 106, no. 1, pp. 202–10, July 2011. [Online]. Available: http://www.ncbi.nlm.nih.gov/pubmed/21511705

[29] J. Roh, W. Z. Rymer, E. J. Perreault, S. B. Yoo, and R. F. Beer, "Alterations in upper limb muscle synergy structure in chronic stroke survivors." *Journal of neurophysiology*, vol. 109, no. 3, pp. 768–81, Feb. 2013. [Online]. Available: http://www.ncbi.nlm.nih.gov/pubmed/23155178

[30] V. Cheung and L. Piron, "Stability of muscle synergies for voluntary actions after cortical stroke in humans," *Proceedings of the ...*, 2009. [Online]. Available: http://www.pnas.org/content/106/46/19563.short

[31] D. J. Clark, L. H. Ting, F. E. Zajac, R. R. Neptune, and S. a. Kautz, "Merging of healthy motor modules predicts reduced locomotor performance and muscle coordination complexity post-stroke." *Journal of neurophysiology*, vol. 103, no. 2, pp. 844–57, Mar. 2010. [Online]. Available: http://www.pubmedcentral.nih.gov/articlerender.fcgi?artid=2822696&tool=pmcentrez&rendertype=abstract

[32] V. Cheung and A. Turolla, "Muscle synergy patterns as physiological markers of motor cortical damage," *Proceedings of the ...*, pp. 1–5, 2012. [Online]. Available: http://www.pnas.org/content/109/36/14652.short

[33] J. G. Webster, *Encyclopedia of Medical Devices and Instrumentation*, 2nd ed. John Wiley & Sons, 2006.

[34] "Semian," http://www.seniam.org/.

[35] M. C. Tresch, V. C. K. Cheung, and A. D'Avella, "Matrix factorization algorithms for the identification of muscle synergies: evaluation on simulated and experimental data sets." *Journal of neurophysiology*, vol. 95, no. 4, pp. 2199–212, Apr. 2006. [Online]. Available: http://www.ncbi.nlm.nih.gov/pubmed/16394079

[36] D. D. Lee and H. S. Seung, "Learning the parts of objects by non-negative matrix factorization." *Nature*, vol. 401, no. 6755, pp. 788–91, Oct. 1999. [Online]. Available: http://www.ncbi.nlm.nih.gov/pubmed/10548103

[37] D. Seung and L. Lee, "Algorithms for non-negative matrix factorization," *Advances in neural information processing ...*, no. 1, 2001. [Online]. Available: http://luthuli.cs.uiuc.edu/~daf/courses/optimization/Papers/lee01algorithms.pdf